Elements on the effects of viscosity on flotation mechanisms

Maxence Cahlik

THÈSE

En vue de l'obtention du

DOCTORAT DE L'UNIVERSITÉ DE TOULOUSE

Délivré par :

l'Institut National des Sciences Appliquées de Toulouse (INSA de Toulouse)

Présentée et soutenue le *09/11/2023* **par :**

Maxence CAHLIK

Éléments sur les effets de la viscosité sur les mécanismes de flottation

---

JURY

Frédéric AUGIER	Chercheur IFPEN	Rapporteur
Davide BENEVENTI	Directeur de recherche	Rapporteur
Zhujun HUANG	Maitresse de conférences	Membre du Jury
Dominique LEGENDRE	Professeur des université	Président du Jury

---

École doctorale et spécialité :

MEGEP : Génie des procédés et de l'Environnement

Unité de Recherche :

Toulouse Biotechnology Institute

Directeur(s) de Thèse :

Pascal GUIRAUD et *Antoine BOUCHOUX*

Rapporteurs :

Frédéric AUGIER et *Davide BENEVENTI*

Remerciements

Mon séjour de cinq ans au sein de l'équipe Transfert Interface Mélange au sein du laboratoire Toulouse Biotechnology Institute, m'a permis de réaliser le travail présenté dans ce mémoire. Ces années ont été une étape importante de ma vie pour les connaissances scientifiques quelles m'ont apportées et pour les personnes que j'ai pu rencontrer.

Tout d'abord, je souhaite remercier Gilles Truan, le directeur de TBI, de m'avoir accueilli au sein du laboratoire durant ces années. Je tiens également à remercier chaleureusement Pascal Guiraud et Antoine Bouchoux pour avoir dirigé cette thèse. Votre investissement et vos remarques pertinentes m'ont permis d'avancer à travers les différentes problématiques de modélisation ou d'expérimentation, de compréhension et d'organisation. Vos nombreuses questions lors de nos réunions m'ont permis d'apprendre a être plus rigoureux dans ma communication et moins douter de mes compétences.

Dans un second temps, je tiens à remercier les membres de mon jury de thèse avec qui j'ai apprécié échanger. Je remercie Dominique Legendre d'avoir accepté de présider ce jury et pour l'intérêt que vous avez porté à mes travaux. Je remercie également Frédéric Augier ainsi que Davide Beneventi pour le temps que vous avez consacré à lire et à rapporter mon travail. Merci à Zhujun Huang d'avoir accepté de participer au jury de thèse et d'avoir fait le déplacement depuis Grenoble.

Je remercie également l'ensemble de l'équipe TIM pour son acceuil, tout particulièrement Ali, Claude et José sans qui la partie expérimentale de mon travail n'aurait pas pu voir le jour. Je remercie aussi tout les doctorants que j'ai pu croisé et notamment avec qui j'ai pu partager le bureau 208. Merci pour votre soutien, les longues discussions en fin de journée, et les scéances de volley ou beach volley.

Et enfin merci à tout mes proches pour leur soutien sans faille. Merci à mes parents, frères, mes colocs et Apo de m'avoir soutenu et écouter me plaindre sur mes multiples problèmes souvent numériques. Merci aussi aux copains du foot (Tom, Nico, Jerem, Olivier, Wyatt...), les heures passées avec vous sur et hors des terrains

m'ont permis de bien évacuer la pression et me faire oublier de temps en temps le travail. Encore merci à Apo pour sa patience lors de mes nombreuses soirées et week-ends passées à travailler ainsi que ses corrections de mon anglais (et conseils de mise en page).

A Mametnic

Résumé

Pour augmenter la production de pétrole des puits existants, des polymères modifiant la rhéologie de l'eau utilisée pour l'extraction sont ajoutés avant son injection. Ces polymères, ici le HPAM, augmentent la viscosité, favorisent l'extraction, mais engendrent des problèmes sur la séparation des émulsions en fin de chaîne de traitement de l'eau d'extraction, en particulier sur la séparation par flottation.

Ce travail a pour objectif de comprendre l'impact qu'a le HPAM sur la flottation. Il combine une approche expérimentale et des méthodes de modélisation et de simulations. L'étude expérimentale préliminaire montre que, dans la gamme industrielle de concentration considérée, le HPAM modifie la viscosité, mais ne change pas la tension de surface du milieu aqueux. La viscosité est constante sur la plage de variations des contraintes imposées, soit par l'écoulement du fluide dans le flottateur, soit par le passage d'une bulle. Le fluide est donc considéré comme newtonien. A l'aide d'un nouveau pilote expérimental de flottateur, nous avons mis au point la méthode pour réaliser une émulsion reproductible pour son alimentation. Nous avons montré que la présence de polymère tend à diminuer la taille des gouttelettes d'huile produites, et, à l'inverse, à augmenter la taille des bulles. Cette influence sur ces deux paramètres permet déjà d'apporter une explication macroscopique à la chute observée d'efficacité des flottateurs industriels lorsque du HPAM est présent dans l'eau. Le pilote mis en place pour l'étude de la flottation a montré plusieurs limitations pour la mesure de ces pertes d'efficacité, dues aux très faibles teneurs en huile du milieu à traiter rendant délicates les mesures de concentration avec les métrologies testées. Cependant, des pistes pour accéder à cette teneur en huile ont été testées et plusieurs solutions alternatives ont été identifiées.

L'étude numérique consiste à évaluer l'effet de la viscosité sur les mécanismes microscopiques de flottation conduisant à la capture de particules (ici des gouttes d'huile) par des bulles en ascension. Dans une première approche, le modèle de capture de Nguyen (1998) (collision hydrodynamique entre la particule et la surface de la bulle suivie de l'attachement par drainage du film interstitiel sous l'effet des forces à courte distance) a permis d'identifier qu'à l'échelle locale, l'impact du HPAM à

travers la viscosité dépend principalement de la taille des gouttes et des bulles. Nous avons montré que l'efficacité de capture d'une bulle décroît avec l'augmentation de la viscosité p our des bulles millimétriques (en mode IAF, flottation à air induit), alors qu'en mode DAF (flottation à air dissout) avec des bulles de quelques dizaines de micromètres, la viscosité n'a presque pas d'effet. Afin de garder une résolution purement numérique, cette étude préliminaire a été menée grâce à plusieurs hypothèses additionnelles au modèle existant dont certains paramètres internes devraient être calées expérimentalement.

Dans une deuxième approche, un nouveau modèle retournant à la définition même de l'efficacité d'attachement a été proposé afin de limiter ces hypothèses additionnelles. Cette approche a montré qu'un paramètre critique au calcul de cette efficacité, l'épaisseur initiale du film liquide au début de l'étape d'attachement, est impossible à définir proprement sans apport expérimental. Ceci nous a permis de remettre en cause la méthode traditionnelle de modélisation de l'efficacité de capture par découplage des étapes de collision et d'attachement. C'est pourquoi nous avons tenté, dans une troisième approche, de déconstruire ce modèle en retournant à un calcul de trajectoire d'approche de la goutte vers la surface de la bulle. Cette méthode initialement utilisée par Sarrot (2006) puis Huang (2009) pour modéliser la collision a été modifiée en ajoutant les forces à courte portée actives dans l'étape d'attachement (forces de Van der Waals, électrostatique et s'opposant au drainage du film liquide). L'évolution de ces forces et de celles dues aux interactions hydrodynamiques le long de la trajectoire, et leur sensibilité à la viscosité, tendent à confirmer les conclusions réalisées avec le modèle de Nguyen. Cependant, dans l'état actuel de sa modélisation, la force s'opposant au drainage possède une magnitude trop importante pour pouvoir atteindre la capture. D'autres forces en plus de celles considérées doivent être prises en compte pour pouvoir finaliser ce modèle de capture.

Abstract

To increase oil production from existing wells, polymers that modify the rheology of the water used for extraction are added before it is injected. These polymers, in this case HPAM, increase viscosity and promote extraction, but also cause problems for emulsion separation at the end of the extraction water treatment chain, particularly for separation by flotation.

The aim of this work is to understand the impact of HPAM on flotation. It combines an experimental approach with modelling and simulation methods.

The preliminary experimental study shows that, in the industrial concentration range considered, HPAM modifies the viscosity, but does not change the surface tension of the aqueous medium. The viscosity is constant over the range of stress variations imposed, either by the fluid flowing through the flotation device, or by the passage of a bubble. The fluid is therefore considered Newtonian. Using a new experimental flotation pilot, we have developed the method for producing a reproducible emulsion for its feed. We have shown that the presence of polymer tends to reduce the size of the oil droplets produced and, conversely, to increase the size of the bubbles. This influence on these two parameters already provides a macroscopic explanation for the observed drop in the efficiency of industrial flotation devices when HPAM is present in the water. The pilot set up to study flotation showed a number of limitations when it came to measuring these efficiency losses, due to the very low oil content of the medium to be treated, making it difficult to measure concentration using the meteorology tested. However, ways of accessing this oil content were tested and several alternative solutions were identified.

The numerical study consists of evaluating the effect of viscosity on the microscopic flotation mechanisms leading to the capture of particles (here oil droplets) by rising bubbles. In a first approach, the capture model of Nguyen (1998) (hydrodynamic collision between the particle and the surface of the bubble followed by attachment by drainage of the interstitial film under the effect of short-range forces) made it possible to identify that, at the local scale, the impact of HPAM through viscosity depends mainly on the size of the droplets and bubbles. We have shown

that bubble capture efficiency decreases with increasing viscosity for millimeter-sized bubbles (in IAF mode, induced air flotation), whereas in DAF mode (dissolved air flotation) with bubbles of a few tens of microns, viscosity has almost no effect. In order to maintain a purely numerical resolution, this preliminary study was carried out using several additional hypotheses to the existing model, some of whose internal parameters would have to be calibrated experimentally.

In a second approach, a new model returning to the very definition of attachment efficiency was proposed in order to limit these additional hypotheses. This approach showed that a parameter critical to the calculation of this efficiency, the initial thickness of the liquid film at the start of the attachment stage, is impossible to define properly without experimental input. This led us to question the traditional method of modeling capture efficiency by decoupling the collision and attachment stages. This is why, in a third approach, we attempted to deconstruct this model by returning to a calculation of the approach trajectory of the drop towards the surface of the bubble. This method, initially used by Sarrot (2006) and Huang (2009) to model the collision, was modified by adding the short-range forces active in the attachment stage (Van der Waals forces, electrostatic forces and forces opposing drainage of the liquid film). The evolution of these forces and those due to hydrodynamic interactions along the trajectory, and their sensitivity to viscosity, tend to confirm the conclusions reached with Nguyen's model. However, in the current state of his modelling, the force opposing drainage is of too great a magnitude to be able to achieve capture. Other forces in addition to those considered need to be taken into account in order to finalize this capture model.

Contents

Nomenclature

α	Gas hold up	$[m^2]$
ϵ	Air permittivity	$[F.m^{-1}]$
ϵ_0	Vacuum permittivity	$[F.m^{-1}]$
κ	Debye constant	$[m^{-1}]$
λ	Constant of Carreau equation	$[s]$
μ_0	Viscosity at zero shear	$[Pa.s]$
μ_f	Fluid viscosity	$[Pa.s^{-1}]$
μ_s	Solvant viscosity	$[Pa.s]$
$\dot{\gamma}$	Shear rate	$[s^{-1}]$
ρ_d	Droplet density	$[kg.m^{-3}]$
ρ_f	Fluid density	$[kg.m^{-3}]$
ρ_p	Particle density	$[kg.m^{-3}]$
ρ_w	Water density	$[kg.m^{-3}]$
$\sigma_{d,b}$	Surface tension between the droplet and the bubble	$[\ N.m{-}1]$
$\sigma_{d,l}$	Surface tension between the droplet and the liquid	$[\ N.m{-}1]$
$\sigma_{l,b}$	Surface tension between the bubble and the liquid	$[\ N.m{-}1]$
τ	Relaxation time	$[s]$
θ	Angular position	$[rad]$
θ_a	Contact angle	$[^\circ]$

θ_{col}	Maximal angle of collision	$[^\circ]$
θ_{cr}	Critical angle of attachement	$[^\circ]$
ζ_b	Bubble surface potential	$[V]$
ζ_p	Particle surface potential	$[V]$
a	Reduced radii	$[m]$
A_{cr}	Coefficient for induction time calculation	$[s.m^{-1}]$
A_i	Hamaker constant of component i	$[J]$
B_{cr}	Coefficient for induction time calculation	$[-]$
C	Oil concentration	$[ppm]$
C^*	Critical overlap concentration	$[kg.m^{-3}]$
C_D	Drag coefficient	$[-]$
C_i	Concentration of ion i	$[mol/L]$
C_M	Added mass coefficient	$[-]$
d_b	Bubble diameter	$[m]$
d_d	Droplet diameter	$[m]$
d_{ini}	Droplet initial distance from bubble center	$[m]$
d_p	Particle diameter	$[m]$
E	Entering coefficient	$[N.m-1]$
e	Elementary charge	$[C]$
E_A	Attachment efficiency	$[-]$
E_{capt}	Capture efficiency	$[-]$
E_C	Collision efficiency	$[-]$
E_d	Detachment probability	$[-]$
E_S	Stability efficiency	$[-]$

F	Resulting force	$[N]$
F_{drag}	Drag force	$[N]$
F_e	Electrostatic force	$[N]$
F_{VdW}	Van der Waals force	$[N]$
g	Gravity acceleration	$[m.s^{-2}]$
H	Film central thickness	$[m]$
h	Film thickness	$[m]$
h_0	Initial film thickness	$[m]$
h_c	Film critical thickness	$[m]$
I	Ionic strength	$[mol.L^{-1}]$
I	Ionic strength	$[mol/L]$
k_b	Boltzmann constant	$[J.K^{-1}]$
K_{N_2}	N_2 Henry's constant	$[Pa]$
K_{O_2}	O_2 Henry's constant	$[Pa]$
M_w	Molecular weight	$[kg.mol^{-1}]$
N_A	Avogadro constant	$[mol^{-1}]$
Q_g	Gas flow rate	$[m^3.s^{-1}]$
Q_L	Liquid flow rate	$[m^3.s^{-1}]$
Q_{ww}	White water flow rate	$[m^3.s^{-1}]$
r_{att}	Radius of the attachment surface	$[m]$
r_{col}	Radius of the colliding surface	$[m]$
r_C	Oil disappearence term	$[ppm.s^{-1}]$
Re_b	Bubble Reynolds number	$[N.m-1]$
S	Column cross section	$[m^2]$

S	Surface coefficient	$[N.m{-}1]$
St_d	Droplet Stokes number	$[-]$
T	Temperature	$[K]$
t	Time	$[s]$
t_i	Induction time	$[s]$
t_s	Sliding time	$[s]$
$u_{s,d}$	Dimensionless droplet settling velocity	$[-]$
V	Volume occupied by a polymer chain	$[\ m^3]$
V_b	Bubble velocity	$[m.s^{-1}]$
$V_{i,r}$	Radial component of the velocity of i	$[m]$
V_p	Particle velocity	$[m.s^{-1}]$
$V_{s,d}$	Droplet settling velocity	$[m.s^{-1}]$
x_{air}	Air molar fraction	$[-]$
z	Height of the column	$[m]$
z_i	Charge number of ion i	$[-]$
P	Pressure	$[Pa]$

List of Figures

Introduction

La flottation est utilisée dans divers procédés industriels pour séparer ou récupérer des minéraux, de l'huile, des protéines ou des cellules d'une suspension aqueuse. Elle est basée sur l'injection de bulles de gaz (par exemple, air, azote) dans l'eau et sur l'attachement des objets (par exemple, particules minérales, gouttelettes d'huile) aux bulles. Les attelages ainsi créés ont une densité inférieure à celle des objets seuls. Plus important encore, ils ont une flottabilité négative, ce qui signifie que leur densité est inférieure à celle de l'eau. Cela a pour conséquence de les faire remonter vers la surface. Au cours de leur ascension, les attelages peuvent entrer en collision les uns avec les autres et/ou capturer d'autres objets, créant ainsi des agrégats de taille plus importante. Les attelages et les agrégats se rassemblent alors à la surface, formant une mousse qui est récupérée par écrémage ou déversement.

Dans l'industrie pétrolière de production, d'énormes volumes d'eau sont injectés dans les champs pour conduire le pétrole vers le puits de production. Le pétrole est ensuite séparé de l'émulsion huile dans l'eau qui en résulte par une cascade d'opérations différentes. La flottation est utilisée à la fin de cette cascade, ce qui permet de récupérer les gouttelettes de pétrole de la taille d'un micron qui restent dans l'émulsion. L'efficacité de la flottation dans ce cas précis est bien établie et documentée [Deng et al., 2005, Arthur et al., 2005]. Cependant, face à une demande croissante, l'industrie pétrolière utilise désormais des techniques de récupération du pétrole telles que le CEOR (Chemical Enhanced Oil Recovery), qui compliquent le tableau [Nilan et al., 2014]. Une technique CEOR courante consiste à augmenter la viscosité de l'eau injectée dans le gisement en ajoutant une petite quantité, ~ 500 ppm, de HPAM (polyacrylamide partiellement hydrolysé). La faible augmentation de la viscosité (typiquement x2) est suffisante pour balayer un plus grand volume du réservoir, extrayant ainsi une plus grande quantité de pétrole des champs qui peuvent encore contenir $20-40\%$ de pétrole lorsque la récupération est effectuée en utilisant uniquement de l'eau [Abidin et al., 2012, Aguiar and Mansur, 2016]. Cependant, un inconvénient important du CEOR réside précisément dans les performances des étapes de l'opération de séparation du pétrole et de l'eau, avec d'énormes baisses

d'efficacité, en particulier dans les unités de flottation [Dalmazzone et al., 2012]. à titre d'exemple, le CEOR a été introduit en 2005 à l'échelle industrielle dans le champ pétrolifère chinois de Daqing [Deng et al., 2005]. Le temps nécessaire pour séparer le pétrole par décantation - un processus également basé sur une flottabilité négative - a alors été multiplié par quatre par rapport à une eau dépourvue de HPAM [Deng et al., 2002]. Un autre exemple, à l'échelle du laboratoire cette fois, est l'étude d'Argillier et al. qui ont utilisé une simple colonne de flottation dans différentes conditions de fonctionnement [Argillier et al., 2014]. Leurs résultats indiquent que la séparation huile/eau est beaucoup plus lente en présence de HPAM, d'un facteur cinq. Le degré de purification est également affecté, avec une concentration d'huile restante dans l'eau vingt fois plus élevée qu'en l'absence de HPAM.

Ces augmentations des temps de séjour et/ou des concentrations d'huile résiduelle sont des inconvénients majeurs pour l'industrie pétrolière. Ceci est particulièrement gênant dans les installations offshore où l'espace est limité. En effet, les normes actuelles obligent l'opérateur à traiter sur place toute l'eau utilisée pour l'extraction. La perte d'efficacité de la séparation nécessite donc d'augmenter le nombre et/ou la taille des unités de flottation sur la plate-forme, ce qui est très difficile, voire impossible, à réaliser dans certaines installations.

Les mécanismes qui expliquent la perte d'efficacité de la flottation en présence de HPAM ne sont pas encore totalement compris. Dans le présent travail, nous proposons d'étudier cette question de manière théorique, *i.e.* en utilisant des modèles adéquats qui décrivent le fonctionnement à la fois localement (à travers l'efficacité de capture) et à l'échelle du processus (à travers les phénomènes de ré-entrainement). Nous nous concentrons sur la conséquence directe de l'ajout de HPAM, à savoir l'augmentation de la viscosité du milieu. En outre, nous examinons les effets indirects possibles - et parfois observables sur place - de l'ajout de HPAM, les bulles d'air et/ou les gouttelettes d'huile notamment ont des *tailles différentes* que dans le cas où l'eau n'est pas viscosifiée.

Le chapitre suivant a pour but de donner une image générale du problème. Il rappelle d'abord le principe du processus de flottation avant d'introduire les deux classes principales de processus de flottation et leur fonctionnement. Après cet aperçu du processus général de flottation, nous nous concentrons sur la flottation dans l'industrie pétrolière pour voir si et comment l'effet de la viscosité sur l'unité de flottation a été étudié. La faible bibliographie sur l'utilisation de la flottation pour l'eau viscosifiée nous permet d'avoir un premier aperçu de la façon dont la présence de polymère peut affecter les paramètres critiques de la flottation tels que la taille des bulles ou des gouttelettes/particules. Enfin, le mécanisme de capture

est discuté dans la dernière partie de ce chapitre.

Comme mentionné ci-dessus, plusieurs paramètres ont un effet sur la flottation. Le deuxième chapitre traite expérimentalement de l'évolution de ces paramètres en présence de HPAM. Dans ce chapitre, la solution utilisée est d'abord examinée avant de chercher à comprendre l'effet du polymère sur la viscosité. Le comportement constaté est ensuite comparé aux travaux existants. Le dispositif expérimental utilisé pour étudier l'effet du HPAM sur la flottation est ensuite présenté. Ce pilote nous permet d'évaluer l'effet du polymère sur des paramètres critiques tels que la taille des bulles ou des gouttelettes. Bien que les résultats, du point de vue de la flottation, ne soient pas très concluants, ils nous permettent d'établir une base pour de futures études et surtout de disposer de données expérimentales importantes pour réaliser nos simulations.

Le chapitre trois présente l'ensemble des résultats de l'efficacité de capture basés sur le modèle de Nguyen. Son modèle est d'abord rappelé avant d'examiner l'effet des gouttelettes, des bulles et de la viscosité sur l'efficacité de capture. Un bref aperçu de l'influence possible d'autres paramètres (potentiel zêta, tension de surface ou force ionique) est ensuite proposé. Pour mener à bien cette étude de l'efficacité de capture à l'échelle de la bulle, plusieurs hypothèses sont ajoutées au modèle existant afin de réaliser une simulation sans avoir recours à l'expérimentation.

Le quatrième chapitre examine la validité des hypothèses formulées précédemment. Cela a conduit à une déconstruction complète du modèle de capture. Les bases d'une nouvelle méthode de calcul de l'efficacité de la capture sont présentées. Ceci conclut notre étude de l'impact de HPAM à l'échelle de la bulle.

Le dernier chapitre traite de l'influence de l'ajout de polymère à l'échelle du procédé. Cette étude est réalisée par la simulation d'une unité de flottation dans différentes configurations (batch, co-courant, contre-courant). Ensuite, l'entrainement des bulles à l'intérieur de l'unité de flottation est étudiée. Ceci nous permet d'étudier l'effet de la viscosité sur les phénomènes de ré-entrainementqui conduisent à une diminution de l'efficacité globale.

Note : cette thèse étant rédigée en anglais, l'introduction et la conclusion de chaque chapitre seront présentées en français et en anglais.

Introduction

Flotation is used in various industrial processes for separating or recovering minerals, oil, proteins or cells from an aqueous suspension. It is based on the injection of gas bubbles (e.g. air, nitrogen) in water and on the attachment of the objects (e.g. mineral particles, oil droplets) to the bubble surface. The clusters that are thus created have a lower density than the objects alone. More importantly, they have a negative buoyancy, meaning that their density is lower that the density of water. This has the consequence to drive them towards the surface of the suspension. During their ascension, the clusters can collide each other and/or capture more objects, thus creating aggregates of larger sizes. The clusters and aggregates then gather at the surface, forming a foam that is recovered by skimming or spilling.

In the oil production industry, huge volumes of water are injected in the fields for driving the oil towards the production well. Oil is then separated from the resulting oil-in-water emulsion through a cascade of different operations. Flotation is used at the end of this cascade, allowing the recovery of the remaining micron-size oil droplets from the emulsion. The efficiency of flotation in this case is well established and documented [Deng et al., 2005, Arthur et al., 2005]. However, facing an increasing demand and a decreasing supply, the oil industry now uses oil recovery techniques like CEOR (Chemical Enhanced Oil Recovery) that complicate the picture [Nilan et al., 2014]. One common CEOR technique consists in increasing the viscosity of the water injected in the field by adding a small amount, ~ 500 ppm, of polymer such as HPAM (partially hydrolyzed polyacrylamide). The little increase in viscosity (typically x2) is sufficient for sweeping a larger volume of the reservoir, thus extracting a larger amount of oil from fields that can still contain $20 - 40\%$ of oil when recovery is performed using water only [Abidin et al., 2012, Aguiar and Mansur, 2016]. However, one important drawback of CEOR precisely lies in the performances of the oil/water separation operation steps, with huge drops in efficiency especially in the flotation units [Dalmazzone et al., 2012]. As an example, CEOR was introduced in 2005 on the Chinese Daqing oil field at the industrial scale [Deng et al., 2005]. The time needed to separate the oil by decantation - a

process that is also based on a negative buoyancy - increased by a factor of four as compared to water [Deng et al., 2002]. Another example, at the lab scale this time, is the investigation of Argillier et al. who used a simple flotation column in different operating conditions [Argillier et al., 2014]. Their results indicate that the oil/water separation is far much slower in the presence of HPAM, by a factor of five. The degree of purification is affected as well with a remaining oil concentration in the water that is twenty times higher than in absence of HPAM.

Those increases in residence times and/or residual oil concentrations are huge drawbacks for the oil industry. This is especially troublesome in offshore facilities where space is limited. Indeed, the current standards oblige the operator to treat on-site all the water used for the extraction. The loss in separation efficiency thus necessitates to increase the number and/or the size of the flotation units on the platform, which is very challenging if not impossible to achieve in some installations.

The mechanisms that explain the loss in flotation efficiency in the presence of HPAM are still not fully understood. In the present work, we propose to investigate this question theoretically, *i.e.* by using (adequate) models that describe the operation both locally (through the capture efficiency) and at the scale of the process (through recarrying phenomena). We focus on the direct consequence of HPAM addition, meaning the *increase in viscosity* of the medium. In addition, we consider the possible - and sometimes observable on-site - indirect effects of HPAM addition, where air bubbles and/or oil droplets have *different sizes* than in the case where water is not viscosified.

The following chapter is intended to give a general picture of the problem. It first recalls the principle of the flotation process before introducing the two main classes of flotation processes and how they work. After this overview of the general flotation process, we focus on flotation in the oil industry to see if and how the effect of viscosity on the flotation unit has been studied. The light bibliography on the use of flotation for viscosified water allows us to have a first glimpse of how the presence of polymer can affect critical flotation parameters such as bubble or droplet/particle size. Finally, the capture mechanism is discussed in the last part of this chapter.

As mentioned above, several parameters have an effect on flotation. The second chapter deals experimentally with the evolution of these parameters in the presence of HPAM. In this chapter, the solution used is first examined before attempting to understand the effect of the polymer on the viscosity. The behaviour found is then compared with existing work. The experimental set-up used to study the effect of HPAM on flotation is then presented. This pilot allows us to evaluate the effect of

the polymer on critical parameters such as bubble or droplet sizes. Although the results are not very conclusive concerning flotation, they allow us to establish a basis for future studies and to have crucial experimental data to perform our simulation.

Chapter three presents all the results of the capture efficiency based on Nguyen's model. His model is first recalled before looking at the effect of droplet, bubble and viscosity on the capture efficiency. A brief overview of the possible influence of other parameters (zeta potential, surface tension or ionic strength) is then proposed. In order to carry out this study of capture efficiency at the bubble scale, several hypotheses are added to the existing model in order to perform a simulation without relying on experiments.

The fourth chapter discusses the validity of the hypothesis made previously. This led to a complete deconstruction of the capture model. The basis for a new way of calculating capture efficiency is presented. This concludes our study of the impact of HPAM at the bubble scale.

The last chapter deals with the influence of the addition of polymer at the process scale. This study is carried out by simulations of a flotation unit in different configurations (batch, co-current). Then the re-carrying of the bubble path inside the flotation unit is studied. This allows us to study the effect of viscosity and other parameters due to HPAM presence on the re-carrying phenomena which lead to a decrease of global efficiency.

Note: as this thesis is written in English, the introduction and the conclusion of each chapter will be presented in French and in English.

Chapter 1

State of the art & objective of the thesis

1 Flotation principle

Flotation is a separation process aiming to separate a liquid or solid phase in suspension from a continuous liquid phase. The principle is based on particles or drop capture. The capture is made with a collector usually a gas header allowing particles to ascend and to be gathered in a sort of foam at the top of the unit. This foam is then skimmed or spilled toward the outside of the flotation unit.
This process is based on a physical principle called buoyancy. Buoyancy is basically a name for the density difference between two phases (particles or bubbles and water). If its value is positive, the entity will ascend to the surface and if it is not the case, it will sink. Either way, the continuous phase and the suspension one will be separated.
In the case of flotation, particles are always floated, gathered at the top of the unit. It is then important to differentiate three different cases :

- Natural flotation : particles are much lighter than the liquid phase, thus they float easily without the assist of a collector;
- Assisted flotation : particles are slightly lighter than the liquid phase, therefore the presence of a collector is needed to enhance the separation;
- Induced flotation : particles are heavier than the liquid phase, thus lighter collectors are needed to reduce the density of the particles and allow the flotation to be possible. In this case, the flotation efficiency depends strongly on the physico-chemical interactions between the liquid phase, the particles and the collectors.

As a matter of fact, the purpose of gas bubbles and other collectors is to enhance the separation. The bigger the difference in density (between the two phases) is the faster the separation will be. Thus, gas headers which collect particles from the suspension phase will lighten them and allow the particles to raise faster. Cluster formed by the complex bubble particle is often named flock but it also can refer to particles aggregate.

Another advantage of flotation is that the capture of the particle thanks to a bubble can be enhanced [Richerand and Peymani, 2015, Argillier et al., 2014], or even be selective by using the chemical affinity of the suspension phase with the liquid (and continuous) phase or gas forming bubbles [Barbery, 1981].

2 Flotation process

2.1 Different classes of flotation process

There are two main types of flotation devices which are distinguished by their bubble generation patterns and the size of generated bubbles.

2.1.1 Micro flotation: Dissolved air flotation (DAF)

The first class of flotation process is the micro flotation. As its name states, this type of flotation devices works with very thin bubbles between 10 to 100 μm [Al-Shamrani et al., 2002].
One way to generate such a range of bubbles is by electrolysis, applying a voltage between a cathode and an anode [Mickova, 2015, Burns et al., 1997]. Hydrogen bubbles are produced at the cathode and oxygen ones at the anode. It is usually used for the flotation of minerals.
Micro bubbles can also be produced chemically from the fermentation of organic matter or different chemicals reactions.
The last and most common way to generate micro bubbles is done by saturating the liquid, usually the water, to be treated with gas (classically air). To achieve this saturation, the pressure in the contact unit is increased and the gas and the liquid are brought into contact. The increase in gas saturation in water is described by Henry's law (equation 1.1 for air) [Schers and Van Dijk, 1992, Takahashi et al., 1979, Edzwald, 2010]. In equation 1.1, x_{air} is the air molar fraction in water which depends on the pressure P and Henry's constants (K_{N_2} for the nitrogen & K_{O_2} for

the oxygen with the values 9.08×10^5 & 4.26×10^4 Pa at $20°C$).

$$x_{air} = 0.8\frac{P}{K_{N_2}} + 0.2\frac{P}{K_{O_2}} \tag{1.1}$$

Thus in the industry, water is pressurized up to around 4 to 6 bars [Edzwald, 2007, Richerand and Peymani, 2015] with air and brought to saturation or close to saturation. This saturated water is passed through a needle valve or a special head allowing the fluid to undergo a significant pressure drop. This allows the water to release the previously dissolved gas and thus creates bubbles [Rykaart and Haarhoff, 1995]. The size of generated bubble depends on the pressure applied. Up to 3 bars, diameters of generated bubbles tends to decrease with the increase in pressure. After this pressure level, bubble size is no longer impacted by an increase in pressure [Oikonomidou et al., 2018] but bubbles are generated easily when pressure is increasing. Indeed, when the pressure drop increases, the formation of bubble is thermodynamically more favorable [Ward et al., 1970]. This method generates very thin bubbles which tend to form very stable couplings with particles which greatly increase the efficiency of the flotation. We can note that, depending on the size of the oil drops (if they are larger than the bubbles), the buoyancy is not very significant [Richerand and Peymani, 2015]. Thus longer flotation times are observed. This way is named Dissolved Gas Flotation (DGF), after the method used to produce bubble. Usually, this bubble generation is done from recycling a part of the treated water [Zouboulis and Avranas, 2000, Rubio et al., 2002].

For now and go on, micro flotation is called Dissolved Air Flotation as it is the method used experimentally in this thesis to produce bubbles.

2.1.2 Induced air flotation (IAF)

The second method is called Induced Gas Flotation (IGF). This name is also given because of the method of producing bubbles. Bubbles, usually made up of air, are produced in various ways by direct air injection. This can be achieved by direct injection of air through capillaries into the flotation cell. The size of the bubbles will then be conditioned by the internal diameter of the capillaries. This makes it possible to generate a large number of bubbles of the same diameter. Other methods can be used to create a distribution of bubble sizes, by injecting the air through a sinter, or by injecting the air mechanically using a turbine. The air is sucked from the outside environment and injected into the cell. These various methods of generation create what are known as macro-bubbles with a diameter around 1 mm [Richerand and Peymani, 2015].These macro-bubbles form less stable

couplings than micro-bubbles but increase buoyancy significantly. In the same way as for the DGF, the limiting factor is the size of the oil drops collected. Indeed, the smaller the drops, the greater the difference in size between bubble and drop and therefore the probability of the coupling breaking increases. Thus the flotation in IGF mode will be less efficient than in DGF mode but often much faster. This is why this method is often preferred in the oil industry.

2.1.3 Induced dissolved air flotation (IDGF)

Finally, another type of flotation cell is currently being studied. This one is called Induced Dissolved Gas Flotation (IDGF) and is a combination of the two previous methods [Richerand and Peymani, 2015]. This creates a very wide distribution of bubble sizes ranging from tens of micrometers to millimeters. Such a distribution improves the efficiency of flotation. Indeed, it allows the capture of the finest oil drops with the smallest bubble sizes as in the DGF process and the largest with macro-bubbles such as an IGF. In addition, other types of couplings can be formed, the micro-bubbles attaching to the oil allow the macro-bubbles to attach more stably to the oil. Thus, the efficiency of a DGF type flotation device is obtained with residence times equivalent to those of the IGF type.

2.2 Application fields

Flotation is used in many industrial fields, where there is a need to separate multiple phases with various properties. Only some reference are given here to illustrate these applications.

Initially, it appeared in the mining industry field either for sulfide (copper, lead, zinc ...) or coal [Barbery, 1981, Ityokumbul, 1993], it allows to get the different ores at the end of the process.

This process is also used in the treatment of industrial wastewater [Liu et al., 2013, Zhang and Guiraud, 2013], in the food industry for vegetal oil [Meyssami, 2005] or to treat the water used to clean poultry [Reed and Woodard, 1976] or even for machinery lubricant [Bensadok et al., 2007, Chawaloesphonsiya et al., 2018]. It is also used to remove ink during paper recycling [Barbery, 1981, Julien Saint Amand, 1999, Beneventi et al., 2008]Similarly, flotation is used in drinking water production systems [Rubio et al., 2002] to remove the various sediments that may be present.

Finally, flotation is used in the oil industry at the end of the water treatment chain to remove the last oil residues from the water used to extract it from the

well [Silset, 2008,Dudek and Øye, 2018,Eftekhardadkhah et al., 2015]. This is where this study comes in. Paragraphs 3 and 4 are dedicated to this specific application.

2.3 Design of industrial flotation unit

2.3.1 IAF designs

The design of a flotation unit depends on its application and category. Indeed, the mining industry tends to use mainly IAF devices such as Wemco (figure 1.1) or Outokumpu (figure 1.2) kinds of cell. In those cells, bubbles are produced mechanically either by sucking the air at the top of the unit with a turbine (Wemco design) or by injecting air. It produces bubbles between 0.2 and 2 mm. This kind of unit, even if quite efficient, tends to be associated with high maintenance issues. In this kind of cell, the dispersed phase is gathered at the top of the unit.

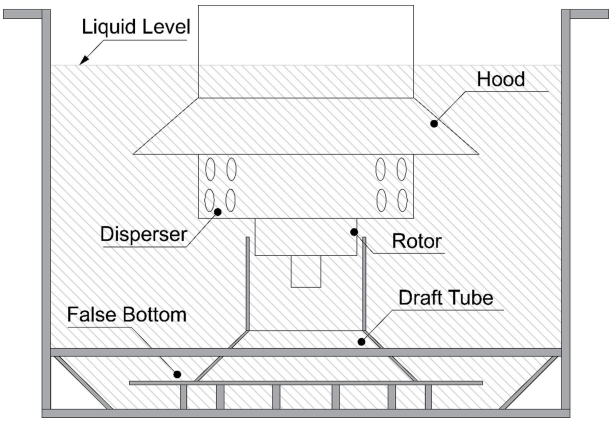

Figure 1.1: Wemco design flotation unit [Yan et al., 2021]

Another kind of IAF is an hydraulic one. Air is introduced with recycled water through a nozzle (figure 1.3). It allows to produce smaller bubbles between 400 and 800 μm [Bennett and Peters, 1988]. This kind of design decreases the residence time of the fluid to treat efficiently [Richerand and Peymani, 2015].

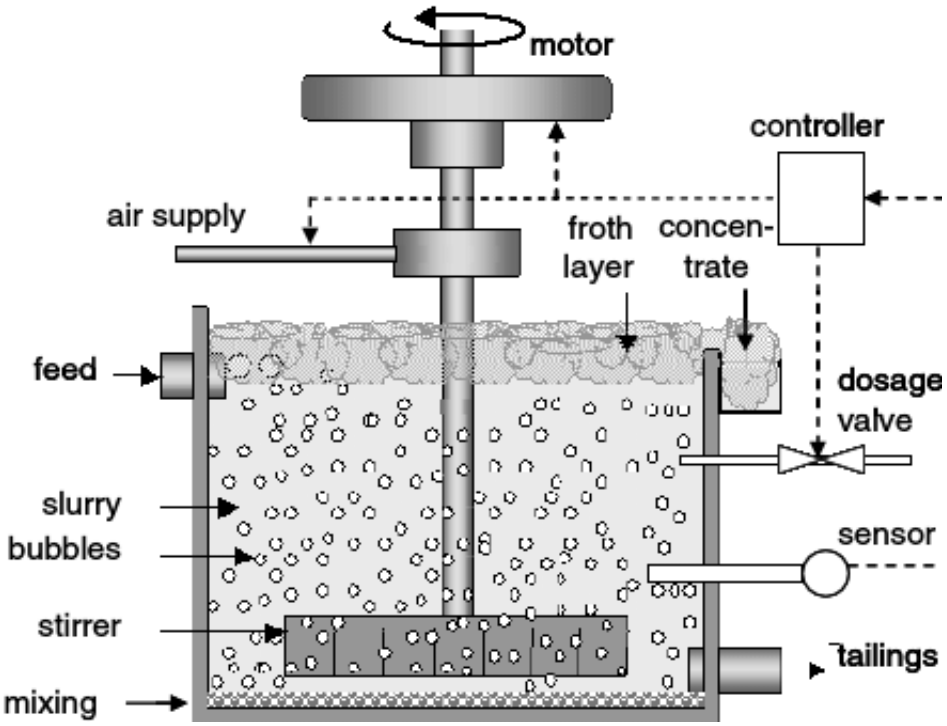

Figure 1.2: Outokumpu design flotation unit [Mondal et al., 2021]

The last kind of IAF device is the column of flotation (figure 1.4). Various methods can be used to produce bubble in a flotation column unit. Porous media are usually used as sparger. This kind of device is quite use in the oil industry even if the use of spargers can be an issue. Indeed, spargers are porous and might fool in presence of organic matter.

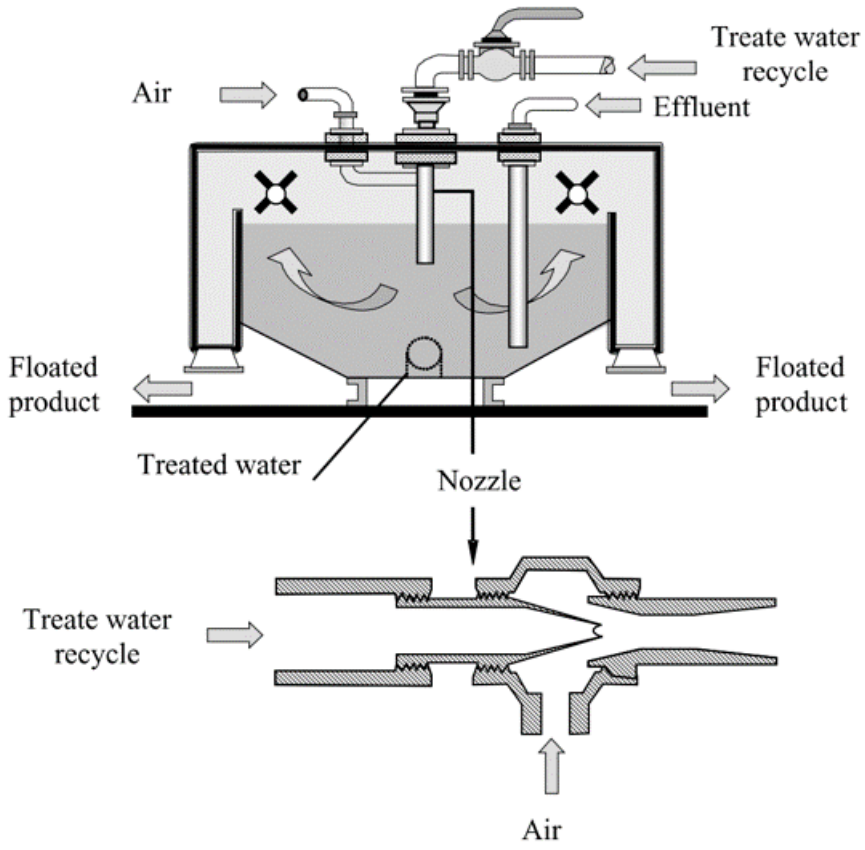

Figure 1.3: Eductor style flotation unit [Rubio et al., 2002]

2.3.2 DAF design

The other kind of flotation use throughout the world are DAF. Those ones, sometimes cylindrical [Besson, 2013] or more often parallelepiped, have always the same general design (figure 1.5), the only difference is the method used to produce bubbles. The large quantity of thin bubbles is produced either with a saturator vessel (most classical method) or DGF pumps. With a saturator vessel bubbles between 10 and 100 μm are produced. That method is quite simple: a part of a recirculating fluid is pressurized inside a vessel before being abruptly release (trough a nozzle or valve). DGF pumps produced slightly smaller bubbles by using a pump to mix both water and air. The turbulence and high shear stress allow the production of bubbles.

After a pretreatment of the feed by flocculation to eventually form flocks, as seen on figure 1.5, a DAF flotation cell is composed of two zones. A contact zone where bubbles and droplets are mixed together allowing bubbles to capture droplets. This functions quite like a flotation column. The second zone is the separation one. The treated water is gathered at its bottom and the dispersed phase at the top.

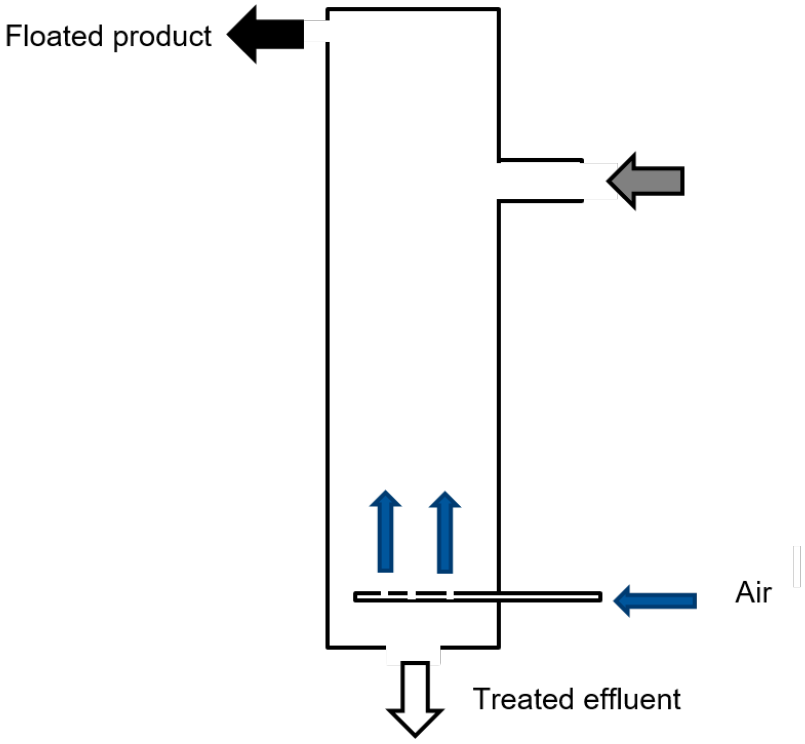

Figure 1.4: Example of flotation column unit

Such a design might cause some issues, as it relies on the bubble trajectory inside the separation zone to achieve a successful separation [Leppinen and Dalziel, 2004]. Indeed, if bubbles are carried by the liquid flow, they travel immediately toward the clean water exit. This can impede the separation. A way to avoid this issue is to reduce the liquid flow to let enough time to the slowest bubble to ascend.

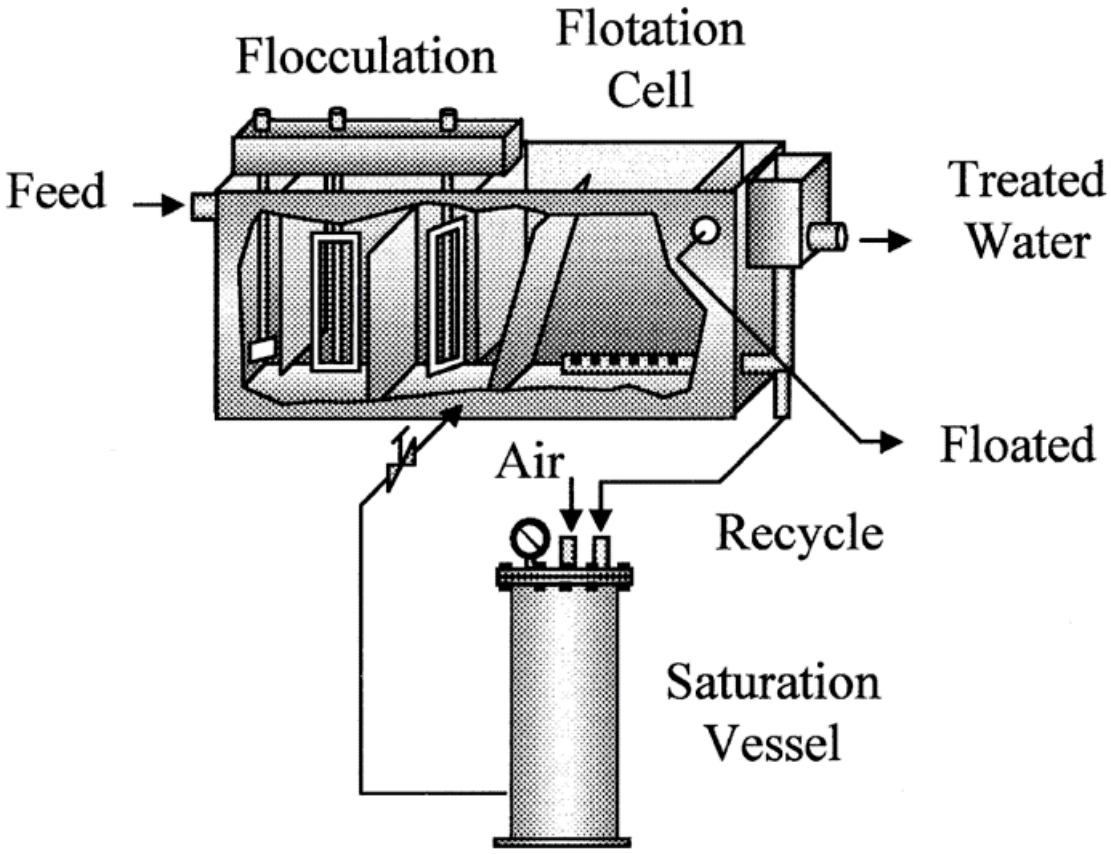

Figure 1.5: Example of DAF flotation unit [Rubio et al., 2002]

3 Flotation in the oil industry

Water is always present at the well when producing oil, but in the oil industry, the use of water is also a way to increase the oil recovery . In fact, to be able to extract oil, water is injected inside the well to push the oil out. However, in order to dispose of the water or even to re-inject it, the produced water has to be cleaned. The produced water goes through various separation processes which efficiency depends mainly on the size distribution of the oil-in-water emulsion (see an example of water treatment chain on figure 1.6). The wastewater goes first trough a gravity separator such as decantation, which allows to get rid of the bigger oil droplets and the main part of the residual oil. But to reach required oil discharge standard (set to 30 ppm by the Oslo Paris convention) [Atarah, 2011], other separation processes such as flotation are used. Flotation is usually chosen for emulsion with droplets sizes up to $30\mu m$ [Ham et al., 1983]. To design properly flotation devices and have an idea of their efficiencies, accurate data or expression describing the oil droplet capture efficiency are needed. This is why studies of various effects have been led.

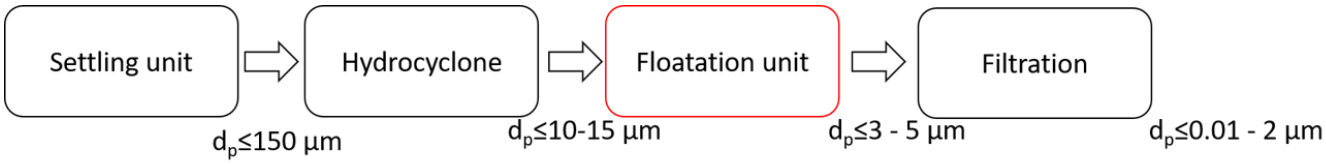

Figure 1.6: Example of a wastewater treatment chain in the oil industry [Deng et al., 2005]

One of the most studied effect is the impact of bubble size on flotation efficiency. This parameter has been studied both experimentally and through numerical calculation. Even if the modeling aspect will be studied later on, it has been shown early on with experiments that an increase in bubble size leads to a drop in flotation efficiency [Cassell et al., 1975, Ramírez-Muñoz et al., 2012].
The impact of droplet size has also been widely studied. When the droplet size is increasing its capture by a bubble is far more probable. Hence, the flotation efficiency is increasing with the droplet size [Dobby and Finch, 1987, Yoon and Luttrell, 1989, Ralston et al., 1999]. This leads to the use of demulsifier to increase the flotation rate [Ichikawa, 2007, Bensadok et al., 2007].
Other aspects such as pH variation, salts concentration, zeta potential variation have been studied. For instance, it has been shown that an increase in salts (such as NaCl or KCl) concentration leads to a better flotation rate [Ralston et al., 1999, Chakibi et al., 2018]. With this study, Chakibi also studied the impact of zeta potential and showed that when this one is decreasing, the flotation efficiency is decreasing. In addition, Dudek showed that flotation is most effective at neutral pH and that a change to basic pH tends to reduce the flotation rate [Dudek and Øye, 2018].

However, the impact of viscosity on the flotation efficiency has been neglected and only a few studies have been performed so far. This question arises in the current context of a constant increase in demand for oil and a decrease in supply. Indeed, in order to increase oil recovery, the water used to recover it is viscosified. This allows to sweep a larger volume of oil wells.

4 Flotation in viscosified water

4.1 At the origin, a way to improve oil recovery

As stated before, in the oil industry, flotation is often used to recover oil present in an oil-in-water emulsion. Such devices are often placed at the end of the water

treatment line in oil fields [Deng et al., 2005, Patel, 2005]. This process allows to recover small droplets larger than 3 micrometers.

Usually, it is just a separation between oil and water. However, facing increasing needs of oil, decreasing of supply and partial exploitation of oilfields (they still contain between 20 and 40 % of oil) [Abidin et al., 2012], the oil industry is using CEOR (Chemical Enhanced Oil Recovery) methods [Nilan et al., 2014]. The process is simple, adding some chemical compounds in the water usually used to extract oil. In the case studied here a small amount (around 500 ppm) of a polymer named HPAM (Hydrolyzed Polyacrylamid) is added along with the water. The use of HPAM in the production water leads to an increase in its viscosity. This phenomenon allows to sweep a larger volume of the reservoir [Aguiar and Mansur, 2016], and thus, extract a larger amount of oil. The viscosified water sweeps a wider range of path allowing to increase the volume swept and the amount of oil recovered.

4.2 A huge drop in separation efficiency actually observed

In practice, the increase of viscosity due to the presence of polymer leads to a huge drop in separation efficiency, mainly in flotation units [Dalmazzone et al., 2012].
It is often used alongside with surfactants in the water to be treated at the well outlet. This form of CEOR is called ASP (Alkali/Surfactant/Polymer) [Qi et al., 2013] [Dalmazzone et al., 2012]. In this form, the role of the polymer is to viscosify the aqueous phase, while the surfactants and alkali will modify the surface tension by reducing it [Deng et al., 2002]. It turns out that in the case of that method, the emulsions formed are extremely stable. This leads to separation problems, mainly in flotation units [Dalmazzone et al., 2012]. This method is for example used on the Chinese Daqing oil field at an industrial scale [Deng et al., 2005]. In 2005, on this field, they favored the decantation process (a process similar to flotation based on the difference between the densities of the entities to be separated). The time required to carry out decantation is multiplied by four when the ASP method is used. This drop in efficiency is suppose to be due to the increase in viscosity but the presence of surfactant might also have an impact on it [Deng et al., 2002]. Furthermore, when ASP method is used, emulsions tends to be more stable, both in oil-in-water [Deng et al., 2005] or water-in-oil [Kang et al., 2011] ones. The case of oil-in-water is for us more interesting as this is the kind of emulsion that aims to be separated by flotation. Thus, on Daquing field, the droplet size distribution goes from 35 to 3 μm in presence of polymer. Hence, the decreasing capture.
One of the methods found to reduce the loss of flotation efficiency was the use of demulsifiers, which made it possible to reduce it to times equivalent to those

obtained with water without polymer or surfactant. However, this requires large quantities of chemicals. In fact, it uses up to 50 mg/L of demulsifier for 3×10^8 tons of water per year. [Deng et al., 2005]. This product is used to destabilize the oil-in-water emulsion stablilized by the presence of the polymer and surfactants but is quite expensive. This is why it is ultimately not viable to use demuslifier in this case.

This decrease in flotation efficiency was investigated experimentally by Argillier et al. [Argillier et al., 2014] using a flotation column. Their results have shown that in presence of HPAM alone, the separation of oil and water through flotation is far much slower. Indeed, it appears that the time needed to reach the maximal separation with the used unit is multiplied by five in presence of HPAM. Furthermore, it shows that the quantity of oil remaining at the end of the separation is twenty time bigger in presence of polymers.

It is then possible to deduct that in presence of polymers like HPAM, the separation is less efficient. There is actually a larger part of oil remaining in the water at the exit of the flotation unit. Those increase in necessary residence times and residual oil concentrations are huge drawbacks for the oil industries and especially for offshore facilities (at sea). In fact, in the case of an offshore facility there is a limited space and it is necessary to treat all the water used for the extraction on site in order to reach the rejection standards. Thus, an increase in the residency time might not be possible to set up, due to the volume to treat and the needed space. As a matter of fact, the outlet flow of the well remains the same. So, to increase the residence time in the flotation unit, more flotation units or larger ones are needed to be able to treat all of wastewater. This is leading to larger needs in space. Therefore, it is a necessity to find the origin of those issues in order to seek solutions and to be able to use this separation method in an effective way.

4.3 Some ideas for the drop of flotation efficiency due to viscosity

The increase in viscosity suitable for oil recovery inside the well can result in some issues regarding the effluent separation. Actually, flotation is a gravity separation unit and its efficiency is a result of an increase buoyancy for the bubble-drop aggregates, flocks or complex. Basically, an increased of buoyancy leads to an increase in ascension velocity. Therefore, assuming the complex or simply the droplet behave as tiny rigid spheres, the velocity of an entity follows Stokes law (equation 5.1), where V_p is the rising velocity of the entity, d_p the entity diameter, $\rho_w - \rho_p$ the difference

of density and μ_f the viscosity of the water continuous phase. We have chosen this law here to represent simply the velocity. In the rest of the thesis, the velocity is modeled by using the Schiller & Naumann drag coefficient (see Annexe A for the expression of the velocity and drag coefficient).

$$V_p = \frac{d_p^2 g(\rho_w - \rho_p)}{18\mu_f} \tag{1.2}$$

This equation shows easily that flotation will be affected by a modification of water viscosity, even without considering flotation mechanisms efficiency, due to a drop of rising velocities with the increases in viscosity.

Furthermore, looking at an industrial flotation device such as DAF device made of two main compartments (figure 5.1), leads to think that the polymer can have an impact at different scales. In this device (on figure 5.1), wastewater and air are injected at the bottom of the unit in compartment 1, the contact zone. In this zone, the capture phenomenon, is observed at the bubble scale. Bubbles, droplets and flocks then ascend toward the top of the unit (following the law depicted in equation 5.1) before being carried towards the surface of the unit into the second compartment. The path of the hetero-aggregate (formed of oil droplets and bubble) in the first compartment depends on the bubble size. Big bubbles are moving to the surface before being skimmed towards the compartment 3 which is the recuperation one (path in black on figure 5.1). However, thin bubbles are carried by the flow towards the compartment 4 and the clean water exit (path in blue on figure 5.1). Thus, the viscosity can have an impact in different part of the cell. In the first compartment, the viscosity can have an impact on the capture of droplets by the bubble and ascent velocity of all entity present. Then, viscosity might also have an impact in the second and fourth compartments, through the ascent velocity meaning that the separation of the foam and water might be less efficient.

For now and then, the study is being conducted without any chemical compounds other than HPAM and salts, mainly to understand the impact of the increase in viscosity through the presence of this polymer. After this overview of the context and scientific issues of our work, the next paragraph focus on the exiting knowledge concerning the flotation mechanisms.

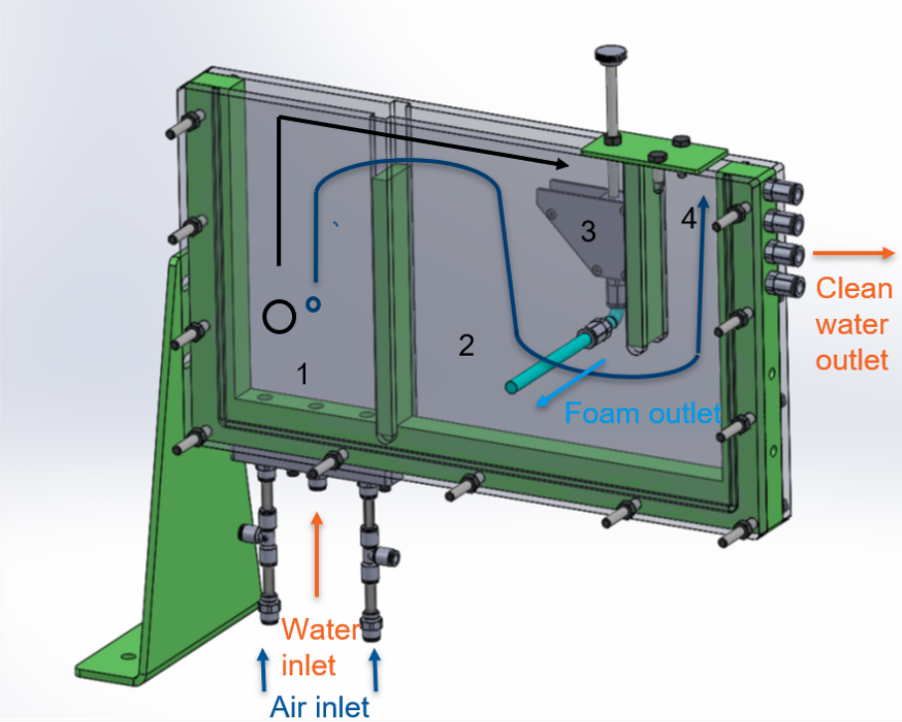

Figure 1.7: Illustration of the operation of a flotation unit function of bubble size

5 Flotation mechanisms

Flotation is based on the fact that a separation can be accelerated through the capture of the phase to separate (in this case oil droplets) with bubbles. The essential mechanism of flotation is thus the capture of particles. The capture efficiency is defined by the number of particles captured by a rising bubble on the number of particles present in the volume swept by this bubble (figure 1.8) and can be expressed as:

$$E_{capt} = \frac{Number\ of\ captured\ particles}{Number\ of\ particles\ in\ the\ volume\ swept\ by\ the\ bubble} \tag{1.3}$$

The ideal case occurs when all the particles within the bubble trajectory are captured by the bubble. In this particular case, the capture efficiency has the value of 1.

Capture is a multistage mechanism. It falls in three elementary steps [Derjaguin and Dukhin, 1993, Derjaguin, 1993], and to each of them there is an efficiency attributed [Ralston and Dukhin, 1999]. The first and most studied step is the collision which is mainly driven by the hydrodynamics around the bubble. To this step an efficiency named collision efficiency E_C is attributed. Then, function of the droplets and bubbles trajectory or velocity, the behavior of interfaces and interfacial proper-

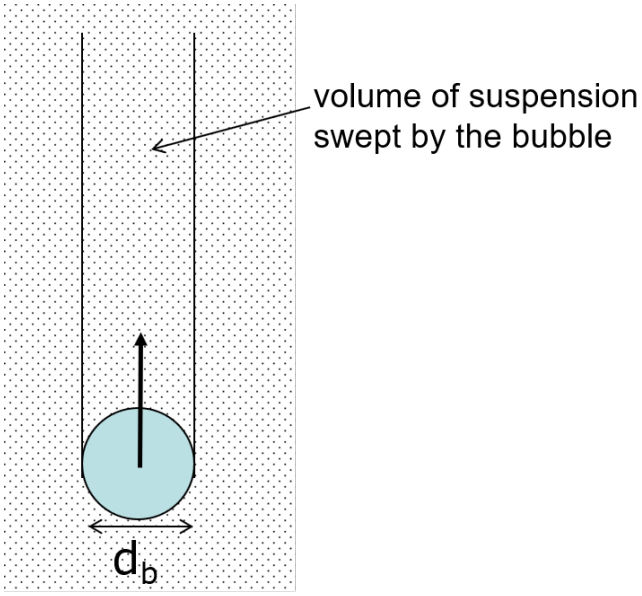

Figure 1.8: Definition of capture efficiency

ties, attachment may occur. An efficiency named attachment efficiency E_A is then defined. Finally, if the attachment is successful the result of the capture depends on the stability of the coupling between the bubble and the attached particle or droplet. Indeed, during its ascension towards the surface, the droplet can detach from the bubble surface for various reasons. A stability efficiency E_S has then been introduced. This efficiency is defined as $1 - E_d$, with E_d the attached droplet probability of detachment. In the context of this thesis, the studied droplets are smaller than 100 μm meaning that the detachment probability can be neglected [Yoon, 2000]. This means that the coupling is stable, $E_S = 1$. The capture efficiency E_{capt} is then expressed as follow:

$$E_{capt} = E_C E_A \tag{1.4}$$

The following paragraphs give details upon collision and attachment.

5.1 Collision

As stated, collision occurs when the droplet enters in contact with the bubble. Different scenarios can happen. Basically, tiny droplets tend to behave has tracers and follow the streamline (see figure 1.9). Thus, collision occurs when droplets trajectories encounter the bubble surface. Once it has been set, three different effects can lead to collision:

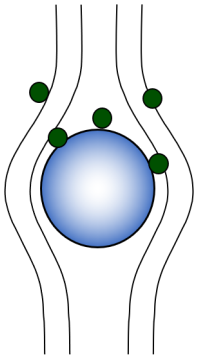

Figure 1.9: Scheme of the collision step

- Interception: droplets behave as tracers [Ralston and Dukhin, 1999], this type of collision occurs when the Stokes number (equation 1.6) of the droplet is far lower than 0.1. This means that the inertia of the droplet is neglected.

- Gravity effect: the droplet shifts from its trajectory away from the streamline toward the bubble. This kind of collision occurs wether the droplet dimensionless settling velocity $u_{s,d}$ (equation 1.5) is greater than 1.

- Brownian effect: droplets acquire a random motion by colliding with the surrounding molecules. A collision under Brownian effect might occurs for droplets thinner than 1 μm and for a Péclet number lower than 10^{-5} [Ramirez et al., 1999].

In the context of this thesis, we study droplets with a diameter varying between 1 and 100 μm at most and bubbles from 1 to 1000 μm. In order to stay in the correct range for modeling, the droplet diameter is always considered smaller than the one of the bubble. Thus, Brownian motion collision can not occur. The gravity effect does not play a role either. Indeed, according to table 1.1, the droplet dimensionless settling velocity is under 1 on all the range of variation.

$$u_{s,d} = \frac{V_{s,d}}{V_b} \; with \; V_{s,d} = \frac{1(\rho_d - \rho_f)d_d^2 g}{18\mu_f} \tag{1.5}$$

This lets us with interception as the main mechanism of collision with droplets which Stokes number variation (table 1.2) are almost in the proper range. Indeed, for droplets around $100\mu m$ inertia should be taken into account.

$$St_d = \frac{1}{9}\left(\rho_d + \frac{1}{2}\rho_f\right)\frac{d_d^2 V_b}{\mu_f d_b} \tag{1.6}$$

d_b (μm) \ d_d (μm)	1	50	100
1	1.7×10^{-4}	–	–
500	1.7×10^{-9}	4.2×10^{-6}	1.7×10^{-5}
1000	9.1×10^{-6}	2.3×10^{-6}	9.1×10^{-6}

Table 1.1: Variation of dimensionless settling velocity number in water at 1 Cp

Models of collision by interception are then more likely to be used in our case.

d_b (μm) \ d_d (μm)	1	50	100
1	8×10^{-8}	–	–
500	1.6×10^{-5}	0.04	0.16
1000	1.5×10^{-5}	0.04	0.14

Table 1.2: Variation of Stokes number in permuted water at 1 Cp

Those models have been widely studied since the middle of the XX century by authors such as [Sutherland, 1948] who set the base of current collision models (for a review of these models see [Sarrot, 2006, Huang, 2009]). They are based on the following hypotheses:

- $V_{s,d} << V_b$ so the droplet velocity is neglected.
- $St_d << 1$ (cf. table 1.2) so the droplet inertia is neglected, it behaves as tracers.

To these commune hypothesis another one is added function of the behavior of bubble surface. In our study, the bubble is considered as contaminated or fully retarded meaning that the bubble surface is immobile and behaves as a solid sphere. A study of the impact of the behavior of interface on collision model has been led by Sarrot et al. [Sarrot et al., 2005]. From solving Navier Stokes equations with DNS (Direct Numerical Simulation), he models the collision efficiency as a function of interface contamination.
Two interesting and extreme cases are addressed:

- Totally clean and mobile bubble interface:

$$E_{C,Clean} = \frac{d_d}{d_b} \frac{15 + 3Re_b^{0.75}}{15 + Re_b^{0.75}} \tag{1.7}$$

- Fully contaminated and immobile bubble interface:

$$E_{C,Contaminated} = \frac{3}{2}\left(\frac{d_d}{d_b}\right)^2\left(1+\frac{Re_b^{\frac{2}{3}}}{5}\right) \tag{1.8}$$

These equations show that collision depends only on the droplets diameter d_d, the bubble diameter d_b and Reynolds number of the bubble Re_b. The dependence of collision efficiency on droplets and bubble diameters is a function of the behavior of the bubble interface. Indeed, equation 1.7 shows a linear dependence of collision efficiency on entities diameter for a clean bubble. But equation 1.8 shows a square dependance of collision efficiency on droplets and bubble diameter for a contaminated bubble.

In our study bubble surface is considered as contaminated (cf. Annexe A). The use of DNS to obtain these models allows to solve all the trajectory of droplets that are inside the cylinder of diameter $d_d + d_b$. Thus it shows that an extreme trajectory exists from which collision can no longer occurs (figure 1.10). This trajectory define the maximal angle of collision θ_{col}. This angle has been put in evidence both numerically [Dai et al., 1999] and experimentally [Dobby and Finch, 1986, Schulze, 1989] (table 1.3). It depends mainly on Reynolds number.

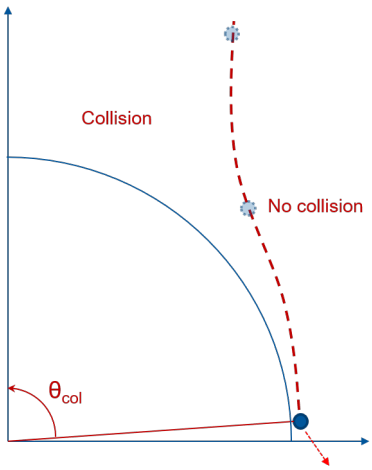

Figure 1.10: Definition of collision angle θ_{col}

The mechanism of collision is in our case the interception as all other phenomena have little to no impact at our scale. The collision efficiency is the one of a contaminated bubble and depends exclusively on hydrodynamics through bubble and droplets diameters along with the Reynolds number of the bubble. The increase

Woo 1971([Dobby and Finch, 1986])	Dai et al., 1999
$\theta_{col} = 78.1 - 7.37log(Re_b)\ for\ 20 < Re_b < 400$	$sin^2\theta_{col} = 2\beta\left[(1+\beta^2)^{\frac{1}{2}} - \beta\right]$
$\theta_{col} = 98.0 - 12.49log(10Re_b)\ for\ 1 < Re_b < 20$	$\beta = \frac{4d_d\rho_d}{3Kd_b(\rho_d - \rho_f)}$
$\theta_{col} = 90.0 - 2.5log(100Re_b)\ for\ 0.1 < Re_b < 1$	$K = \frac{\rho_d V_b d_p^2}{9d_b\mu_f}$

Table 1.3: Models of θ_{col}

of viscosity and the presence of HPAM can thus only have a direct impact on it through the Reynolds number Re_b.

5.2 Attachment

Attachment mechanism begins after the droplet has collided with the bubble. At first, a liquid film is formed between the droplet and the bubble. Then, the droplet begins to slide along the bubble surface (figure 1.11). During its slide, the film between the droplet and the bubble is thinning. If the droplet slides long enough on the bubble surface, the liquid film becomes thin enough to break and the droplet attaches with the bubble (with the creation of a 3 phases contact line). Otherwise once it reaches a certain point, the droplet is carried away of the bubble. So basically, the attachment phase depends on the ratio of two times:

- The sliding time t_s, time during which the drop slides along the bubble surface;
- The induction time t_i, time during which the drop slides along the bubble surface.

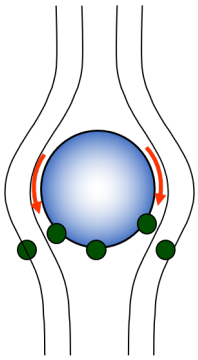

Figure 1.11: Scheme of the attachment step

Thus, if the induction time is shorter than the sliding time, attachment occurs. Figure 1.12 shows the different cases that can occur after the collision. The blue

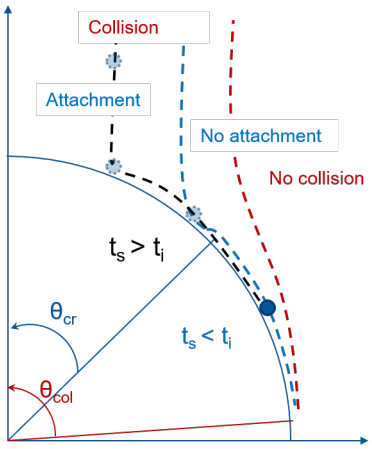

Figure 1.12: Definition of the critical angle of attachment θ_{cr}

line symbolizes the last trajectory where attachment occurs. Behind this streamline, the droplet does not have enough time to drain the liquid film before being carried away at the angle θ_{col}. This angle representing, as stated before, the maximum angle of collision (angle from which collision is no longer possible) is also giving the point where the droplet is carried away if it has not already attached [Nguyen Van, 1993]. This blue line also gives us the critical angle of attachment θ_{cr}, point from which attachment is no longer possible as the droplet does not slide long enough to drain the film.
This two angles have been introduced by [Dobby and Finch, 1987, Yoon and Luttrell, 1989] in order to define the attachment easily. Indeed, the attachment efficiency is initially defined as follow:

$$E_a = \frac{number\ of\ attached\ droplets}{number\ of\ colliding\ droplets} \tag{1.9}$$

This equation can be expressed as follow [Dobby and Finch, 1987]:

$$E_a = \frac{Attachment\ surface}{Collision\ surface} = \frac{sin^2\theta_{cr}}{sin^2\theta_{col}} \tag{1.10}$$

In equation 1.10, the angle θ_{col} depends only on hydrodynamics. It can be obtained either from experiments [Dobby and Finch, 1986] or from models [Dai et al., 1999] (table 1.3).

The angle θ_{cr} is a bit more complicated to obtain but can also be obtain experimentally from the induction time or from mathematical modeling. The easiest and more recent one, is the one presented by Dai et al. in 1999 and enhanced by [Koh

and Schwarz, 2006]:

$$\theta_{cr} = 2arctan\left[exp\left(\frac{t_i\left(2(V_d+V_b)+V_b\left(\frac{d_d}{d_b+d_d}\right)^3\right)}{d_d+d_b}\right)\right] \; with \; t_i = A_{cr}d_d^{B_{cr}} \quad (1.11)$$

In this equation, coefficients A_{cr} and B_{cr} are function of experimental conditions. The coefficient B_{cr} is independent of the droplet, the bubble diameter and the ionic strength. A_{cr}, as equation 1.12 shows, depends on the contact angle θ_a between the droplet and the bubble. This angle depends on the physico-chemical properties of the system and can be calculated from Young equation (equation 1.13) [Ives, 1983]. The only issue with this formula for our study is that a potential variation of viscosity has not be taken into account in the calculation of this coefficient.

$$A_{cr} = \frac{75}{\theta_a} \quad (1.12)$$

$$cos\theta_a = \frac{(\sigma_{d,b}-\sigma_{d,l})}{\sigma_{l,b}} \quad (1.13)$$

Before ending this part there is still one point to talk about. In the case of oil droplets, the stability of the hetero-aggregate formed during the attachment can be increased. Indeed, according to various studies [Moosai and Dawe, 2002, Dudek and Øye, 2018], once the liquid film breaks the oil droplet can spread and coat the bubble (figure 1.13). This phenomena is depending on the entering E and spreading S coefficients (equation 1.14 and 1.15) [Ross, 1950] and the size ratio between the bubble and the droplet.

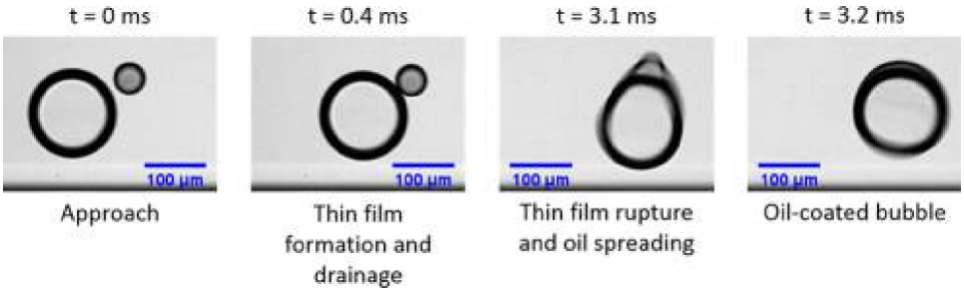

Figure 1.13: Stages of bubbledrop interactions, leading to the formation of an oil film on a gas bubble [Dudek and Øye, 2018]

$$E = \sigma_{l,b} + \sigma_{d,l} - \sigma_{d,b} \quad (1.14)$$

$$S = \sigma_{l,b} - \sigma_{d,l} - \sigma_{d,b} \quad (1.15)$$

If both these coefficients are positive the bubble may get coated and it may favor the film rupture. However, the droplet has to be big enough in order to spread around the bubble. This is why [Dudek and Øye, 2018] gave the additional criterion of size ratio for bubble coating. Droplets must be at least half the size of the bubble for the coating to happen. Furthermore it has been shown [Chakibi, 2017] that in presence of HPAM surface tensions are not modified. Meaning that those coefficients do not change in the presence of a polymer or with the increase in viscosity.

6 Conclusion

The negative effect of liquid phase viscosity on flotation efficiency is currently well documented, but no rational explanations can be found in the scientific literature.

The hydrodynamics of flotation cells clearly show the importance of the rising velocities of bubbles, particles and heteroaggregates. Obviously, their rising velocities depend on the viscosity of the continuous phase. This macroscopic effect will be studied in detail in Chapter 5, together with the effect of droplet and bubble size modification in the presence of polymer.

Flotation mechanisms include in their modeling the Reynolds bubble number Re_b. Various collision efficiency models based on Re_b have been developed by different authors such as Sarrot, Huang or even Nguyen. These models can be used to study the effect of viscosity on collision efficiency. This will be done in Chapter 3.

Experiments in the literature also show an effect of the polymer on bubble and droplet size. Since the collision efficiency depends on these diameters, a first experimental step is necessary to see the effect of viscosity change on these diameters. This will be one of the results of the experiments in the second chapter.

Attachment is less studied in the literature. The only model suitable in our case is the one found in Nguyen's modeling work. We will try to use it in the third chapter to better understand the effect of viscosity on this second flotation mechanism involved in the capture of a droplet by a bubble.

Conclusion

L'effet négatif de la viscosité de la phase liquide sur l'efficacité de flottation est actuellement bien documenté, mais aucune explication rationnelle ne peut être trouvée dans la littérature scientifique.

L'hydrodynamique des cellules de flottation montre clairement l'importance des vitesses de montée des bulles, des particules et des hétéroagrégats. Il est évident que leurs vitesses de remontée dépendent de la viscosité de la phase continue. Cet effet macroscopique sera étudié en détail au chapitre 5, ainsi que l'effet de la modification de la taille des gouttelettes et des bulles en présence de polymère.

Les mécanismes de flottation incluent dans leur modélisation le nombre de Reynolds des bulles Re_b. Différents modèles d'efficacité de collision basés sur Re_b ont été développés par différents auteurs tels que Sarrot, Huang ou encore Nguyen. Ces modèles peuvent être utilisés pour étudier l'effet de la viscosité sur l'efficacité de collision. C'est ce que nous ferons au chapitre 3.

Les expériences de la littérature montrent également un effet du polymère sur la taille des bulles et des gouttelettes. Comme l'efficacité de la collision dépend de ces diamètres, une première étape expérimentale est nécessaire pour voir l'effet du changement de viscosité sur ces diamètres. Ce sera l'un des résultats des expériences du deuxième chapitre.

L'attachement est moins étudié dans la littérature. Le seul modèle adapté à notre cas est celui trouvé dans le travail de modélisation de Nguyen. Nous essaierons de l'utiliser dans le troisième chapitre pour mieux comprendre l'effet de la viscosité sur ce second mécanisme de flottation qu'est la capture d'une gouttelette par une bulle.

Chapter 2

Experiments

Ce chapitre a pour but de présenter tous les travaux expérimentaux de la thèse, depuis les fluides utilisés jusqu'au dispositif expérimental et aux résultats. Dans un premier temps, les propriétés de toutes les solutions (huile, solution polymère et saumure) sont présentées, de leur composition à leur comportement rhéologique. Une partie sur le pilote de flottation et sa métrologie est ensuite abordée avant de parler de l'impact du polymère sur la distribution de la taille des gouttelettes ou des bulles.

This chapter aims to present all the experimental work of the thesis, from the used fluids to the experimental device and results. First, the properties of all the solutions (oil, polymer solution and brine) are presented from their composition to their rheological behavior. A part about the flotation pilot and its metrology is then tackled before talking about the impact of polymer on droplet or bubble size distribution.

1 Solutions properties

In this part, the properties of all solutions used in our experiments are shown. It begins by the brine features with its composition, pH and conductivity in presence of polymer. Then, a presentation of the rheological device and protocol is done before tackling the subject of oil. Later, a presentation of the polymer with the literature revolving around it is made and compared to the rheological properties found for our solutions.

1.1 Chemical compounds & solutions composition

1.1.1 Brine

The solutions are made from permuted water, a mixture of salts given by an industrial (see table 2.1) and 500 ppm polymer concentrations (HPAM). The brine solution has a ionic strength of 1.2 $mol.L^{-1}$. It has been assumed that at these

Products	Concentrations (mol/L)	Concentrations (kg/L)
$Water$	-	-
$NaCl$	8.08×10^{-2}	4.72×10^{-3}
$CaCl_2$	6.71×10^{-3}	7.45×10^{-4}
$MgCl_2$	5.89×10^{-3}	5.61×10^{-4}
KCl	1.49×10^{-3}	1.11×10^{-4}

Table 2.1: Salt mix for the reference brine

salts concentrations the viscosity, density and tension surface of the brine is equal to the one of deionized water. This assumption is made in accordance with the literature [Fanaie and Khiadani, 2020] that shows a variation of less than 1% for each of this parameters. Every calculations in this document are then done for brine solution (except if other specifications are given).

1.1.2 Polymer: Hydrolyzed Polyacrylamide (HPAM)

Partially hydrolyzed polyacrylamide, HPAM (FLOPAAM 3130s sold in powder form by SNF, in this study), consists of 2 types of chemical functions (figure 2.1): amide-type functions and carboxyl-type functions. It is a linear polymer in extended

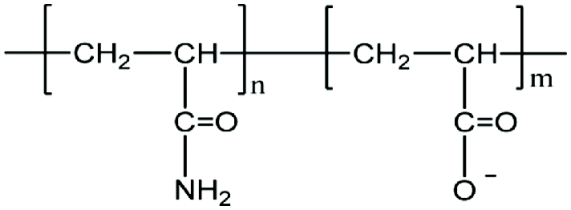

Figure 2.1: Chemical structure of HPAM

solution conformation due to the electrostatic repulsion between the carboxylate groups [Choplin and Sabatié, 1986]. Moreover, because of the presence of many chemical groups, there is no or very little interpenetration between the different chains due to steric discomfort. In our case, the hydrolysis of the polymer is between

25 and 35 % [Wever et al., 2011]. That means that there are between 25 and 35 percent of the amide functions hydrolyzed.

At neutral pH, all the carboxyl groups in the chain are oxidized to carboxylate groups [Ait Kadi et al., 1987].
The C^* of a polymer is the concentration at which the different polymer chains start to overlap one another [Rubinstein and Colby, 2003], is expressed as $C^* = \frac{M_W}{VN_A}$ with V the volume of the solution occupied by the polymer chain and M_W the molecular weight of the polymer. This value marks the transition from the diluted to the semi-diluted state of the polymer. It represents the point at which the chains begin to overlap. For a lower concentration, the chains are scattered throughout the total volume. Whereas for a higher concentration, the different chains overlap and share the same space. Moreover, HPAM is a polyelectrolyte i.e. it is a polymer with a multitude of ionic sites that can interact with each other, therefore its C^* will depend on the salinity of the solution in addition to its molecular weight M_w.
In the case of the FLOPAAM 3130s, the HPAM used during our experiments, C^* has a value of 1100 ppm in a 6 g/L saline solution [Chakibi, 2017]. This means that the study is done in diluted regime as our maximum polymer concentration is 500 ppm. Thus, there will be no interaction between polymer chains. FLOPAAM 3130s has a lower molecular weight (around 3 MDa) than polymers usually used and studied on oil fields to simulate its degradation through the well and other separation unit. The polymer chain is therefore shorter than in other studies, but it represent well the situation in the water treatment process.
It is also interesting to note that the water density is almost not changed by the presence of HPAM or salts. An increase of less than 1% is observed [Richerand and Peymani, 2015].

1.1.3 Oil: FINAVESTAN A80B

A model oil is used in all the experiments. This oil, FINAVESTAN A80B provided by TotalEnergies, does not require any particular safety measure and is often use in pharmaceutical or agri-food industry. This white oil is the result of highly advanced refining processes which gives them a very high level of purity. It is odorless, tasteless and colorless.
This oil FINAVESTAN A80B has a density of $854 kg/m^3$. Other parameters such as viscosity and surface tension have been measured. These results will be present later on in this chapter.

As a first step before conducting any experiment with the pilot, a number of parameters needed for further experiments must be determined.

1.2 Solutions pH & conductivity

Now that the composition of the solutions has been determined, the focus is made on the parameters needed for the flotation experiments. First, as stated before, pH has an impact on HPAM behavior, this is why the first parameters to be gathered are the conductivity and pH of the solution. The very low conductivity of permuted water 13.3 $\mu S.cm^{-1}$ increases slightly along with the concentration of polymer (table 2.2). Nevertheless, for HPAM solution in brine, the conductivity stay around the one of the brine. Indeed, brine has a conductivity of 9.5 $mS.cm^{-1}$ which means that it is modified by less than 1% when adding 500 ppm of polymer. This is basically explained by the fact that brine conductivity is much higher than the one of a polymer solution.

The increase of pH in presence of polymer remains limited, it goes from 6.4 in permuted water up to 6.74 with 500 ppm of HPAM. This increase is quite logical because the polymer has a carboxyl group that tends to make the solution basic. However, when the solution of polymer is made in the brine, the solution seems buffered. Indeed, according to table 2.2, the pH is only slightly modified. This can be explained by the fact that ions in solution are screening carboxyl group, making them inactive.

	pH	Conductivity
Permuted water	6.4	13.3 $\mu S.cm^{-1}$
Brine	6.4	9.5 $mS.cm^{-1}$
HPAM in permuted water	6.74	58.4 $\mu S.cm^{-1}$
HPAM in brine	6.41	9.52 $mS.cm^{-1}$

Table 2.2: pH and conductivity of 500 ppm HPAM solutions

1.3 Surface tension determination

1.3.1 Tensiometer: du Noüy ring

To measure the surface tension between our different phases, a du Noüy ring tensiometer (figure 2.2) is used. This device has a quite simple operating system.

First, it is necessary to check that the support of the tensiometer is perfectly horizontal. Horizontal position adjusting screws allow to change its position and a small bubble helps to evaluate it. Once the position of the support is deemed right, the measurements can begin. A measurement begins by setting the rotating mark on zero and checking that the flail is between the black marks (near the point A

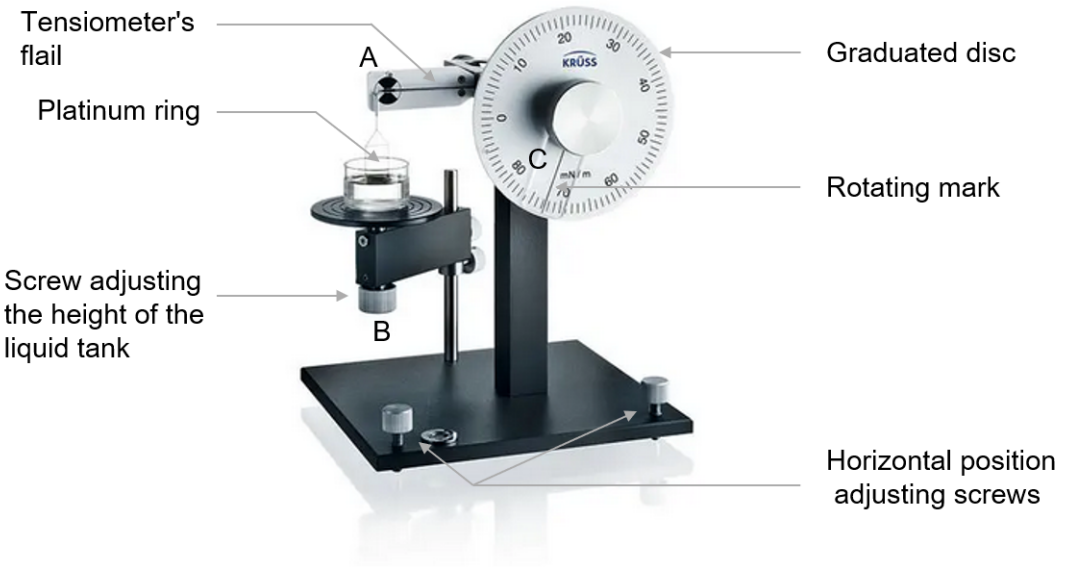

Figure 2.2: Du Noüy ring tensiometer

on figure 2.2). Then a tank is filled with the fluid to study (in the case of surface tension measurement between this fluid and air) and put on the platform. Once this is done, the platinum ring is put on the small hook located at the end of the flail and ensure that it is below the liquid surface. Now, that the tensiometer is set, simply use the screw (marked B on figure 2.2) that adjusts the height of the liquid tank until the tensiometer's flail goes bellow the A marks. When it is happening, set the flail back between the marks by using the rotating mark. These steps are repeated until the ring rips the surface. At this point the rotating mark will be on the surface tension value.
This protocol is slightly modified when the du Noüy ring is used for the surface tension between two liquids. At the beginning of the experiments, the tank is filled with the heavier liquid, the platinum ring is set inside it as for measurement between liquid and air. The lighter liquid is then added slowly to avoid any mixing between the two. The surface tension between these two liquids is reached when the ring rips the interface and goes inside the lighter liquid.

1.3.2 Surface tension values

The protocol presented in the previous part allows us to measure the surface tension at each interface present in our cases. Surface tension values are sum up in table 2.3. These results shows that neither the polymer or salts presence have a noticeable

impact on the surface tension. This observation is confirmed by [Chakibi, 2017] who showed that the presence of HPAM does not affect the surface tension between air and water.

Interface	Surface tension ($mN.m^{-1}$)
Oil/air	30.5
Permuted water/air	68
Brine/air	70
Viscosified brine/air	71
Brine/oil	31
Viscosified brine/oil	28.5

Table 2.3: Surface tension of all our interfaces for 500 ppm HPAM solution

1.4 Viscosity determination

1.4.1 Rheometer

A Rheomars III provided by Thermo-Fisher (figure 2.3) is used to perform the rheological measurements. This device allows to measure the viscosity as a function of the shear rate with a temperature regulation. The temperature is set at the temperature in the laboratory, at $20°C$.
A flat cone geometry (figure 2.4) is used to perform the measurements. This geometry is not necessarily more appropriate than a Couette-type geometry (a moving cylinder rotating around a fixed cylinder), as it is less accurate at low shear stress. However, measurements with a glucose solution (whose behavior and viscosity are tabulated as a function of concentration and temperature) showed a problem with the Couette geometry. Indeed, the results with this modulus are not stable and show a rheofluidizing effect at low shear rates. Since glucose solutions are known to have a Newtonian behavior, we chose the plane cone modulus which gives results closer to the tabulated data.

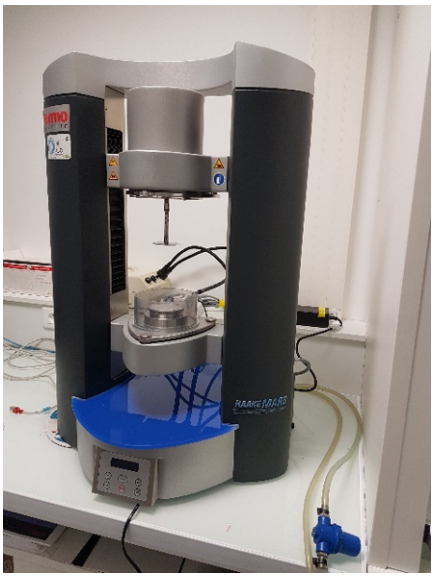

Figure 2.3: Rheomars III

Figure 2.4: Flat cone mobile unit $C60/1°TiL$

1.4.2 Protocol

The protocol used to perform each rheological experiments is the same and following one:

- Normal force initialization
- Mobile lowering and stand by at 2 mm
- Mobile lowering with a slow rotation (10 tr/min) to the measurement position
- Pre-shear at 73 s^{-1} during 300 s
- Pre-shear at 0 s^{-1} during 60 s (mobile at rest)
- Step from 0.1 to 10 s^{-1}
- Step from 10 to 1000 s^{-1}
- Step from 1000 to 10 s^{-1}
- Step from 10 to 0.1 s^{-1}

The initialization of the normal force is necessary to have accurate measurements. The mobile is lowered in two steps to avoid an outpouring of liquid around it. If an outpouring occurs, the surrounding of the mobile must be clean. Indeed, the outpouring increases the surface of the fluid and will distort the measurement if not cleaned. The second step is done with a slow rotation to avoid air to be trapped inside the fluid. Once everything have been set, the measurement can begin. The first pre-shear at 73 s^{-1} is performed to evaluate the viscosity and compare it to the one of 1.6 Cp given by industrial measurements performed all at this shear rate. The fluid is then brought to rest during a minute before starting the rheogram. The rheogram is performed in two main parts. The first is done with an ascending shear rate and then the shear rate are treated in a decreasing manner. This allows to see if the rheology of the fluid depends on its history i.e if it is a thixotropic fluid. A fluid is said thixotropic if the ascending and decreasing part does not overlap.
This ascending and decreasing part are both composed of two mains steps. One in low shear rate with a stabilization time of 120 s. This means that the software of the rheological device wait up to 2 min before returning a viscosity value. The lower shear rate are studied in 30 steps from 0.1 to 10 s^{-1} (when ascending). This long stabilization time coupled with numerous small steps allows to increase the precision at low shear rate. The other main steps is much faster as the stable viscosity value is reached much faster. The stabilization time is indeed set at 30 s and only 20 steps between 10 and 1000 s^{-1} are performed.

1.4.3 Qualification of the validity range with glucose solution

To be sure of the range of validity of our rheological experiments, a first one with a solution of glucose (40% in weight in water) have been led. This experiment was necessary to know on which range the future measurements are usable. Indeed, as stated before, glucose solutions have a well known rheological behavior. A 40% glucose solution in weight as a newtonian behavior and a viscosity of 5.4 Cp [Telis et al., 2007]. Figure 2.5 shows the evolution of the shear of the glucose solution function of the shear rate. This figure shows that the solution behave as a newtonian fluid (in accordance with the literature) at a viscosity of 5.4 Cp with shear rate between 0.5 and 1000 s^{-1}. In this range, there is just a small variation of viscosity around 3 % at most. However, for shear rate lower than 0.5 s^{-1}, the solution has a strange behavior. This can be explained by the fact that the tolerance of the device might be reached. The conical plane module might also not be the most appropriate for such low shear rate.

With these results, it can be concluded that for the further experiments, variation

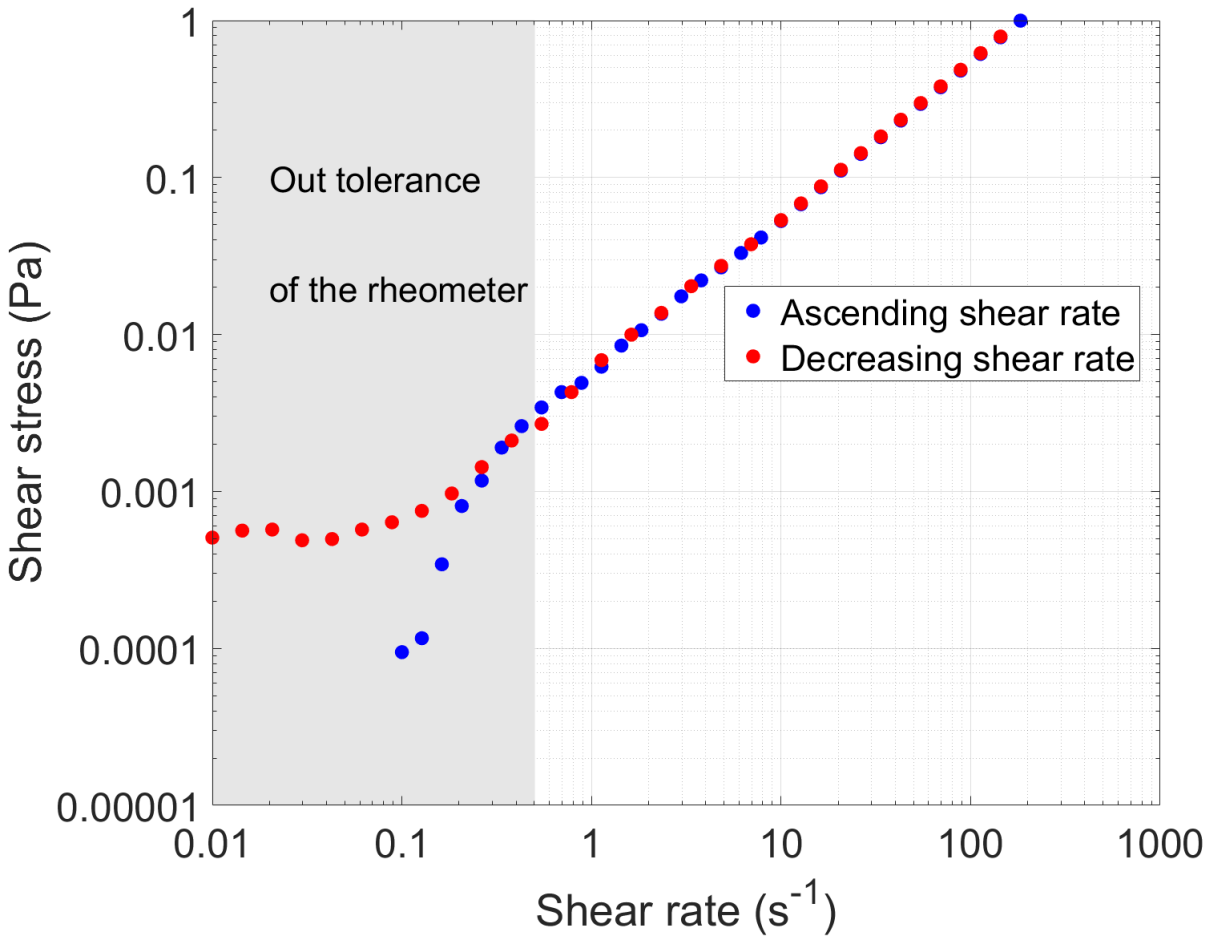

Figure 2.5: Shear stress versus shear rate for a 40% glucose solution in weight

for shear rate lower than 0.5 s^{-1} should not be considered.

1.5 Oil rheology

The oil viscosity has been measured with the protocol presented before and the Rheomars III. It appears that oil behave as a newtonian fluid (see figure 2.6), if abstraction is made of the range between 0.1 and 1 s^{-1} where the viscosity value seems to be a bit random. Anyway, the oil viscosity is 29 Cp for now and then. This value is the value of the plateau between 1 and 1000 s^{-1}.

1.6 HPAM solution rheology

There are many parameters that can modify the rheology of a polymer solution, i.e. its resistance to stress and deformation, which mainly represents the impact of these

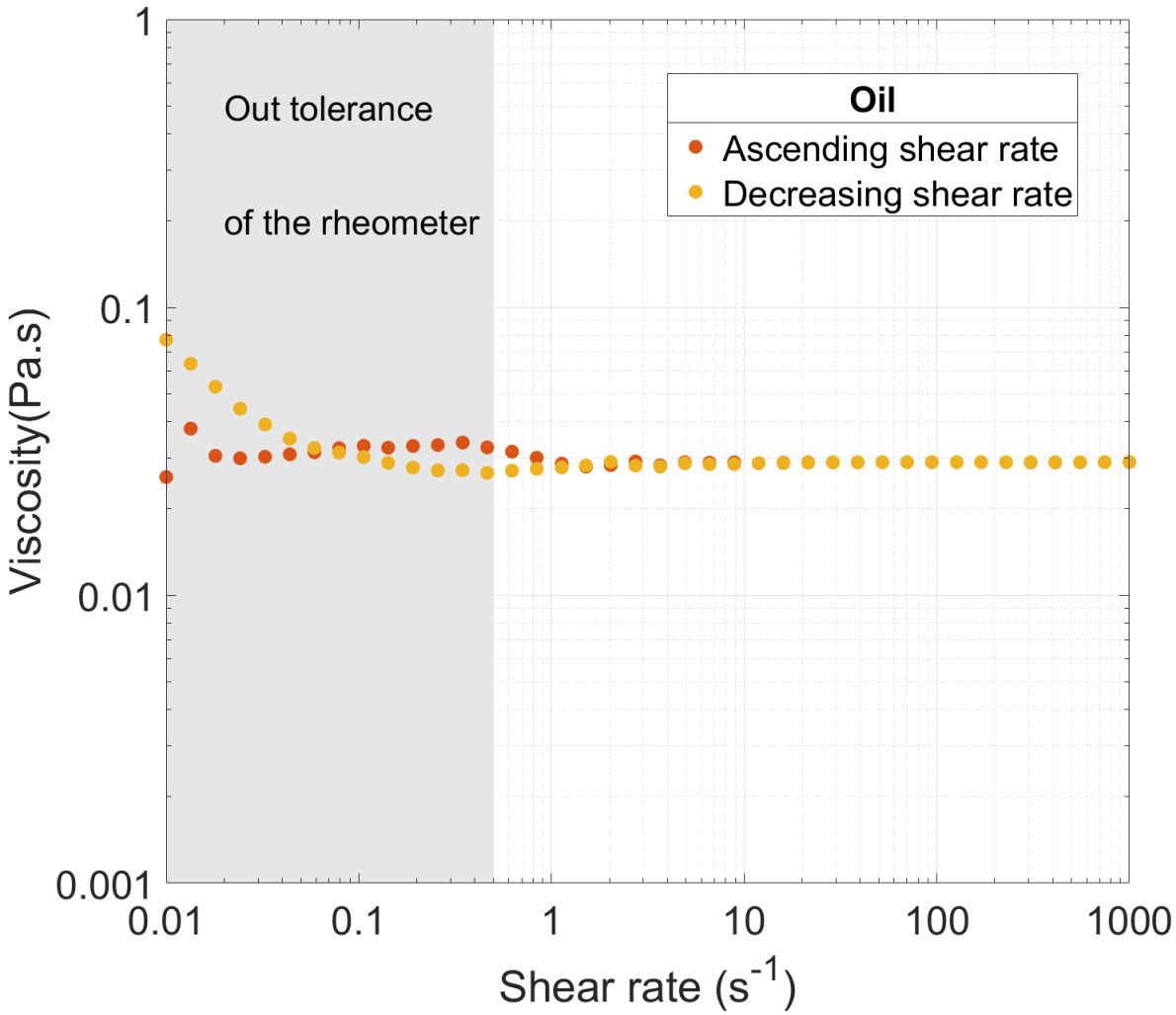

Figure 2.6: Viscosity versus shear rate for the model oil FINAVESTAN A80B

actions on the viscosity of the solution. In the case of HPAM, if an abstraction of the classical effect of the concentration of polymers in solution is made, the following five parameters impact the rheology:

- The degree of hydrolysis of the polymer [Spildo and Sæ, 2015] [Wever et al., 2011];
- The presence of salts in the solution [Wever et al., 2011] [Zaitoun and Potie, 1983] [Choplin and Sabatié, 1986];
- Temperature of the solution [Wever et al., 2011];
- The molecular weight of the polymer [Wever et al., 2011].

The following sub-sections will therefore focus on the most important effects that could be modified in theexperiments carried out as part of the forthcoming study, namely the presence of salts and the degree of hydrolysis of the polymer. In addition, the study of the solution containing the polymer subjected to shear stress will be carried out.

1.6.1 Impact of degree of hydrolysis

The degree of hydrolysis is the amount of amide function hydrolyzed to acrylate function.
Generally speaking, the viscosity of the solution increases as the degree of hydrolysis increases. This is easily explained using the form that the polymer will take. Indeed, the greater the number of acrylate functions, the greater the electrostatic repulsion between the different parts of the polymer, which will force the polymer to be in an increasingly extended configuration. This will therefore lead to an increase in the space occupied by the polymer and therefore an increase in the viscosity of the solution [Ward and Martin, 1981]. However, from a hydrolysis of more than 70 % the viscosity falls back to values similar to those of a hydrolysation of 35 %, so the evolution of the viscosity as a function of the degree of hydrolysis is bell-shaped. [Spildo and Sæ, 2015]. It should be noted that beyond a certain degree of hydrolysis the polymer is no longer soluble in water [Lewandowska, 2007].

1.6.2 Impact of shear rate

HPAM is a rheopectic polymer i.e. its viscosity increases with time at a constant shear rate [Wever et al., 2011] [Choplin and Sabatié, 1986]. In addition, it has a rheofluidifying and rheothickening effect depending on the situation. That is to say that the viscosity of this polymer decreases (rheofluidifying) or increases (rheothickening) with the shear rate. Indeed, below a critical shear rate threshold (the threshold at which the polymer changes from a rheofluidifying effect to a rheothickening effect) which varies according to the different parameters stated above [Wever et al., 2011], the polymer chains align and disentangle themselves, which facilitates the passage of the fluid between the chains (little interaction between the different chains) and thus decreases the viscosity. Beyond this same threshold or in porous media (such as in an oil reservoir), the elongation and interpenetration of the chains is forced by shear [Wever et al., 2011]. This leads to an increase in the space occupied by the polymer and the interactions between the chains and consequently the viscosity. These evolutions can be obtained analytically using the Carreau relation for shear

rates below the critical shear rate [Ait Kadi et al., 1987] :

$$(\mu_f - \mu_s) = \frac{(\mu_0 - \mu_s)}{(1 + (\lambda\dot{\gamma})^2)^{(1-n)/2}} \tag{2.1}$$

And the power law for shear values above the critical shear rate [Ait Kadi et al., 1987] :

$$(\mu_f - \mu_s) = m\,|\dot{\gamma}|^{n-1} \tag{2.2}$$

With μ_s the solvant viscosity (in our case water), μ_0 the viscosity at zero shear, $\dot{\gamma}$ the shear rate, and λ a constant of Carreau model.

1.6.3 Impact of salts

As previously mentioned, HPAM is a polyelectrolyte and contains a large number of electrostatic charges and ionic sites. Thus, an addition of electrolytes such as salts (monovalent, bivalent or more) decreases the apparent size of the macromolecules [Ait Kadi et al., 1987] and consequently changes the volume occupied by the latter. This therefore leads to changes in the rheology of the solution. Indeed, in the presence of salts, the polymer will curl slightly and will take on the appearance of an extended ball [Choplin and Sabatié, 1986]. This results in a decrease in the viscosity of the solution due to the fact that the polymer occupies less space within the solution [Shepitka et al., 1983].
In addition, the addition of salts also causes an increase in the rheothickening effect of the polymer when the critical shear threshold is exceeded. Symmetrically, the addition of salts causes a decrease in the rheofluidifying effect before the critical shear rate [Ait Kadi et al., 1987]. The presence of salts also makes it possible to manage the increase in viscosity with the degree of hydrolysis thanks to a shielding of the acrylate groups by the salts. This effect takes place until all the acrylate groups are shielded. Once this stage is reached, the viscosity starts to increase again. This phenomenon exists only with monovalent salts and is due to the screening of the chemical groups that limits the electrostatic interactions within the polymer and allows the polymer to adopt a more compact conformation.
When using divalent salts or more, they will tend to bind different ionic sites of the polymer, or even sites of different polymer chains. Thus, if there are too many divalent salts (or more), this will cause the polymer to precipitate when its degree of hydrolysis exceeds 33% [Zaitoun and Potie, 1983]. In our case the quantities of divalent salts being very low, this bridging phenomenon should not occur or only slightly. Similarly, dissolution problems due to the presence of these salts will not occur because the polymer used has a degree of hydrolysis between 20 and 30%.

1.7 HPAM rheology results

In our particular case of viscous water used for flotation experiments in condition as close as the one found on the field, additional rheological measurements have been done. These experiments have been led on the Rheomars III to evaluate if our HPAM solution behave as expected in the literature.
These rheological experiments have been made with two kinds of polymer solution for a concentration in HPAM of 500 ppm. The first solution is a polymer solution in deionized water and the other is in brine. Figure 2.7 shows the evolution of both solution viscosity function of the shear stress. By looking at the curves in both deionized water and brine, we can easily say that polymer solution (with concentration up to 500 ppm at least) does not show a thixotropic effect in the range of validity of the rheometer (given by the study of glucose solution). Indeed, the ascending and decreasing part are overlaid at least for a shear rate between 1 and 1000 s^{-1}. The viscosity of these solutions thus do not depend on their history.
In deionized water, figure 2.7 shows a good agreement between our experimental values and the one found by Lopes et al. [Lopes and Silveira, 2014]. In addition, both solutions present a clear rheofluidifying effect. Indeed, the viscosity of both solution decreases with the increase of shear rate. It might be interesting to note that this effect is attenuated by salts presence. This rheofluidifing effect is also found in the experiments led by Carreau et al. [Ait Kadi et al., 1987] or Lopes et al. [Lopes and Silveira, 2014].
As stated previously, his study shows that the addition of salts causes a decrease in the rheofluidifying effect. This reduction of the rheofluidifying effect in presence of salt is also shown in our results (figure 2.7). Indeed, by adding salts a change of more than 50% in slope is observed.

Furthermore, literature state that in presence of salt, the viscosity of a HPAM solution tends to decrease (figure 2.7). In our case in brine, this decrease is also found. Indeed, figure 2.7 shows that in presence of an equivalent of a 6 g/L NaCl solution, the viscosity of an HPAM solution decreases by a factor 6.
This effect of salts presence is also found on figure 2.8 which shows the variation of viscosity of an HPAM solution at a constant shear rate of 73 s^{-1} in brine and deionized water.
However, the rheopectic effect of polymer solutions seen by [Wever et al., 2011] & [Choplin and Sabatié, 1986], is not seen at our concentration around 500 ppm. Indeed, figure 2.8 shows that for a shear rate of 73 s^{-1} the viscosity stays constant with the time in presence of salts or not.

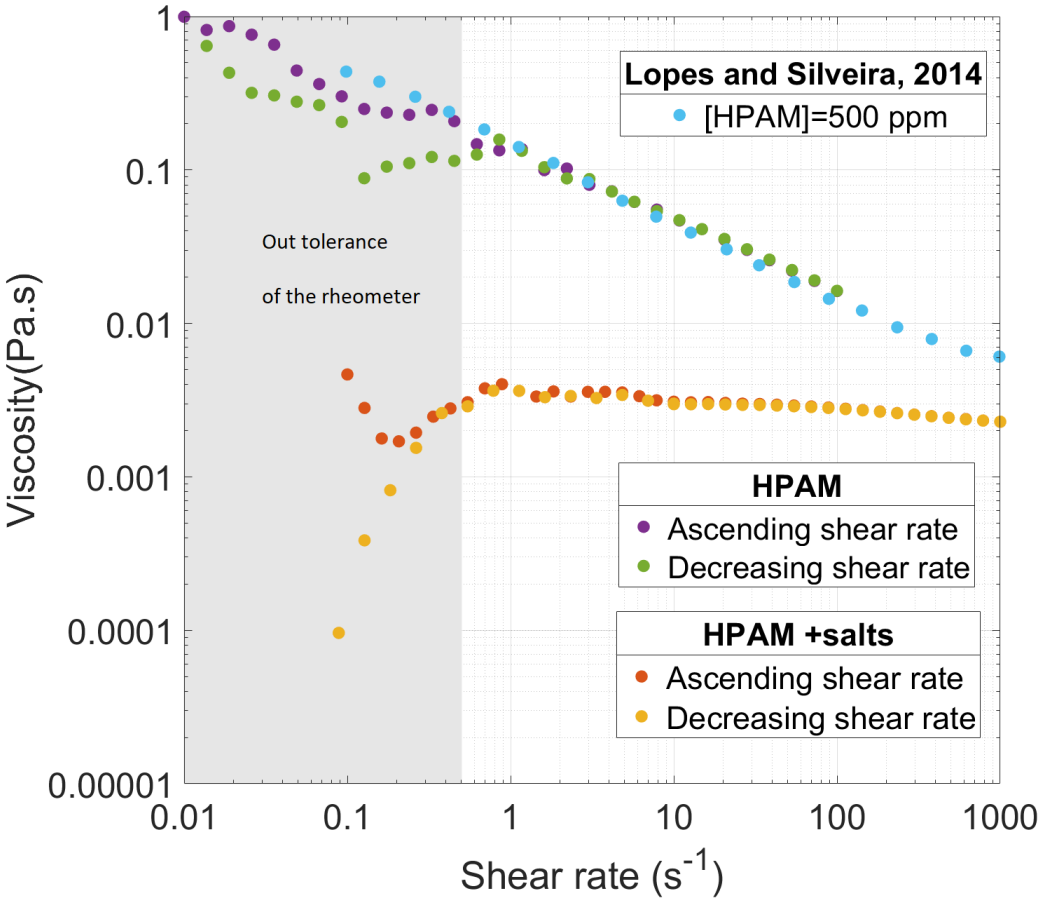

Figure 2.7: Viscosity versus shear rate for 500 ppm HPAM solutions

1.8 Conclusion on HPAM rheology

It has been seen that the rheology of HPAM polymer solution is quite complex. As a matter of fact, function of the shear rate, it presents mainly a rheofluidifying effect when its concentration is around 500 ppm, either in brine or in deionized water. We inted now to evaluate the shear rate experienced by the solution in several situations encountered in flotation devices.
The shear rate variation in a flotation unit can be due to the flow in the unit but also to the bubbles rising.

To evaluate the shear rate variation due to a rising bubble, a study of shear rate γ generated by a bubble has been led function of its size (table 2.4). The shear rate is approximated by a simple formula [Frank et al., 2012]:

$$\gamma = \frac{V_b}{d_b} \tag{2.3}$$

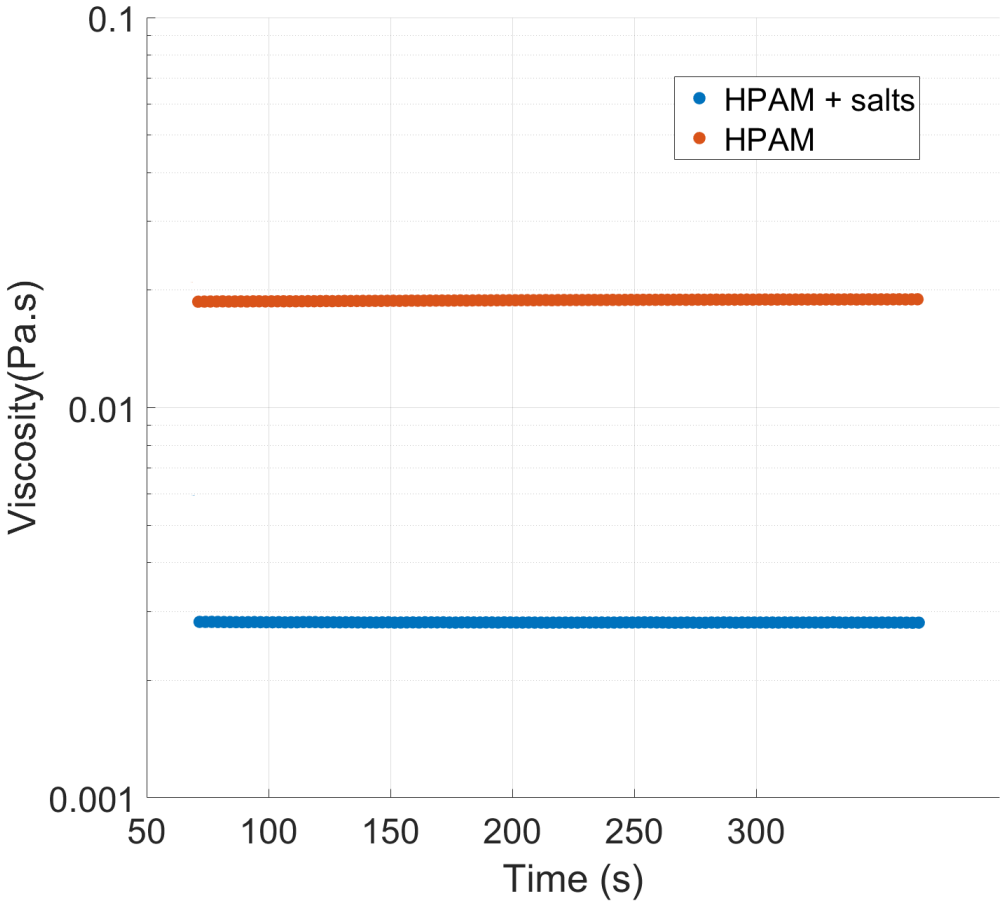

Figure 2.8: Evolution of viscosity function of time at a constant shear of 73 s^{-1} for 500 ppm HPAM solutions in brine and permuted water

Table 2.4 shows that the shear rate generated in the path of a bubble varies between

$d_b(\mu m)$	$\gamma(s^{-1})$
10	5.4
40	21
100	54
1000	543

Table 2.4: Shear rate generated by a bubble function of its diameter

1 and 500 s^{-1}, which matches with the mean shear rate of 100 s^{-1} find in the industry [Ralston et al., 2007]. This leads to a variation of viscosity of around 15% from the mean value given at 73 s^{-1}.

The shear rate variation in the flotation cell when working at its maximum capacity (which is going to be define later in this chapter, paragraph 1.2 Flotation

cell), is evaluated thanks to CFD simulation. The fluid used in these simulations is newtonian with a viscosity of 2.8 Cp (the value found at 73 s^{-1} for a 500 ppm HPAM solution in brine in our experiments).
Figure 2.9 shows that the shear stress vary only between 1.5 et 4 mPa.
When these values are reported on figure 2.10, it allows to evaluate the variation

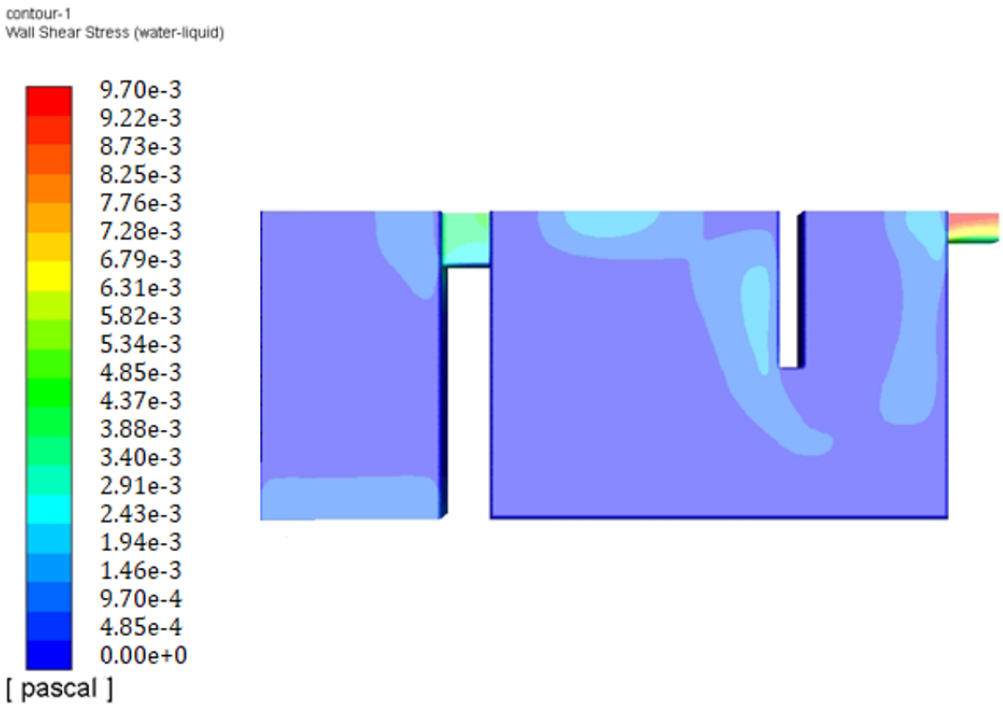

Figure 2.9: Shear rate inside the flotation cell

of viscosity on this range. Indeed, this figure shows the evolution of shear stress function of the shear rate which allows by dividing the first by the second or referring to figure 2.7.

By this mean, we can conclude that the viscosity has a variation of at most 15% compared to the average viscosity of 2.8 Cp (which match with the one at 73 s^{-1}).

This variation of viscosity of less than 15% matches with the one found numerically for the rising bubble. This is why for now and then, the viscosity of the brine solution with polymer is considered as constant in the later calculation. This solution is supposed to behave as a newtonian fluid.

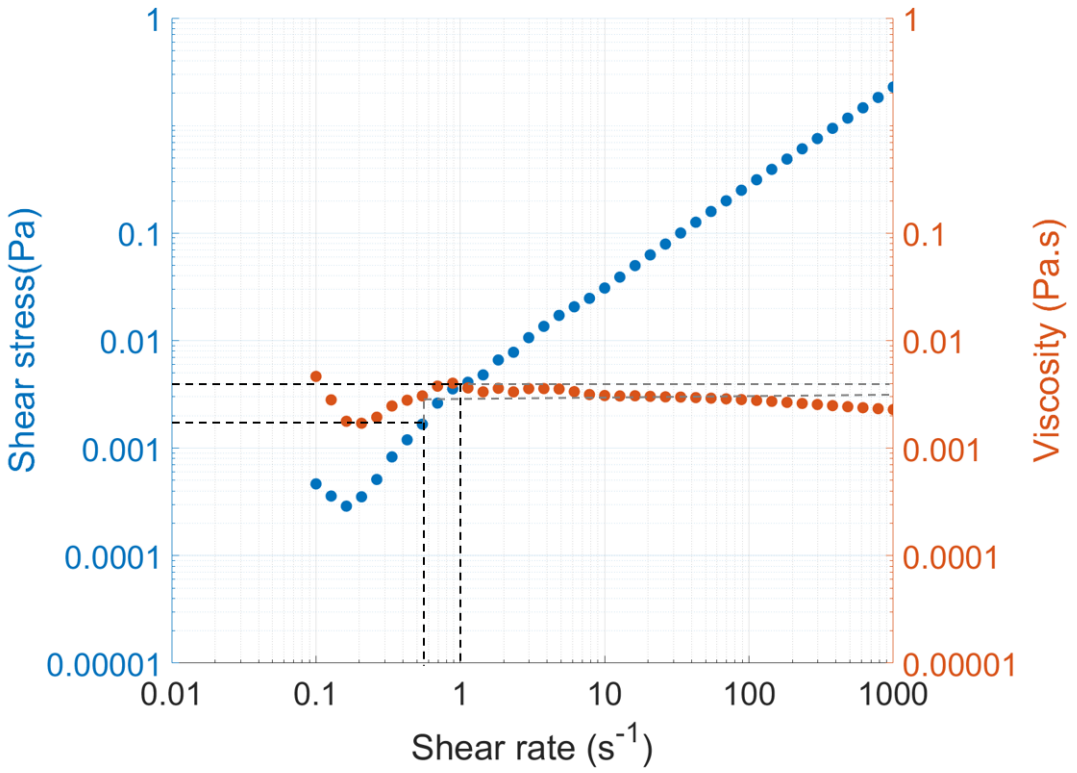

Figure 2.10: Shear stress & viscosity function of shear rate for a solution of HPAM (500 ppm) in brine

2 Pilot

The pilot designed during the first year of the PhD has the purpose to study the flotation effiency with as many variable parameters as possible as the following flowsheet shows.

2.1 General flowsheet (figure 2.11)

At first, salted or viscosified water is prepared in the C1 tank with a mixer.
There is then two possibilities depending on which mode the pilot is working. If it is working in IAF mode, the fluid is carried in the tank C2 where the emulsion is made by emulsifying during 30 min. The emulsion is then injected in a device (Drop 1) allowing to measure the droplet size distribution at the inlet of the flotation cell. At the same time, air is injected with the brine inside the flotation cell through some capillary like device to create milimetric bubbles. These bubbles then capture the droplets present in the emulsion inside the zone marked as 1 on figure 2.11 and ascend to the top of the unit. When bubbles carrying droplet reach the surface, the

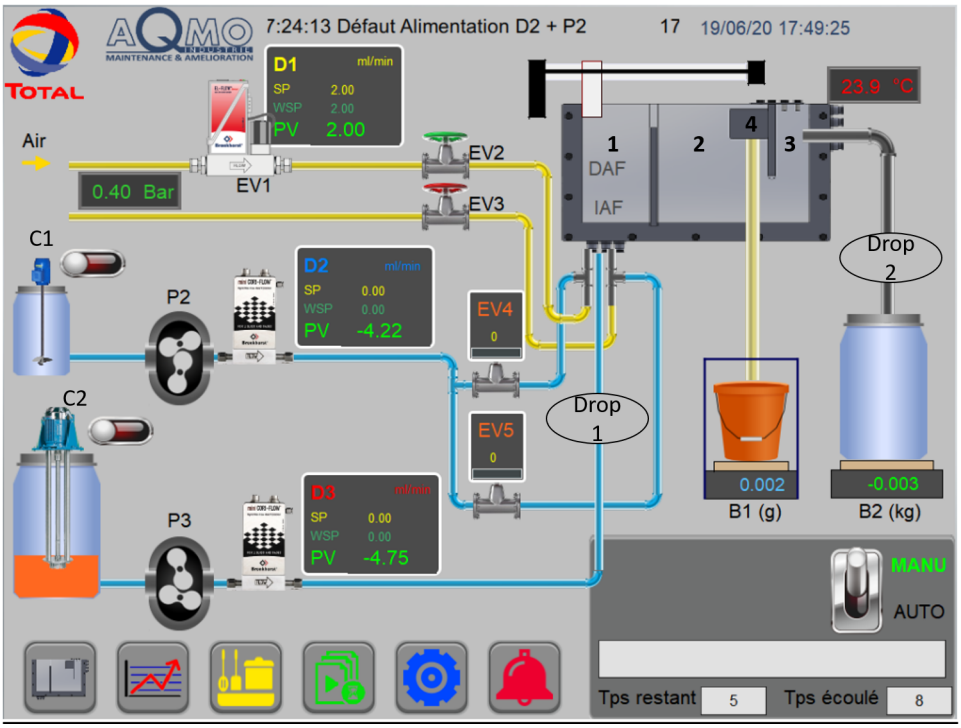

Figure 2.11: Flowsheet of the pilot

oil and air form a kind of foam at the surface which is skimmed into the recuperation tank (zone 4 on figure 2.11). Once inside this tank, the foam flows on the balance B1 by gravity.
The cleaned water circulates from the zone 2 to 3 before overflowing inside a device (Drop 2) which measures the droplets size distribution at the outlet of the cell. At the outlet of this device the clean water flows into a tank on scale B2.

If the pilot is working in DAF mode, a pressurized tank is filled with the brine and pressurized at 5 bar with air to be saturated. To create bubbles, this water is depressurized abruptly at the inlet of the flotation cell creating the so called white water.

2.2 Flotation cell

The flotation cell, has been designed to look like an industrial one, but at a very small scale in order to work in a continuous mode without generating too much fluid.
It is composed of three zones (figure 2.12). The first one is named the capture zone (where capture occurs), has a length of 10 cm. In this zone, bubbles enters in collision with the oil droplets that might attach to the bubble surface. Then, there

is the re-driving and separation zone where the bubble paths depends on the flow rate of the emulsion (and white water if it is operated in DAF mode). This zone measures 16.3 cm. In this zone, bubbles, function of their sizes and the global flow rate, will have different flow paths. Indeed, the bigger the bubble is the faster it will ascend and reach top of the unit. However the smaller the bubble is, the slower it will raise toward the top of the unit and if it reaches a critical size, the bubble will be carried away toward the clean water outlet. This critical size is defined during the conception of this kind of flotation cell. The last zone is where the clean water is recovered and has a length of 8 cm. This cell 20 cm tall has a small volume

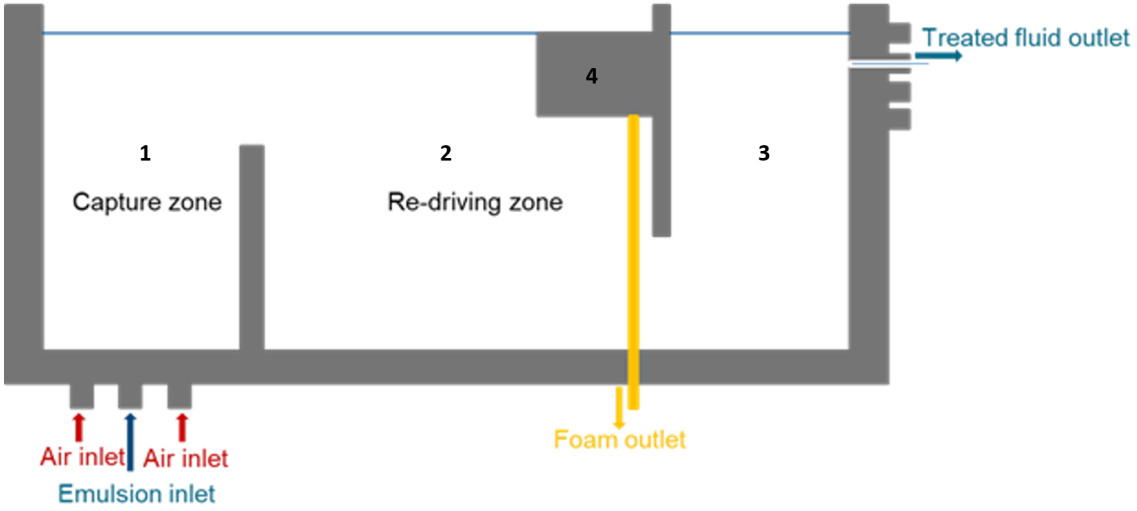

Figure 2.12: Scheme of the flotation cell

around 1.4 L depending on the level of liquid. Indeed, the volume of liquid inside the cell will depend on two parameters, the first and obvious one is the level of water depending on which hole the water is flowing from at the liquid outlet (and the level of the foam gathering compartment numbered 4 on figure 2.12). The second one (less obvious in this scheme) is the thickness of the flotation unit which can be increased by adding plastic pieces before the window. The thickness can go from 2 to 4 cm at is maximum volume.
In order to be able to modulate the height of the capture zone, the height of the separation wall between the capture and re-carrying zones can be modified. As a matter of fact, there are three different separations walls, one of 16.5 cm, another of 13.7 cm and finally the most used of 15 cm.

The flow circulation inside the cell is quite simple. White water and emulsion are injected at the bottom of the capture zone, then bubble ascends toward the top of the unit and get carried in the re-carrying zone. For bubbles bigger than 40 μm

they can get carried by the flow but they ultimately reach the top of the unit which allows the oil they carry to be skimmed in the small oil collector (zone 4 on figure 2.12). Bubbles smaller than 40 μm are carried away toward the recovery zone where the clean water is then recovered by one of the hole at the top of the unit. The size of 40 μm has been defined beforehand during the design of the flotation unit.

2.3 Bubbles generation

As it was planned initially to perform experiments with various kind of bubbles in order to study different flotation mode (DAF with bubble smaller than 200 μm, IAF with milimetric bubble or a mixed mode with both size of bubble), there are two ways to generate bubbles.

2.3.1 Generation in DAF mode

In order to generate bubbles thinner than 200 μm, it has been chosen to create bubbles by using pressurized water. The water used during the experiment, pressurized at 5 bars in a 40 L pressurization tank is depressurized abruptly at the entrance of the flotation cell (figure 2.13). Therefore, the size of the bubbles generated depends on the liquid flow rate and the opening of the needle valve.

2.3.2 Generation in IAF mode

In order to generate milimetric bubbles, the first idea was to use capillaries with an internal diameter of 22 μm. This diameter was chosen in accordance to Tate law to allow the prodution of calibrated bubble of 1 mm.
A device given by YLEC Consultants named CIMYLEC (figure 2.14) was preferred to this use of capillaries. This device has been chosen due to the fact that it was initially supposed to be able to produce bubbles both in IAF and DAF range. However, after some preliminary experiments, it has been shown that the bubble produced were more around the millimeter. This is why this method of generation has been kept only to work in IAF mode.
The exact way this device works has not been explained by YLEC Consultant, but basically mixing a large amount of water inside their devices (at a relatively high flowrate, around 8 L/h) as well as an air flow allow to generate bubbles probably because of a sort of capillary tube.

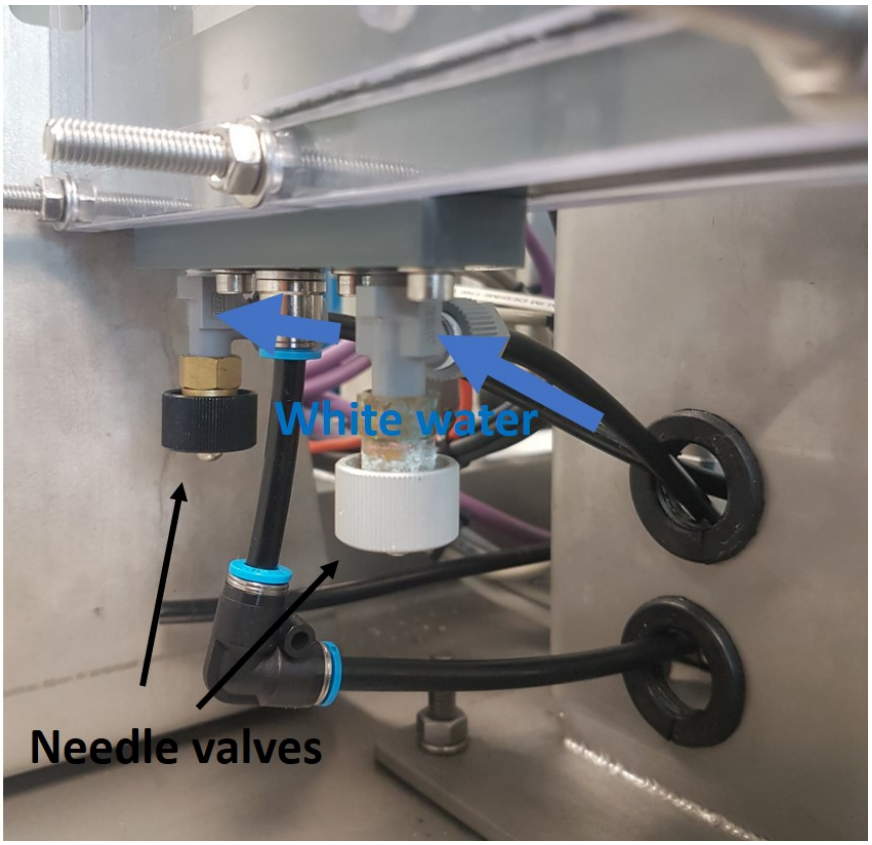

Figure 2.13: Picture of the needle valves and their positions at the entrance of the flotation cell

2.4 Emulsion preparation

The emulsion is created in two stages. The first one is to prepare the fluid to treat. Indeed, if the experiment is not done in permuted water, a solution of water or brine and polymer has to be done. This solution is done beforehand in batch with a propeller mixer ((SEW-USOCOME)) and conveyed to the emulsion tank thanks to a pump.
Once this has been done, small amount of oil (FINAVESTAN A80B), up to 300 ppm is added to the solution. The emulsion is then made by emulsifying the solution for 30 min with a Silverson emulsifyier (Silverson BX, figure 2.15).

2.4.1 Control of flow rates

It is necessary to have access to the different flow rates present in the pilot in order to be able to do mass balance and to evaluate how the installation is working.
As it is shown on figure 2.11, there is two methods used to have access to the flow rate on the pilot. The first way uses flow meters (Bronkhorst mini CORI-FLOW

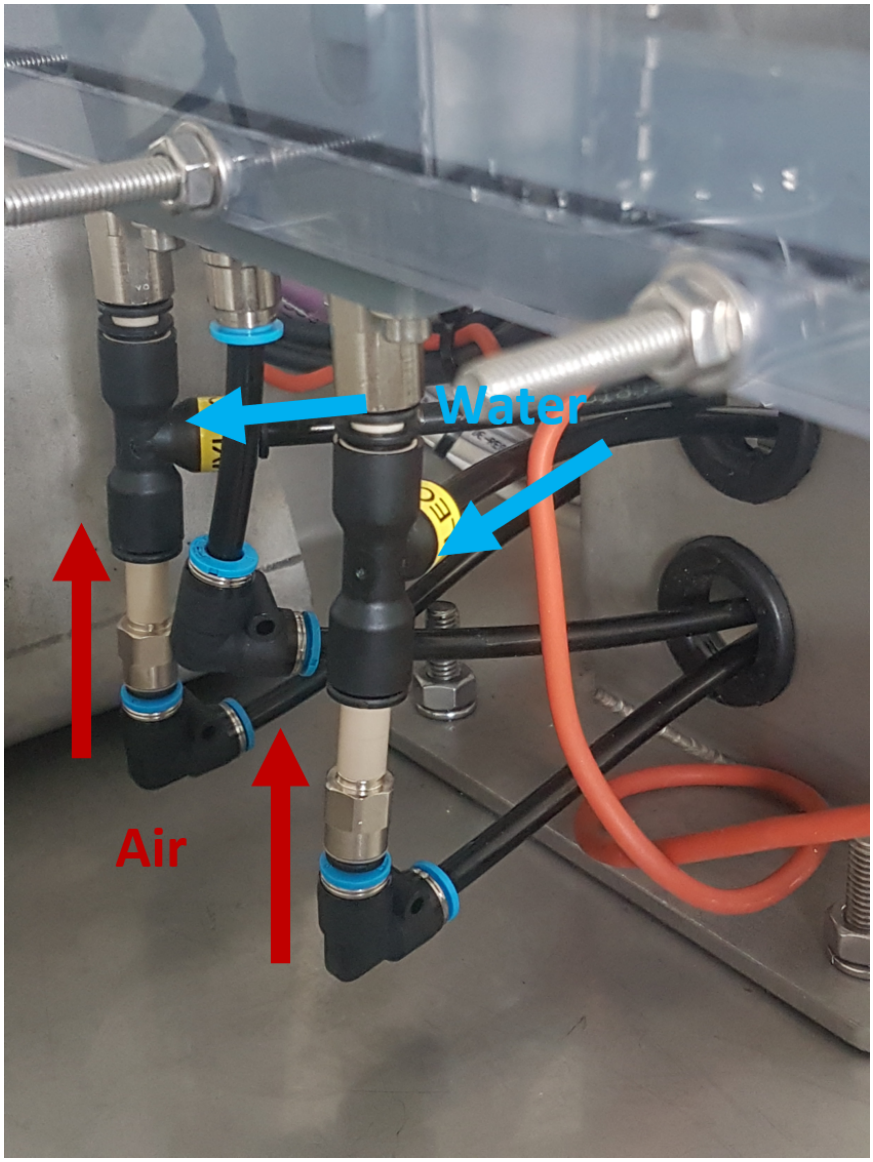

Figure 2.14: CIMYLEC devices on the flotation cell

working up to 250 mL/min). Those flow meters are set on the different inlets of the cell and allow to monitor and regulate the flow rates of white water and emulsion. Flows are ensured thanks to two gear pumps (TUTHILL DGS) with a regulation made by the flow meters through a retro-control working with a PROFIBUS.
The other method is through the use of scales. Those scales are set on the outlet of the flotation cell. Scales have been chosen due to the fact that traditional flow meters only works when the inlet pipe is completely filled, which is not the case for our two outlets. The flow on the foam outlet is measured with a Metler-Toledo scale (PBK989-XS0.6 with a maximum load of 0.61 kg) which is very precise with a quick stabilization time (with an error around 0.001 g and a settling time of 10

Figure 2.15: Silverson emulsifyier with a dispersion head: (a) in the tank, (b) in full

ms). This need of precision is due to the fact that foam is continuously flowing and supposedly extremely light. The second scale set at the clean water outlet is also a Metler-Toledo (PBK989-CC300) with a quick settling time but far less precise (with an error around 0.5 g and a settling time of 10 ms) as the quantity of water to gather here is much greater. The tank set on the scale is indeed made to recover up to 200 L of water.

In addition, a flow meter is set on the air inlet used to produce milimetric bubbles when the pilot is used in IAF mode. This flow meter (EL-FLOW Select) is also provided by Bronkhorst but works only for gas.

2.5 Liquid level control

The control of the liquid level inside the flotation is quite complex to monitor. It is done exclusively by acting on the recuperation tray height and the valve present after the clean water outlet. In order to know how to set these parameters, the clean water outlet flow rate is monitored and set at 80 % of the global fluid inlet.

3 Metrology developments

3.1 Measurement of droplet size distribution

Droplet size distribution is a key parameter for flotation efficiency, this is why a non intrusive home made optical device (which will be named Dropsizer, figure 2.16) has been designed to measured it at the inlet and the outlet of the flotation cell. Droplets size distribution is measured thanks to home made optical devices. These devices allow to measure size online by umbroscopy. As its name suggests, umbroscopy is a method based on the study of the shadow of an object. The principle is to use a light source at infinity to illuminate the object. The refraction of this light, by the variation of optical index when crossing object interface, allows the camera to get the object in dark (shadowgraphy). In the case of the Dropizer, this method is coupled with an optical microscope like device. This optical device is focused on a thin portion of fluid with a 1 mm focal plane in the middle of the cell. Dropsizer

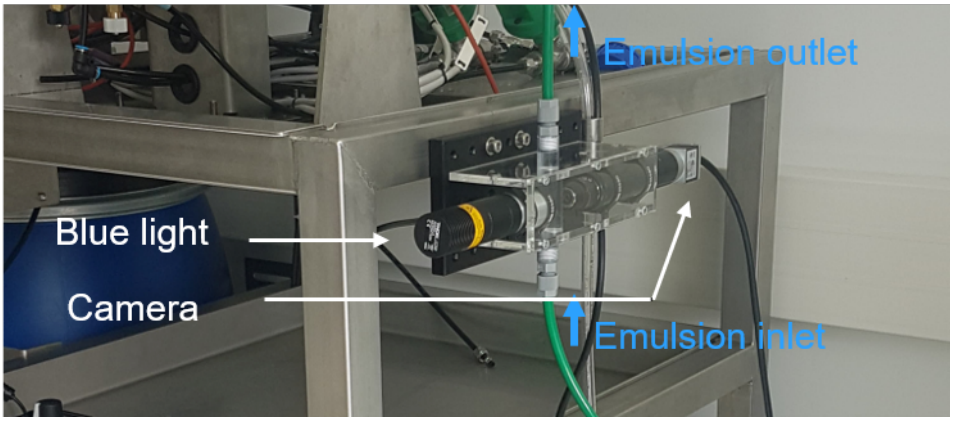

Figure 2.16: Dropsizer device

camera is coupled to an home made software allowing to detect and size the droplets online (without frame processing after experiments). The software get the raw image (figure 2.17a) and then detects objects by the variation of the intensity gradient. To be considered as an object, the variation of the gradient must be higher than a certain threshold. In this way, objects that are not in focus are not considered. This threshold can be modified in order to be able to detect an object even when the intensity of the image background is low. Once detected, each object is isolated and its interface is binarized (figure 2.17b) and filled (figure 2.17c) . From this new picture the sphericity of the object is checked by counting the number of pixels on the minor and major axis. If these two axes are similar, the object is considered

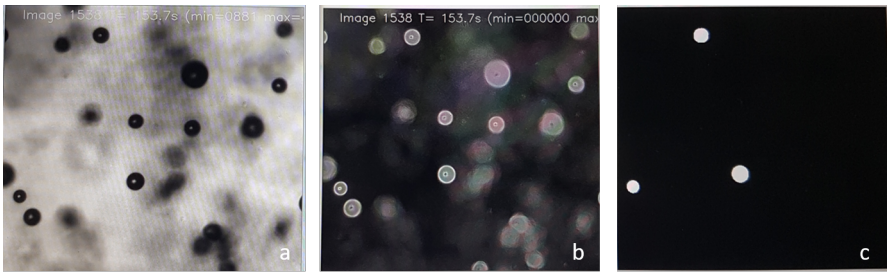

Figure 2.17: Example of the treatment applied to each frame to detect bubbles or droplets

spherical and kept for further processing. The last step is to return the object diameter. If this one is bigger than 4 μm, the object is kept and set in the final size distribution.
The two steps of verification and calculation for a detected object to be kept are necessary to avoid computational artifact. Indeed, all studied droplets are small enough to be always spherical. Furthermore, even if object smaller than 4 μm can be detected, count them as part of the droplet distribution is a mistake. On the frame, a pixel is equivalent to 1.2 μm meaning that for a 2 (or 3 microns) droplet, the spherical droplet is assimilated to a cube of 2 by 2 pixels.

A comparison between the distribution obtain with a dropsizer and a Malvern granulometer is made later on (in paragraph 4. Characterisation of the emulsion produced).

3.2 Measurement of bubble size distribution

Initially, Dropsizers were supposed to be used for bubble size distribution measurement. However, the swarm of bubble produced in DAF mode is too crowded. The quantity of light gathered by the camera become too low. Thus, the entity determination by the intensity gradient become harder and the software is no longer able to identify a bubble.
This is why a Spraytec (a device from Malvern Instrumentation, figure 2.18) is used. This device is usually used to size spray elements thanks to a laser.

The functioning of the Spraytec is relatively simple. On one side of the device, a laser ray with a wavelength of 632.8 nm is transformed to produce an infinite light (with parallel light ray) thanks to a lens. This ray goes trough the bubble spray (place in the center of the device). Bubbles scatter the light which is then refocused by another lens onto some light sensors present on the other side (figure 2.19).

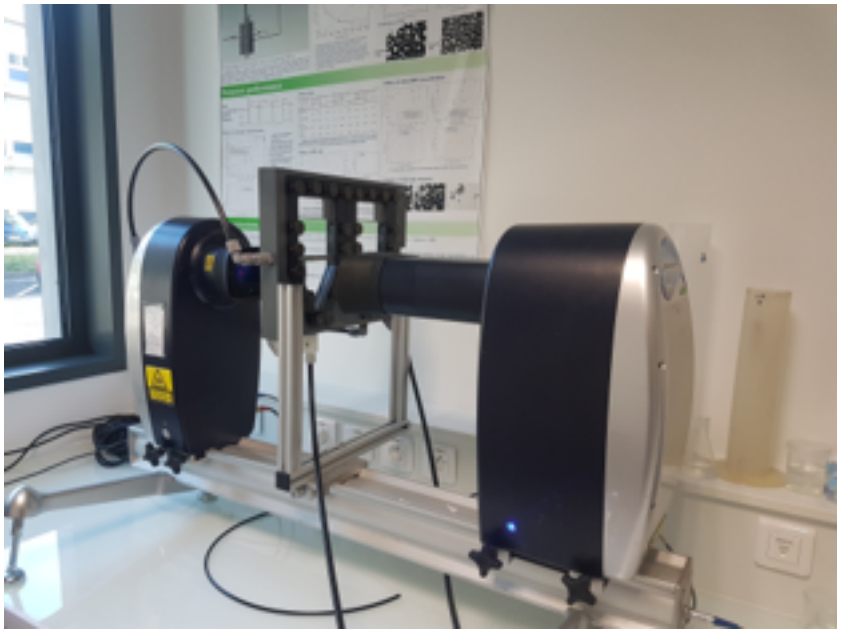

Figure 2.18: Malvern Spraytec device

Function of the temporal light repartition on the sensors, the bubble size distribution is given function of time. This passage from light repartition to bubble size distribution is possible thanks to the Mie theory. This theory gives the scattering pattern of light ray function of the size of obstacles.

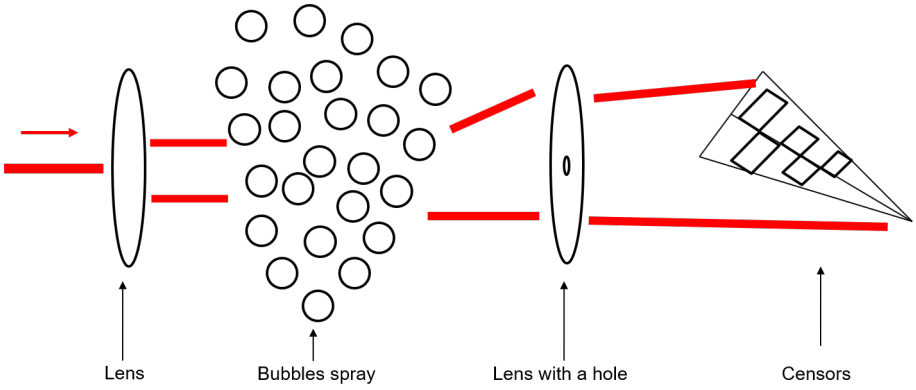

Figure 2.19: Functioning scheme of the Spraytec

3.3 Oil concentration measurement

Many methods have been considered to measure the oil concentration.

3.3.1 Light intensity on dropsizer images

The first was to use the dynamics of the images from dropsizers. Indeed, the concentration and the population of drops will influence the intensity recovered by the cameras. Thus, with a study of the gray level, it should be possible to estimate the oil concentration in water. In order to evaluate if this method works in our case, a gray level scaling have been performed. Emulsions have been performed for different concentration from 50 to 300 ppm (the maximum oil concentration used during experiments). Once made, those emulsions goes through both dropsizers and the mean intensity of each frame is recorded. The intensity of the solution is then averaged on the 30 min of experiments. This gives the following scaling:

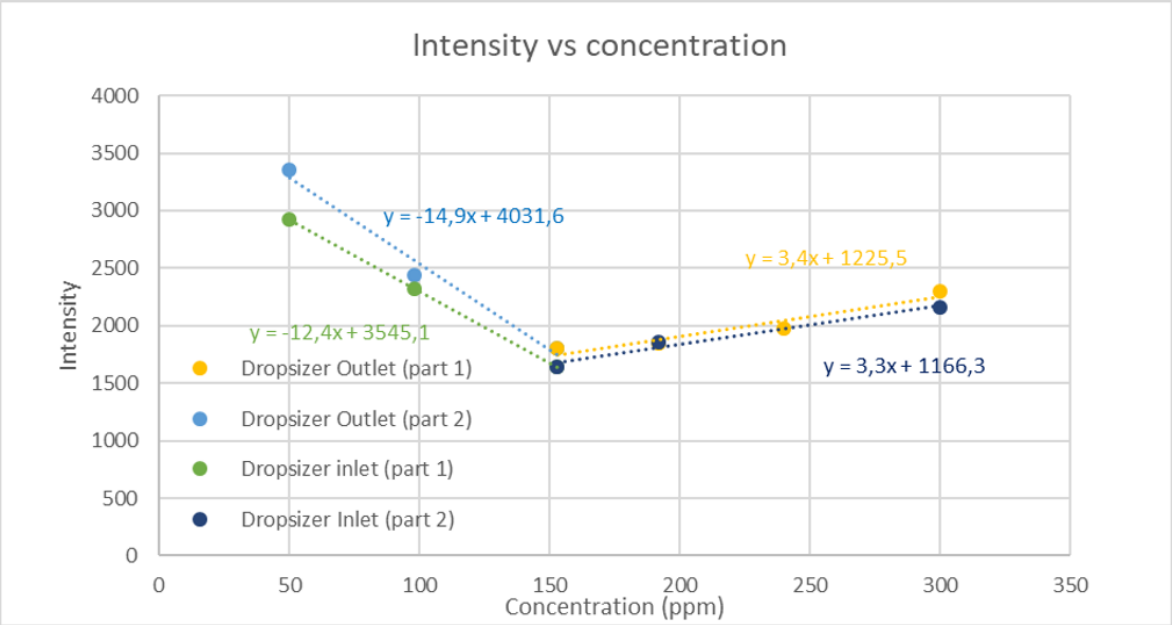

Figure 2.20: Gray scaling of both Dropsizer for oil emulsion

Figure 2.20 shows that when the concentration increases, the intensity drops until a concentration of 150 ppm. From this concentration, the intensity increases slightly with the concentration. However, after several experiments the window allowing the measurement seems to fool despite a clean water cleaning after each use. Indeed, the intensity drops after a few use. Figure 2.21 shows a second scaling and the drop of intensity. For a given concentration, more than a thousand intensity units are lost between the first and second calibration. A relative comparison between the intensity of the input and output dropsizer could be used. However, the variation of one with respect to the other is not always constant, which could pose a problem for small variations in concentration.

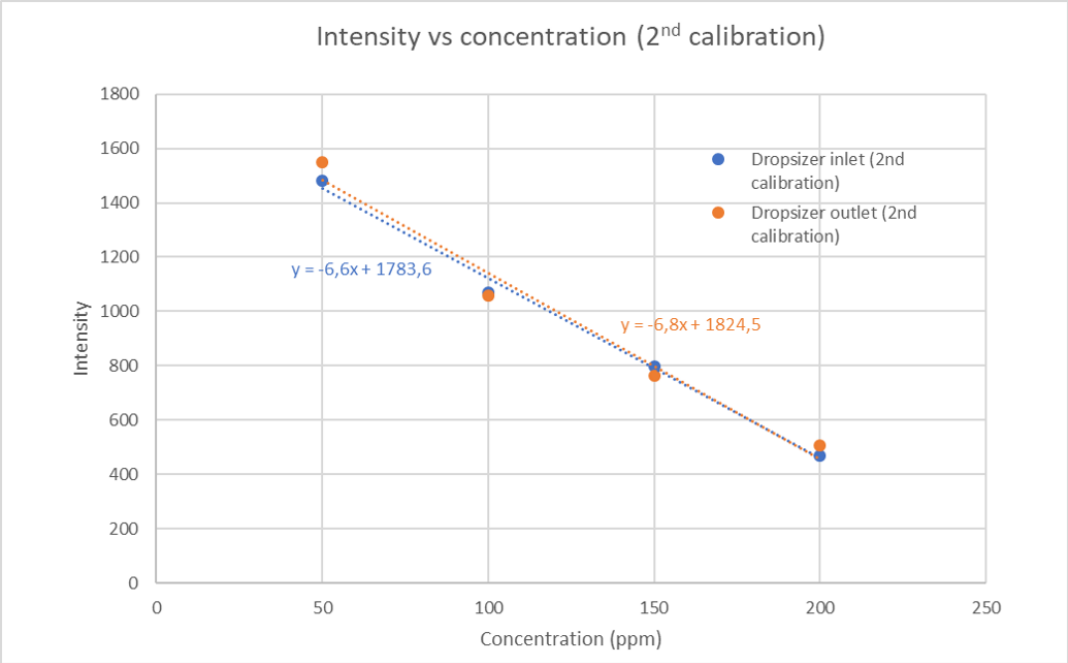

Figure 2.21: Gray scaling of both Dropsizer for oil emulsion after a few experiments

Other methods are more focused on the chemical properties of the emulsion. The Far Infrared spectroscopy (spectroscopy FTIR) and UV fluorimetry to determine the oil concentration of samples in labs have been explored as well as DCO measurements.

3.3.2 Fluorimetry

Fluorometry is a simple method based on the ability of molecules to be excited by a light source and to re-emit that light at different wave length. To study a sample, it is necessary to find the wavelength at which the excitation is maximal, then observe to recover the re-emission at the right wavelength. Based on the amount of light recovered, it is possible to estimate the concentration of the target species present in the sample.
In the case of our synthetic oil, experiments show that the most absorbed wavelength is at 305 nm and the emission peak is at 440 nm. However, when the oil is mixed with water to form an emulsion, a problem arises. The pure water and the emulsion (at the maximum concentration of 300 ppm) emit at the same wavelength and intensity. This makes it impossible to determine the oil concentration by this method, even by calibration.

3.3.3 FTIR Spectroscopy

The FTIR spectroscopy is based on the evolution (in the IR range of wave length) of the absorption of the sample as a function of the concentration. In the case of an oil-in-water emulsion, it is first necessary to extract the organic phase with Tetrachloroethylene (TCE). To perform this extraction, 5 mL of the emulsion is taken to be mixed with 500 μL of TCE. Once this extraction is done, the organic phase composed of TCE and oil is passed to the FTIR spectrophotometer (Thermofisher-Nicolet IS50 FTIR) and an absorption spectrum of this phase is realized.
With this method, a calibration has been performed, absorption spectrum are plotted for various concentration (from 150 to 300 ppm). From these spectrum (figure 2.22) and the absorbance of the sample at $2927 cm^{-1}$, the calibration curve specific to the FINAVESTAN A80B is set (figure 2.23).
However, due to the fact that TCE is a CMR (Carcinogenic, mutagenic or reprotoxic substances), it needs to be manipulate under a hood. Unfortunately the FTIR spectrophotometer can not be placed under such a device in our lab. Thus, this method cannot be used for oil concentration determination in our study.

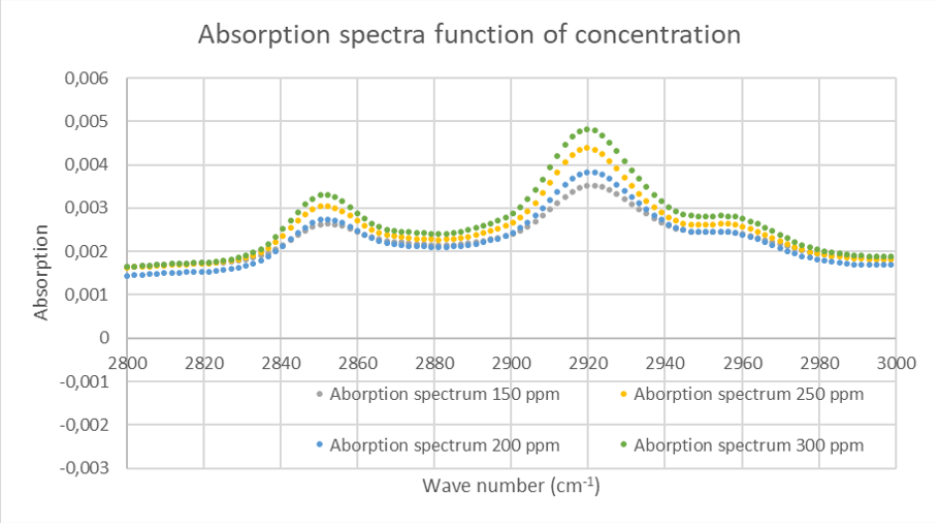

Figure 2.22: Absorption spectrum for TCE and oil solution for oil concentration from 150 to 300 ppm

3.3.4 Chemical Demand of Oxygen: DCO

The last method is to use the Chemical Demand of Oxygen (DCO) of the sample. This method simply evaluate the necessary quantity of oxygen needed to oxide organic molecules, here the oil. To use this method, an emulsion sample is added

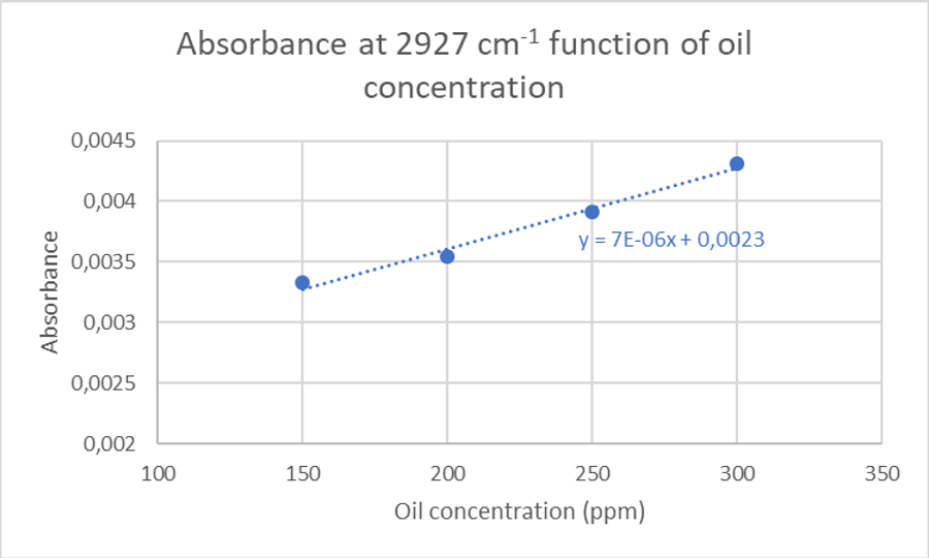

Figure 2.23: Calibration curve to determine oil concentration function of absorbance

in a fixed volume inside a DCO kit (a solution with a catalyst) heat for 2 hours and then pass trough a device which evaluate the quantity of oxygen used by the evolution of solution color.
The only true drawback of this method is that the emulsion sample need to be diluted if the concentration of chlorure ion is superior to 2 g per L (which is the case here when brine is used). Furthermore, HPAM being an organic compound it also can be oxide by oxygen, thus a second scaling is needed in presence of HPAM.

4 Characterisation of the emulsion produced

4.1 Objectives

Emulsion preparation is a critical topic to tackle in the use of this pilot. Indeed, for flotation the emulsion size has a role to play (which will be describe in the next chapter). To perform experiments and be able to modify as much parameters as possible, it is important to find a way to produce calibrated emulsion with similar size distribution. One of the easiest way to modify droplet size is to vary the speed of the emulsifyier. However, the one set on the pilot does not allow such a method. This is why ideally an other way must be found.

4.2 Emulsifying phase

It has been chosen to first study how the emulsion behave during the emulsifying phase and how the droplet distribution varies. In order to evaluate that a given concentration of oil (300 ppm) in deionized water are mixed. At the beginning of the experiment, the flotation cell is filled with deionized water and the optical and numerical background are performed. The acquisition is then launched on the Spraytec before beginning the circulation. The emulsifyier is then launched after 5 min of powering up and works in continue for a full 30 min. After the emulsifying time we aim to have a mean droplet of 15 μm (diameter found at the exist of a well).This first part allows to evaluate the droplet distribution through the emulsifying time. After this time, the emulsifyier is stopped but the flow and acquisition keep going. This step allows to see how the emulsion evolve during time.

These experiments shows that the mean diameter of the droplet distribution tends to decrease with the emulsion time. Indeed, figure 2.24 showing the evolution of the droplet mean diameter function of the emulsifying time stressed that the mean diameter tends to decrease as the inverse of the square root of the time. However, during the experiments with 30 min duration, an increase in temperature of $2°C$ is observed. This increase of temperature can become quite an issue if the emulsifying time is increase as all fluid physicochemical properties depends on temperature.

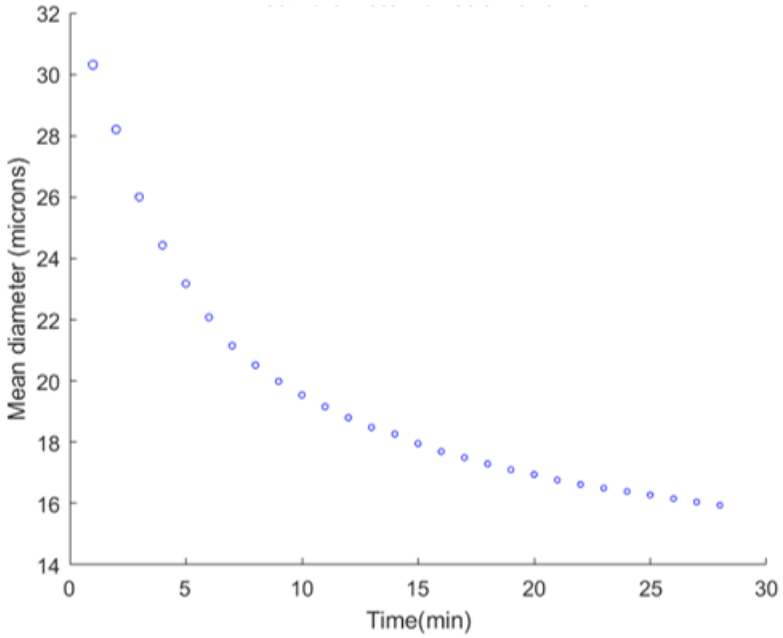

Figure 2.24: Evolution of the droplets mean diameter function of the emulsion time

After 30 min of emulsifying, we have reached our target mean droplet size of 15 μm but how does this emulsion behave with time ?

4.3 Stability

Nevertheless, it is important to see how stable is this created emulsion. The distribution has to be as constant as possible through the experiment duration. The maximum duration of our flotation experiments is at most around 40 min depending on the flow rate. Figure 2.25 shows that the mean diameter tends to decrease when the emulsion resting time is increasing. This leads to two conclusions. The first is that the emulsion seems quite stable, coalescence phenomenon does not occurs inside the emulsion tank. Indeed, the decrease in diameter can be explained by the possible decantation in the tank. However, even if this mean diameter is decreasing with the resting duration, its evolution is quite slow at least in the first 40 min. During this time, a total variation of only 13% is observed, at the scale of residency time (around 6 min), the variation is negligible around 2% . This allows to say that emulsifying the solution for only 30 min seems enough to perform the experiment right after and have a known emulsion (which does not change much during time).

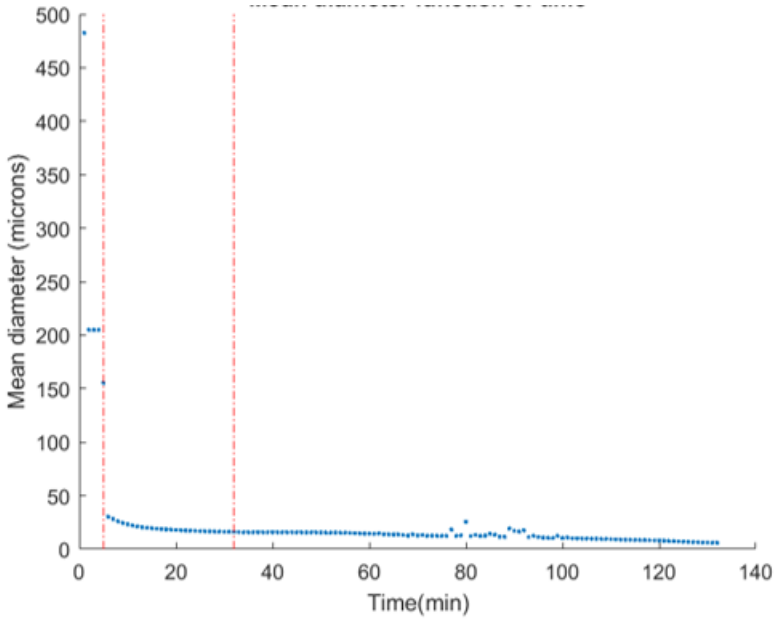

Figure 2.25: Evolution of the droplets mean diameter function of the emulsion resting time

4.4 Variation of d_d

Now that a way to produce the emulsion has been found let see, if it is possible to modify its diameter. Alternating resting and emulsifying sequence might be way to achieve that. Figure 2.26 shows that after emulsifying for 30 min and reaching the quite stable emulsion reach previously and letting it rest for a short amount of time before remulsifying it for the same amount of time seems to allow to decrease the mean size of the emulsion. The found emulsion is also quite stable. Indeed, the droplet mean diameter shows almost no decrease during a 10 min resting time. However, further emulsifying seems to have no effect on the emulsion size or stability. In order to facilitate the emulsion making and due to the fact that our leverage to thin the droplet size is quite low, we have decided that in each of our case, emulsion will be made by emulsifying it for 30 min.

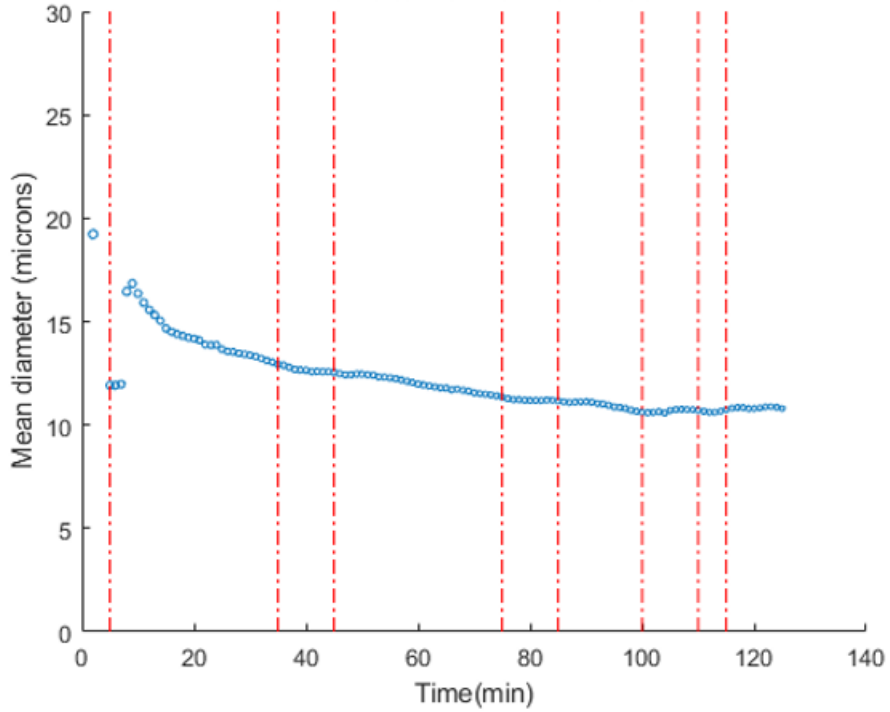

Figure 2.26: Evolution of the droplets mean diameter function of time when alternating resting and emulsifying sequence

4.5 Impact of polymer on droplets size distribution

Once the protocol to make the emulsion has been decided, it is important to see the emulsion behavior in presence of polymer. The effect of HPAM is examined here through the plotting of the droplet size distribution. Dropsizers are used here to

evaluate droplets size distribution. Figure 2.27 shows the evolution of droplet size distribution in two scenarios. The first one in blue in deionized water and the other one in orange in viscosified brine (500 ppm of HPAM in brine). These distributions in number clearly shows that the droplet size distribution is clearly impacted by the presence of polymer and salt. As a matter of fact, the mean diameter decreases from 10 to 7 μm in presence of polymer. This reduction of droplet diameter in presence of polymer is also found in the oil industry. For example a comparison on the same oil field on two wells have been made in China. One well was exploited with water and the other with water viscosified thanks to HPAM. Being on the same oil field means that initially, before one being viscosified, both water should have the same properties. However, a huge difference of diameter is seen on the two wells: on the one exploited with just water the mean diameter of the emulsion at the exit is around 35μm while droplets on the one with polymer are around 3μm [Deng et al., 2005].
This variation of diameter in presence of HPAM might not be similar here due to the fact that the emulsion is not made in the same way.

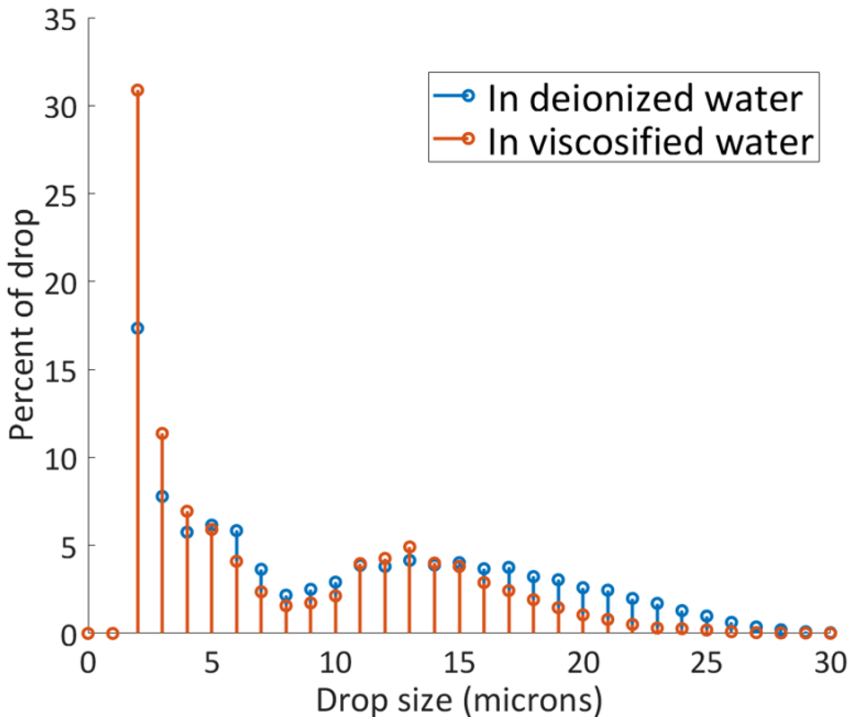

Figure 2.27: Droplet size distribution in percent

It is also interesting to see that the representation of droplet size distribution in number shows a huge amount of very thin droplets around 3μm which are present

in both kind of water (even if the share is larger in visocified water). Those droplets tends to reduce the mean diameter compared to distribution made in volume as their share is smooth in the second representation. However, even if present with probably smaller one (implied by being seemingly the center of a secondary distribution) these droplets are at the limit of detection of Dropizers device. This means that their share can be increased due to numerical artefact during the processing of the frame. Nevertheless, experiments done with a granulometer showing results in volume also show these very thin droplets proving at the same time their presence (figure 2.28)

Furthermore, flotation devices are in the industry often efficient up to this diameter [Deng et al., 2005]. The fact that the share of droplet of this diameter being greater in viscosified leads to an easy conclusion that a flotation unit should be less efficient in viscosified water. Indeed, a greater percentage of droplets will still be present at the end of the process. It has been seen here that droplets size tends to

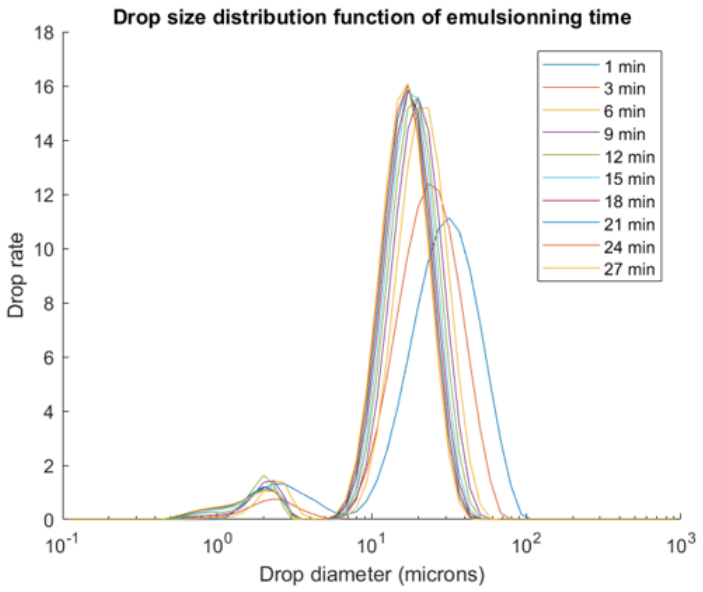

Figure 2.28: Droplet size distribution in volume in deionized water (experiment done with a granulometer)

decrease in presence of polymer, but what about the bubble size ?

4.6 Characterisation of the bubbles in DAF

Now that we know that the droplet diameter is modified by the presence of polymer and salts, it is interesting to study the behavior of the last parameter (beside viscosity) having a direct impact on capture efficiency: the bubble size.

First according to [Besson, 2013] bubble size distribution tends to decrease in presence of salts. His study have been with the same experimental device as us, as known as a Malvern Spraytec. However, figure 2.29 showing the bubble distribution in both deionized water (in blue) and viscosified brine (in orange) stresses a different results. Indeed, in presence of polymer (in viscosified brine), the bubble size tends to increase. The bubble mean diameter thus goes from $60\mu m$ in deionized water to $70\mu m$.

Looking only at the design and functioning of a flotation unit, this increase is quite useful. In fact, an increase in bubble mean size means an increase in allowed flow rate inside the unit. This leads to an increase in the quantity of water treated in one day. This is explain by the fact that a flotation unit is designed in order to allow the largest share possible of bubble to reach the surface and by doing so be useful to the flotation. This is done by setting a maximal inlet flow rate lower than the ascending velocity of a given bubble size. Thus, for a flotation unit designed for deioinized water, the load of the unit should be increase by the presence of polymer.

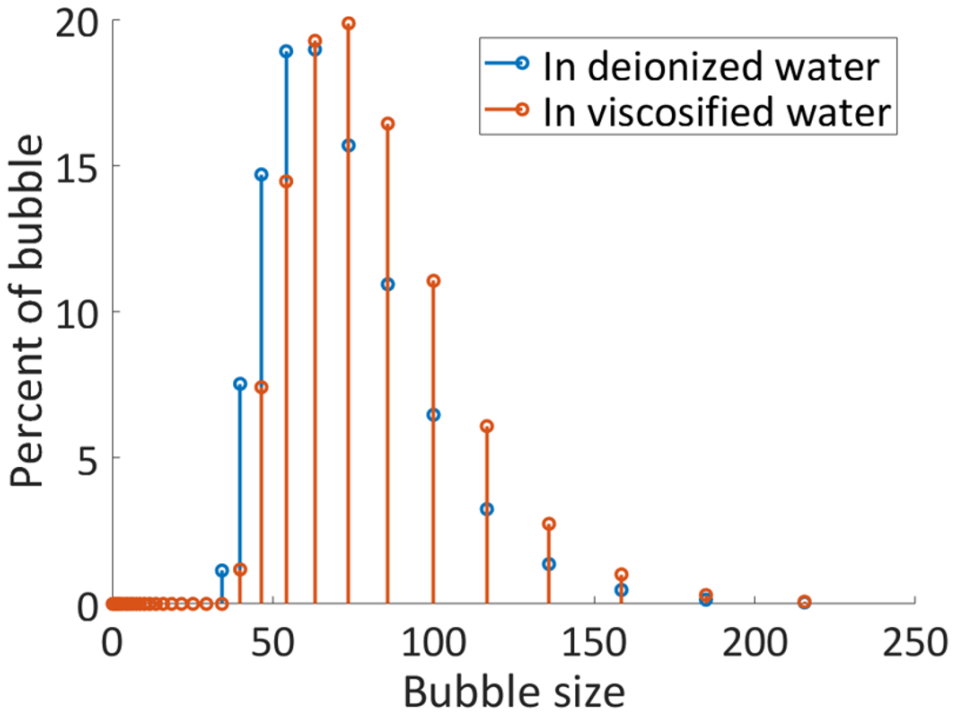

Figure 2.29: Bubble size distribution in percent

5 Conclusion

Various solutions properties have been shown here. First, considering the range of shear stress variation inside a flotation cell, our results show that polymer solutions can be considered as newtonian fluid. Indeed, the variation range of our solutions is small enough to say that the viscosity of our otherwise rheofluidfying polymer solutions is constant.
Furthermore, the pilot has shown several limitation such as the impossibility to reproduce the same emulsion as the one seen on oil field or to have a direct access to oil concentration. However, a way to obtain a calibrated emulsion and interesting results on droplets or bubble size distribution have been found. Indeed, the presence of polymer tends to decrease the droplets size and, on the contrary, to increase bubble size. The impact of this evolution on capture efficiency will be studied in the next part.
In addition, droplets size distributions also show the presence of very thin droplet (smaller than $3\mu m$). These droplets are too small to be separated from water thanks to flotation according to studies on industrial flotation device.

Conclusion

Diverses propriétés des solutions ont été démontrées ici. Tout d'abord, en considérant la plage de variation de la contrainte de cisaillement à l'intérieur d'une cellule de flottation, nos résultats montrent que les solutions polymères peuvent être considérées comme des fluides newtoniens. En effet, la plage de variation de nos solutions est suffisamment faible pour que l'on puisse dire que la viscosité de nos solutions polymères, par ailleurs rhéofluidifiantes, est constante.
Par ailleurs, le pilote a montré plusieurs limitations telles que l'impossibilité de reproduire la même émulsion que celle observée sur les champs pétroliers ou d'avoir un accès direct à la concentration d'huile. Cependant, un moyen d'obtenir une émulsion calibrée et des résultats intéressants sur la distribution de la taille des gouttelettes ou des bulles ont été trouvés. En effet, la présence de polymère tend à diminuer la taille des gouttelettes et au contraire à augmenter la taille des bulles. L'impact de cette évolution sur l'efficacité de capture sera étudié dans la partie suivante. De plus, les distributions de taille des gouttelettes montrent également la présence de gouttelettes très fines (inférieures à $3\mu m$). Ces gouttelettes sont trop petites pour être séparées de l'eau par flottation d'après une étude sur un dispositif de flottation industriel.

Chapter 3

Impact of HPAM on flotation at bubble scale via Nguyen model

Afin d'évaluer l'effet du polymère sur l'efficacité de la flottation, il a été choisi de se concentrer sur son effet sur l'efficacité de la capture. Tout d'abord, l'effet du polymère sur la viscosité est étudié, puis, son effet dû à la variation des autres propriétés physico-chimiques.
L'effet du HPAM sur l'augmentation de la viscosité dépend également de la taille des bulles et des gouttelettes. L'étude des effets des distributions de la taille des bulles et des gouttelettes sur le phénomène de capture sont étudiés. Cette étude est dans ce chapitre réalisée numériquement à l'aide du modèle de Nguyen [Nguyen et al., 1998], pour avoir une idée de la variation potentielle de l'efficacité de capture en fonction des propriétés physico-chimiques, dont la viscosité.

In order to evaluate the effect of the polymer on flotation efficiency, it was chosen to focus on its effect on capture efficiency. Firstly, the effect of the polymer through viscosity is studied, following, its effect through the variation of the other physico-chemical properties.
The effect of HPAM through viscosity also depends on bubble and droplet size distribution, which effect on the capture phenomenon are also examined. This study is first carried out numerically in this chapter using the Nguyen model [Nguyen et al., 1998] to get an idea of the potential variation of the capture efficiency along with the physico-chemical properties.

1 Capture modeling

As it was stated in chapter 1, the capture efficiency E_{capt} is defined as the number of droplets captured by a bubble relative to the total number of droplets present in the volume traversed by the bubble during its ascent. $E_{capt} = 1$ means that all particles within the trajectory of the bubble are captured.

The capture mechanism is traditionally broken down into three elementary steps as shown in Figure 3.1 [Derjaguin, 1993, Ralston and Dukhin, 1999] : collision, attachment and stability.

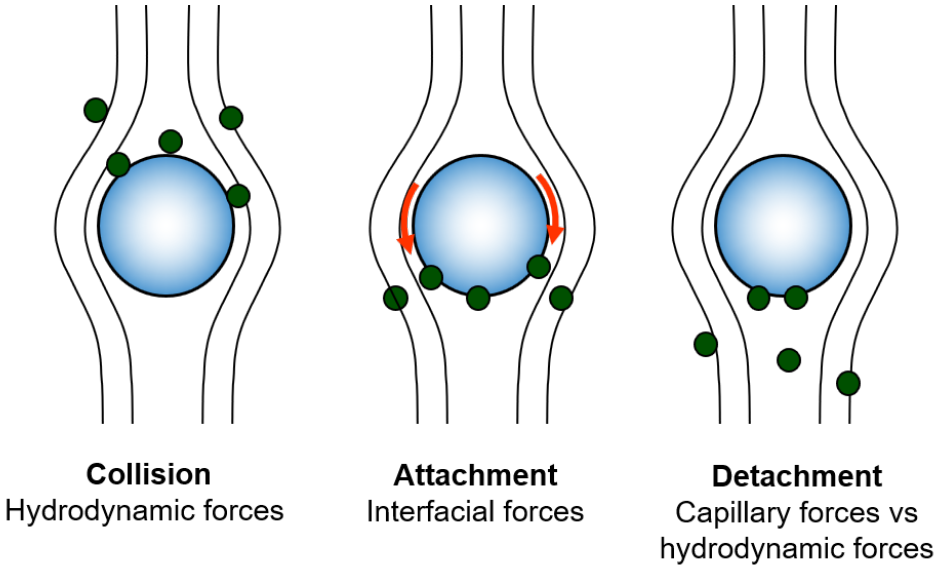

Figure 3.1: The three steps of the mechanism of capture in flotation

Each of these elementary steps is assigned an efficiency value, E_C (collision), E_A (attachment), E_S (stability), so that:

$$E_{capt} = E_C E_A E_S \tag{3.1}$$

(i) Collision: In the case studied here, the droplets are < 100 microns in diameter, i.e. they are small enough to act as tracers and follow flow lines. Therefore, collision occurs when a droplet follows a flow line that is close enough to the bubble for the droplet to attach to the bubble surface (step (ii)). The collision efficiency E_C is the number of droplets that collide relative to the total number of droplets in the bubble path. Note that the term 'collide'does not mean that the droplet actually 'touches' the bubble surface, as a thin layer of liquid remains between the bubble and the droplet before attachment occurs or not.

(ii) Adhesion: After the collision, the droplet either slides along the surface of the bubble or bounces off it. According to Dobby & Finch [Dobby and Finch, 1987], droplets cannot bounce off a surface if their radius is less than 100 μm. So we assume that all colliding droplets will slide on the bubble surface in the direction of flow. Each droplet slides on the bubble for a given 'sliding time', which depends on parameters that will be explained later. Attachment occurs when the sliding time is sufficient to drain the liquid layer between the droplet and the bubble surface. The attachment efficiency E_A is defined by the number of droplets that successfully attach to the bubble relative to the total number of droplets that collide with it.

(iii) Stability: The cluster formed by a bubble with one or more droplets will continue to rise. It is then possible for droplets to detach from the bubble, with Es being the associated stability efficiency. In the case of fine droplets, as in our case but also in the vast majority of other industrial situations, the inertia of the attached droplet (or particle) is so low that the probability of detachment is negligible [Yoon, 2000, Nguyen et al., 1998]. We therefore assume that $E_S \approx 1$, then equation (1) is simplified as follows:

$$E_{capt} = E_C E_A \tag{3.2}$$

E_{capt} is a local scale indicator but gives a direct indication of the overall flotation performance. In section 2.3, we show how E_{capt} is modified by a change in viscosity and/or changes in bubble and droplet size.

To be able to calculate E_{capt}, we first need to express the collision efficiency E_C and the attachment efficiency E_A. The next two sections are therefore dedicated to expressing E_C and E_A.

1.1 Collision efficiency E_C

Collision depends mainly on the hydrodynamics around the bubble. In fact, since droplets behave as tracers, collision occurs when the trajectory of the droplet approaches the surface of the bubble.
To estimate E_C, we use a so-called interception model for the collision between a bubble and the oil droplets. The assumptions of the model we have chosen are:

- Droplet velocity, much lower than the bubble velocity, is neglected;
- Droplets behave as tracers and follow the flow line, their inertia is neglected.

The model proposed by Nguyen et al. in 1998 [Nguyen et al., 1998] is chosen here (equation 3.3) in order to have the same theory origin for both collision and

attachment. The use of this model adds another hypothesis. The bubble surface is considered as a contaminated surface. This means that the bubble behaves as a rigid sphere and that there is no slip velocity at the interface between air and water. This latter hypothesis is made because water is never perfectly clean and small impurities are present. These impurities migrate to the surface of the bubbles and contaminate the bubble interface.

$$E_C = \frac{2V_b D}{9(V_p + V_b)Y}\left(\frac{d_p}{d_b}\right)^2 \left[\sqrt{(X+C)^2 + 3Y^2} + 2(X+C)\right]^2 \tag{3.3}$$

$$X = \frac{3}{2} + \frac{9Re_b}{32 + 9.888Re_b^{0.694}} \tag{3.4}$$

$$Y = \frac{3Re_b}{8 + 1.736Re_b^{0.518}} \tag{3.5}$$

$$C = \frac{V_b}{V_p}\left(\frac{d_b}{d_p}\right)^2 \tag{3.6}$$

$$D = \frac{\sqrt{(X+C)^2 + 3Y^2} - (X+C)}{3Y} \tag{3.7}$$

The Nguyen collision model (equation 3.3), developed from semi-analytical calculations and experimental results, depends on several explicit parameters. The first is the square dependence of E_C with the ratio of the drop diameter d_p over the bubble diameter d_b, which reflects the contamination of the bubble surface.
The collision efficiency E_C depends also on particle and bubble velocities. These are calculated from the Schiller & Naumann correlation (see Annexe A) and are proportional to the viscosity and a function of the bubble Reynolds number.
The dimensionless coefficients X, Y, C and D are Reynolds dependent and related to the bubble (equations 3.4, 3.5, 3.6, 3.7).

From these various equations, there are finally 3 parameters that can influence the efficiency of the collision. The diameters of the bubbles and droplets have a direct effect on this efficiency, viscosity appears indirectly in droplet and bubble velocities and Reynolds numbers.
Furthermore, as seen in a study in Daqing [Deng et al., 2005, Qi et al., 2013], the polymer has an indirect effect on droplet size through viscosity. Indeed, in the presence of polymers, the mean droplet diameter is divided by ten (going from 35 to 3.5 μm in the presence of HPAM). This same effect is observed in our experiments (see chapter 2). Our droplet mean diameter goes from 10 to 7 μm when HPAM is added in the solution.

Now that we have an expression for E_C, we still need to find an expression for

the attachment efficiency E_A.

1.2 Attachment efficiency, E_A

After the collision, a thin film of liquid remains. The colliding particle then slides along the bubble surface, pushed by the liquid flow. As it slides, the liquid film is thinned by various forces until it reaches a critical thickness where the film breaks and a triple point of contact is created. The triple point of contact (TPC) then expands until the particle attaches (Figure 3.2) [Ives, 1983, Nguyen et al., 1998] . A time can be assigned to each of these steps. However, the duration of rupture and TPC expansion is very short, so the time of all these steps, called the induction time, is often assimilated to the draining time. The critical point in modelling attachment theory is therefore to understand how the liquid film is thinned.

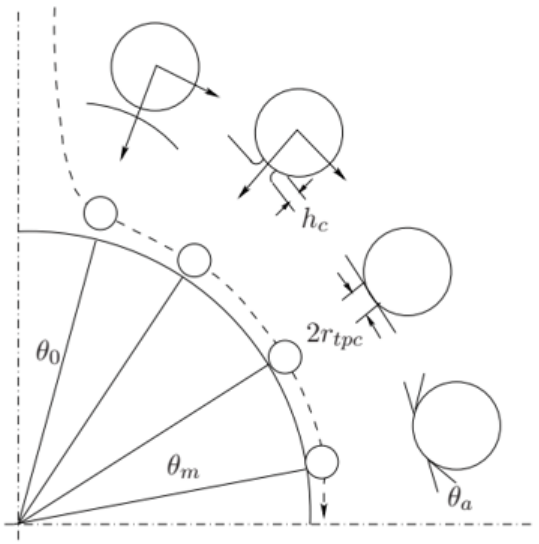

Figure 3.2: Three steps of bubble particle attachment

1.2.1 General concept for attachment efficiency modelling

The attachment model developed by Nguyen express E_A as a function of the ratio of two durations (equation 3.8): the sliding time t_s (time during which the droplet slides along the bubble surface, equation 3.9) and the induction time t_i (time required for the film to thin and break, equation 3.10). This model is based on the same assumptions as the Nguyen collision model seen in the previous part. However, this expression is valid in a fore-and-aft symmetry situation and the sliding time given in equation 3.9 is an average. This condition is not always met, but was

used here to obtain initial results.

$$E_A = sech^2\left(\frac{t_i}{t_s}\right) \tag{3.8}$$

$$t_s = \frac{d_p + d_b}{2V_b A} \tag{3.9}$$

This sliding time is quite easy to evaluate, it depends on the particle and bubble diameter, the bubble velocity V_b and a parameter A (equation 3.12), which is a function of the Reynolds number.
However, the induction time is more complex to evaluate as it depends on the same parameters (bubble velocity, A & B Reynolds dependent constant) but also on the maximum angle of collision θ_{col} (angle from which collision is no longer possible, equation 3.11), function of the Reynolds number and of the critical angle of attachment θ_{cr} (the angle from which no more attachment is possible). This last angle is more complex to evaluate theoretically.

$$t_i = \frac{d_p + d_b}{2V_b(1-B^2)A} ln\left(\frac{tan(\frac{\theta_{col}}{2}}{tan(\frac{\theta_{cr}}{2}}\left[\frac{cosec(\theta_{col} + Bcot(\theta_{col})}{cosec(\theta_{cr} + Bcot(\theta_{cr})}\right]^B\right) \tag{3.10}$$

$$\theta_{col} = arccos(D) \tag{3.11}$$

$$A = \frac{V_p}{V_b} + \frac{d_p}{d_b}X + \left(\frac{d_p}{d_b}\right)^2 M \tag{3.12}$$

$$B = \frac{d_p}{d_b}\frac{Y}{A} + \left(\frac{d_p}{d_b}\right)^2 \frac{N}{A} \tag{3.13}$$

$$M = -\frac{9}{4} - 27\frac{Re_b}{64} + 0.2266Re_b^{1.274} \tag{3.14}$$

$$N = -0.437Re_b^{1.0562} \tag{3.15}$$

1.2.2 Theoretical determination of Nguyen model parameters

Nguyen et al. estimate this critical angle using experimental data valid only for quartz particles. Therefore, we need to understand the mechanism behind the thinning of a liquid film. Unlike collision, adhesion and film thinning are driven by physico-chemical forces that we need to determine.

After the collision, the film between the bubble and the colliding particle is thinned by these forces. The effects of these forces depend on the thickness of the film (or the distance between the bubble and the droplets). The forces considered here are [Derjaguin, 1993, Derjaguin et al., 1984] :

- Van der Waals forces, short-range intermolecular forces, are expressed as follows (according to Lifshitz theory), E being the interaction energy of the system

$$F_{VdW} = -\frac{dE}{dh} \tag{3.16}$$

$$E = -\frac{A_{o,w,a}}{6h}\frac{d_b d_p}{d_p + d_b} \tag{3.17}$$

- Electrostatic forces, forces depending on the charges present in the solution, acting in the intermediate range and expressed as follows

$$F_e = \epsilon\epsilon_0 2\pi a\kappa \frac{2\zeta_p\zeta_b exp(\kappa h) - \zeta_p^2 - \zeta_b^2}{exp(2\kappa h) - 1} \tag{3.18}$$

In these expressions, taken from Nguyen and Evans [Nguyen and Evans, 2004], h is the film thickness. The van der Waals forces depends on the bubble and particle diameters and the Hamaker constant $A_{o,w,a}$ of the system. This Hamaker constant is obtained with the equation 3.19 given by Israelachvili [Israelachvili, 1992] with the phases in contact being oil, water and air.

$$A_{oil,water,air} = \left(\sqrt{A_{oil}} - \sqrt{A_{water}}\right) \times \left(\sqrt{A_{air}} - \sqrt{A_{water}}\right) \tag{3.19}$$

The constants in the equation 3.19 can be found in the literature:

- Water Hamaker constant $A_{water} = 5.73 \times 10^{-20} J$ [Nguyen, 2000]
- Oil Hamaker constant $A_{oil} = 5 \times 10^{-21} J$ [Ichikawa, 2007]
- Air Hamaker constant $A_{air} = 0 J$

The electrostatic force depends on physico-chemical properties such as ζ_b (and ζ_p) the bubble surface potential (and particle surface potential), ϵ the permittivity of the solution and ϵ_0 the permittivity of the vacuum. The Debye constant κ (equation 3.20) reflects the presence of charges in the solution and the thickness of the electrical double layer. The Debye constant depends on the elementary charge e, the ionic strength I, the temperature T and the Boltzmann constant k_b.

$$\kappa = \sqrt{\frac{e^2 I}{\epsilon\epsilon_0 k_b T}} \tag{3.20}$$

Other different forces may be considered, such as steric or hydration forces. These forces are usually neglected [Nguyen and Evans, 2004, Hewitt et al., 1993]. Hydrophobic forces should also be used, but several experiments are needed to have

access to integration constants and decay lengths. It was therefore decided not to include them here.

The effect of these forces is used to calculate the film thinning rate thanks to the Taylor model 3.21. This model is based on the following hypothesis:

- The film is present between a spherical and a planar object or between two spherical objects.
- One surface is assumed to be stationary and the other to be moving towards the first.
- The fluid forming the film is Newtonian.

$$V_{Taylor} = \frac{dH}{dt} = -\frac{mFH}{6\pi\mu_f a^2} \tag{3.21}$$

This model gave us the evolution of the film thickness as a function of different parameters. A mobility factor gives the behaviour of the bubble (m=1 if the bubble behaves as a solid sphere and m=4 if the surface of the bubble is mobile). It then depends on the resultant external forces F, which in our case is the sum of van der Waals and electrostatic forces. The bubble and droplet diameters affect the film thickness through the reduced radii a and the central film thickness H. H can be expressed as follows and depends on the film thickness:

$$H = h - \frac{r^2}{2a} \tag{3.22}$$

The Taylor model, once differentiated, can be integrated between the initial and critical thickness (h_0 & h_c) to obtain the induction time.
In the case studied here, the initial thickness h_0 is given by the thickness at which the van der Waals and electrostatic forces became greater than the hydrodynamic forces (weight and drag). The critical thickness is obtained from Manev et al. 3.23 [Manev and Nguyen, 2005] formula for foam film. This expression depends on physico-chemical properties such as fluid viscosity μ_f, surface tension σ or Hamaker constant $K_{VdW} = \frac{A_{o,w,a}}{6\pi}$;;

$$h_c = \frac{0.98(k_bT)^{\frac{1}{12}} K_{VdW}^{\frac{1}{3}}}{\mu_f^{\frac{1}{6}} \sigma^{\frac{1}{4}} \left(-\frac{mF}{6\pi\mu_f a^2}\right)^{\frac{1}{6}}} \tag{3.23}$$

Now that the initial and critical thicknesses are known, the induction time and therefore the attachment efficiency can be calculated. The next section will first describe the effect of standard parameters such as viscosity, bubble and droplet size on collision efficiency before describing the effect of these parameters on initial

thickness and induction time. This will allow us to consider the effect of viscosity and particle size on attachment and capture efficiencies.

2 Impact of particles size and viscosity on capture efficiency

This section is dedicated to the study of the evolution of the capture efficiency along with a variation of three parameters:

- Bubble size d_b;
- Droplet size d_d;
- Viscosity μ_f;

As the capture efficiency is a product of the collision and attachment efficiencies, the effect of these parameters on these efficiencies will be studied beforehand.

2.1 Impact of viscosity and particles size on collision efficiency

As seen in section 1.1 of this chapter, collision efficiency depends explicitly on bubble and droplet diameter and implicitly on viscosity via the Reynolds number.

In table 3.1 we give the variation of collision efficiency as a function of typical droplet and bubble sizes found in the oil industry. The viscosity is taken to be that of water, i.e. 1 Cp. The bubble sizes are chosen to study the effect of viscosity in different flotation modes. 50 μm is the average bubble diameter used in the DAF mode, while 500 μm is the beginning of the IAF mode. An upper limit of 1 mm for bubble size has been chosen to correspond to the mean diameter in IAF mode.
Droplet size was found to vary with increasing viscosity at the Daquing field in China [Deng et al., 2005, Qi et al., 2013]. Therefore, the lower droplet diameter was chosen to represent the lowest diameter found at this site in the presence of polymer and the upper diameter is that found at Daquing in standard process water.
Figure 3.3 shows the evolution of collision efficiency as a function of bubble size in non-viscosified water (with a viscosity of 1 Cp). This figure shows the evolution of the collision efficiency for two different droplet sizes. The smaller one is close to that found in the viscosified process water at the Daquing oil field ($3\mu m$). The larger one is the one given by Total ($15\mu m$). The first obvious effect shown by figure 3.3 and table 3.1 is that the collision efficiency E_C is strongly influenced by the bubble

d_b (μm) \ d_d (μm)	1	15	30
50	6.8×10^{-4}	1.5×10^{-1}	5.7×10^{-1}
500	1.9×10^{-5}	4.3×10^{-3}	1.7×10^{-2}
1000	8.6×10^{-6}	1.9×10^{-3}	7.7×10^{-3}

Table 3.1: Values of collision efficiency in water at 1 Cp

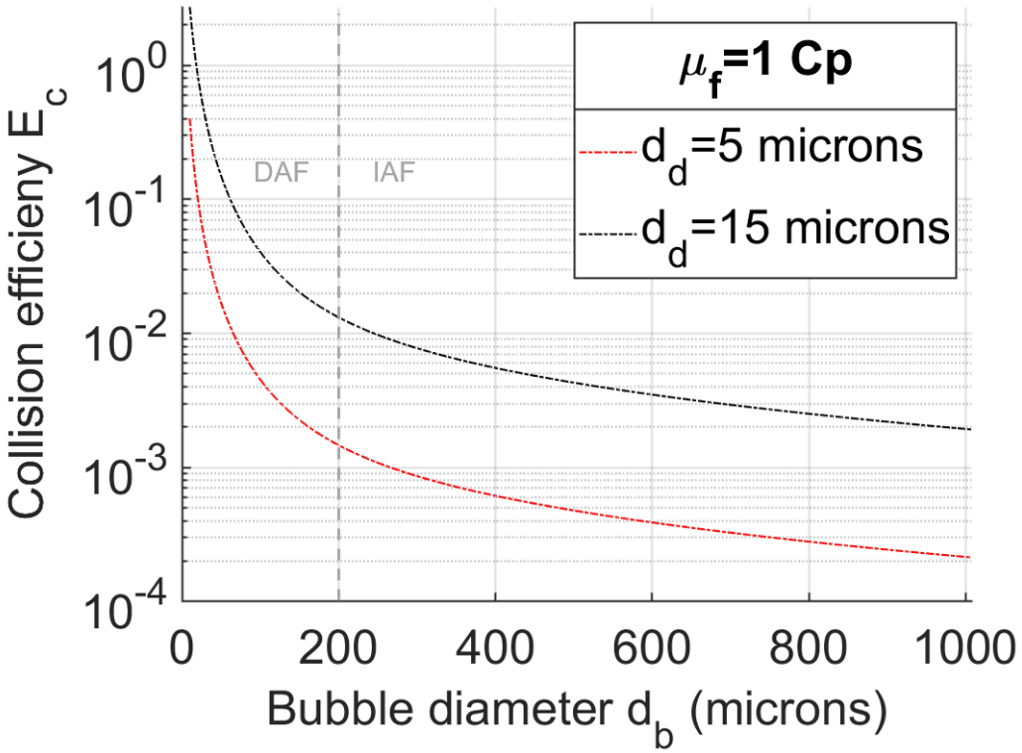

Figure 3.3: Evolution of the collision efficiency function of bubble diameter for two droplet size (5 & 15 μm) in fresh water

diameter d_b and the droplet diameter d_d. In fact, as the bubble diameter increases, the collision efficiency tends to decrease. The fact that larger droplets are more likely to collide with the bubble can also be explained from a hydrodynamic point of view. In fact, in the model studied here, the droplets behave as tracers, which means that they follow the flow line. So the larger the droplet, the more likely it is to collide with the bubble, even if the flow line is further away from the bubble surface.

As in figure 3.3 the bubble size range sweeps from the DAF size range to the IAF size range, it can be concluded that collision will be more efficient in the DAF mode than in the IAF mode. This conclusion does not change when the droplet diameter

is changed from 5 to 15 μm.

It is then obvious that the effect of viscosity on collision efficiency depends on both the bubble and the droplet size range. For this reason, it has been decided to present the results in both a table of values and a graph similar to those realised at 1 Cp. Table 3.2 shows the evolution of all these parameters in viscous water (2 Cp). It shows that the collision efficiency tends to decrease as the viscosity increases for the same d_b and d_d values as table 3.1.
However, this decrease in efficiency needs to be quantified. This is why figure 3.4 shows the evolution of the efficiency function of bubble size for different viscosities. This figure highlights an interesting point which is difficult to see in the table 3.2, namely that the effect of the increase in viscosity depends on the bubble size. In fact, in DAF mode (for bubbles up to $200\mu m$), the variation of the efficiency is very small. It decreases for a $20\mu m$ droplet to only 20% when the viscosity is multiplied by 2. The decrease is slightly higher (up to 30%) when the viscosity is multiplied by 5. However, in IAF mode (for bubbles from $200\mu m$), a multiplication of the viscosity by 2 induces a loss of efficiency up to 30%. This is even worse if the viscosity is multiplied by 5, in which case the collision efficiency is reduced by more than half. It is important to note that these variations are given for the worst case in each mode (for the larger bubble). Therefore, the loss of efficiency for a bubble of around 50 μm (taken as the average bubble in our study in DAF mode) is less than 5%.

d_b (μm) \ d_d (μm)	1	15	30
50	6.7×10^{-4}	1.5×10^{-1}	5.7×10^{-1}
500	1.3×10^{-5}	2.9×10^{-3}	1.2×10^{-2}
1000	5.8×10^{-6}	1.3×10^{-3}	5.2×10^{-3}

Table 3.2: Values of collision efficiency in water at 2 Cp

This study of collision efficiency shows that it is highly dependent on bubble and droplet size. As the bubble size increases, the collision efficiency decreases. Conversely, collision efficiency increases with droplet size.
The effect of viscosity on collision efficiency is also dependent on bubble size. In fact, with a very small bubble, a change in viscosity has almost no effect, whereas with a millimetric bubble, the effect of viscosity is huge. Thus, if we think about the effect of viscosity on the two types of flotation mode, it can be said that it has no effect on collision efficiency in DAF mode and a huge effect in IAF mode.
However, as we have already said, the capture efficiency is a product of the collision efficiency and the attachment efficiency. So let us see how viscosity affects the

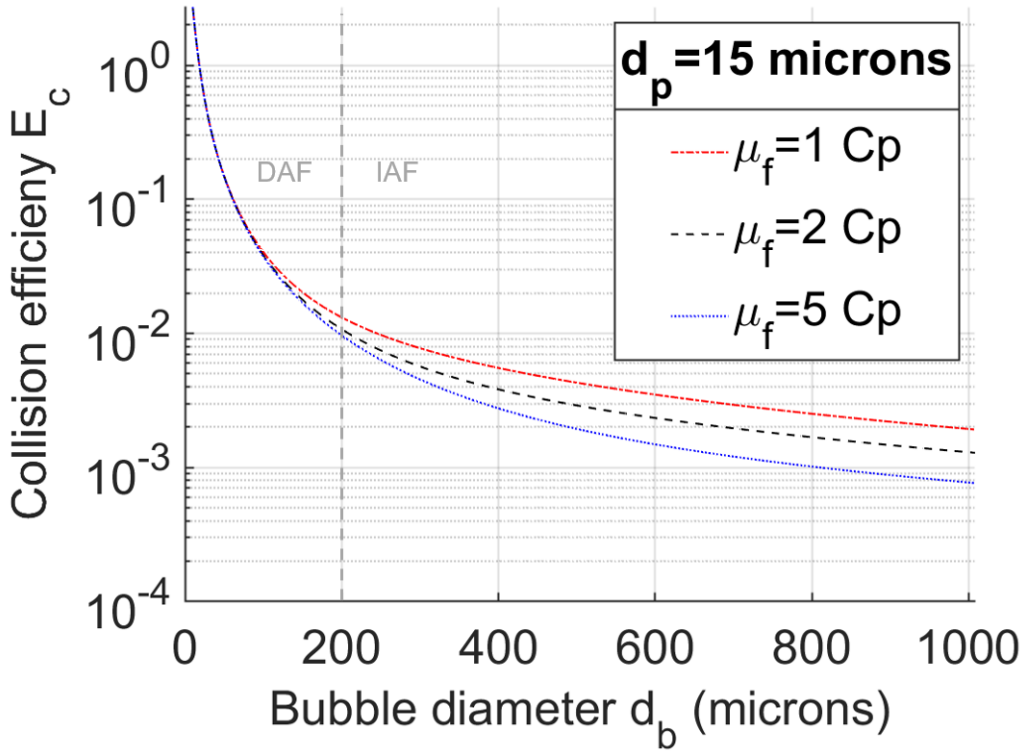

Figure 3.4: Evolution of the collision efficiency function of bubble diameter for a $15\mu m$ droplet in various water viscosity

attachment step before concluding on its effect on capture.

2.2 Impact of viscosity and particles size on attachment efficiency

As mentioned before, the efficiency of the attachment is the ratio of two times:

- The time taken for the droplet to slide along the surface of the bubble, which depends only on the hydrodynamics of the system: the sliding time.
- The time required for the liquid film between the droplet and the bubble surface to drain away: the induction time.

According to the model of Nguyen et al. ([Nguyen et al., 1998]) shown at the beginning of the chapter, the expression of the sliding time is quite simple (equation 3.9). However, the induction time in this model is much more complex to express and depends on experimental data that we do not have in our case. For this reason, a new expression of the induction time is first given along its variation with viscosity and particle size, before evaluating the attachment efficiency.

$$t_s = \frac{d_p + d_b}{2V_b A}$$

2.2.1 Induction time

The induction time is the time it takes for the liquid film between the droplet and the bubble surface to be drained. We have considered that it starts at a thickness h_0, which is the initial thickness, and ends at a thickness h_c, where the film breaks. As mentioned in section 1.2 of this chapter, we decided to calculate it thanks to the Taylor model. This gives us the following expression:

$$t_i = \int_{h_c}^{h_0} \frac{6\pi\mu_f a^2}{mFH} dH \tag{3.24}$$

In the equation 3.24, a is the reduced radius of the droplet and the bubble, m is a coefficient describing the surface of the bubble (equal to 1 if the bubble behaves as a solid sphere) and F is the resultant of the surface forces. This integral also depends on the critical thickness h_c (given earlier in section 1.2) and on the initial thickness h_0, which is yet to be defined.

h_0 is the thickness at which the trajectory of the droplet is no longer dominated by hydrodynamics forces. At this point, the surface forces and the hydrodynamic force are equal before and after the surface forces dominate the trajectory of the drop and force the drainage of the film.
h_0 is the distance at which the surface forces becomes strong enough to move the particle away from the flow line and to drain the liquid film.
Indeed, in the absence of surface forces, particle follow the fluid. The hydrodynamic forces acting on the particle are then equal to zero.
Even if surface forces are very low, they will always be greater than zero ...That means that it is very difficult to find a suitable value for h_0 by comparing the surface forces with the hydrodynamics one being equal to 0...In order to get an initial position h_0, we decided to compare the surface forces to the drag force generated by the velocity of the droplets submitted to the flotability.
This first method is tested with the idea that the main part of the induction time lies in the period of time when the droplet is very close to the bubble surface, i.e. that the precision of h_0 is not so important in the calculation of the induction time by equation 3.24. To define this thickness, a drag force is artificially created, taking into account the velocity of the droplet (induced by flotability), while it should follow the flow line as it behaves as a tracer. This means that the droplets no longer have

the velocity of the fluid. The hydrodynamic force can therefore be expressed as the drag force (equation 3.25).

$$F_{drag} = 3\pi\mu_f d_b(1 + 0.15Re_p^{0.687})(V_{d,r}) \tag{3.25}$$

In this expression, $V_{p,r}$ is the radial component of the droplet rising velocity (equation 3.26).

$$V_{d,r} = \frac{\left(\frac{d_d}{2}\right)^2 g(\rho_f - \rho_d)}{9\mu_f} cos\theta \tag{3.26}$$

θ present in these equations represents the angular position of the droplet.

Technically, we now have all the parameters to calculate the induction time. However, it can be interesting to see how the initial thickness h_0 evolves with viscosity and droplet diameter. This evolution is shown in figure 3.5. Figure 3.5 shows

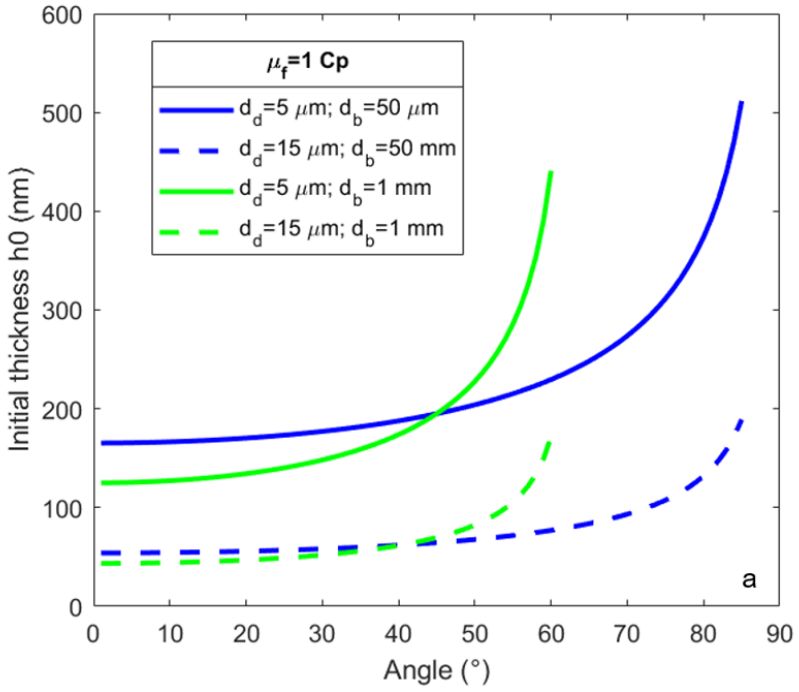

Figure 3.5: Evolution of h_0 function of the angular position for 1Cp

the evolution of h_0 as a function of angular position in permuted water, i.e. at 1 Cp. To have this dependence on angular position, h_0 is calculated at each potential angle of collision.The green curves show its evolution for a milimetre bubble and the blue ones for a $50\mu m$ bubble. We can then see that the larger the bubble, the

lower h_0 is.The line style shows the effect of the drop size on h_0. The discontinuous one is for $15\mu m$ and the continuous one for $5\mu m$. It shows that the droplet size has the same effect as the bubble size. In fact, the larger the droplet, the lower the h_0. These curves also show that h_0 has a plateau value before increasing drastically as the angle gets closer to the maximum collision angle (when the droplet starts to move away from the bubble). This can be explained by the fact is that near this angle the velocity of the fluid increases and the hydrodynamic force is stronger than in the previous part of the trajectory. It was decided to take the value of h_0 at the value of the plateau. These values are given in the table 3.3.

Furthermore, figure 3.6 shows the evolution of h_0 for a water viscosified at 2 Cp.

d_b (μm) \ d_d (μm)	1	15
50	243 nm	87 nm
1000	125 nm	43 nm

Table 3.3: Values of h_0 in water at 1 Cp

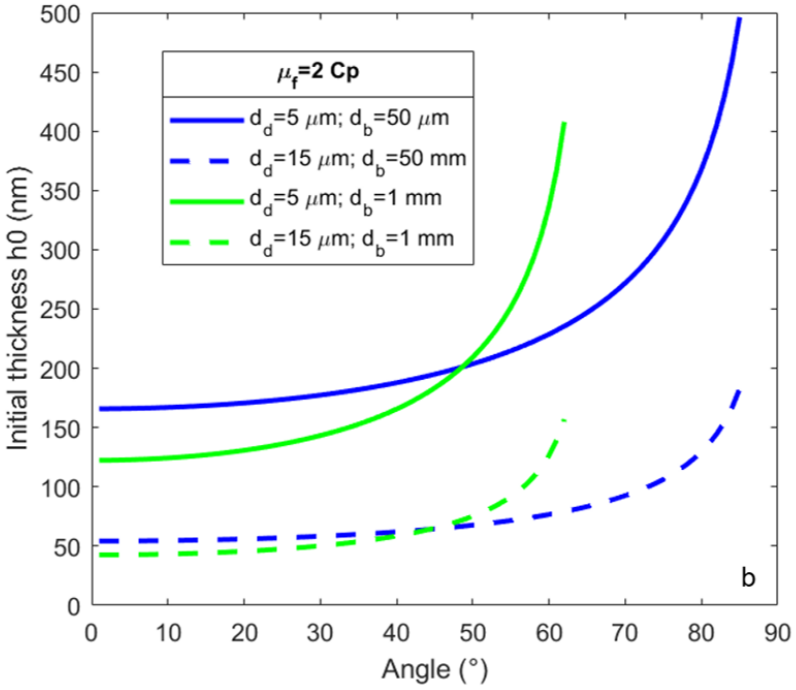

Figure 3.6: Evolution of h_0 function of the angular position for 2 Cp

It appears that as the viscosity increases, the value of h_0 decreases. This decrease

is very small as the table 3.4 shows when the viscosity is multiplied by 2.

d_b (μm) \ d_d (μm)	1	15
50	165 nm	54 nm
1000	122 nm	42 nm

Table 3.4: Values of h_0 in water at 2 Cp

Now that we have all the expressions for the calculation and an idea of the evolution of the h_0 function of all our parameters, we can look at the evolution of the induction time.

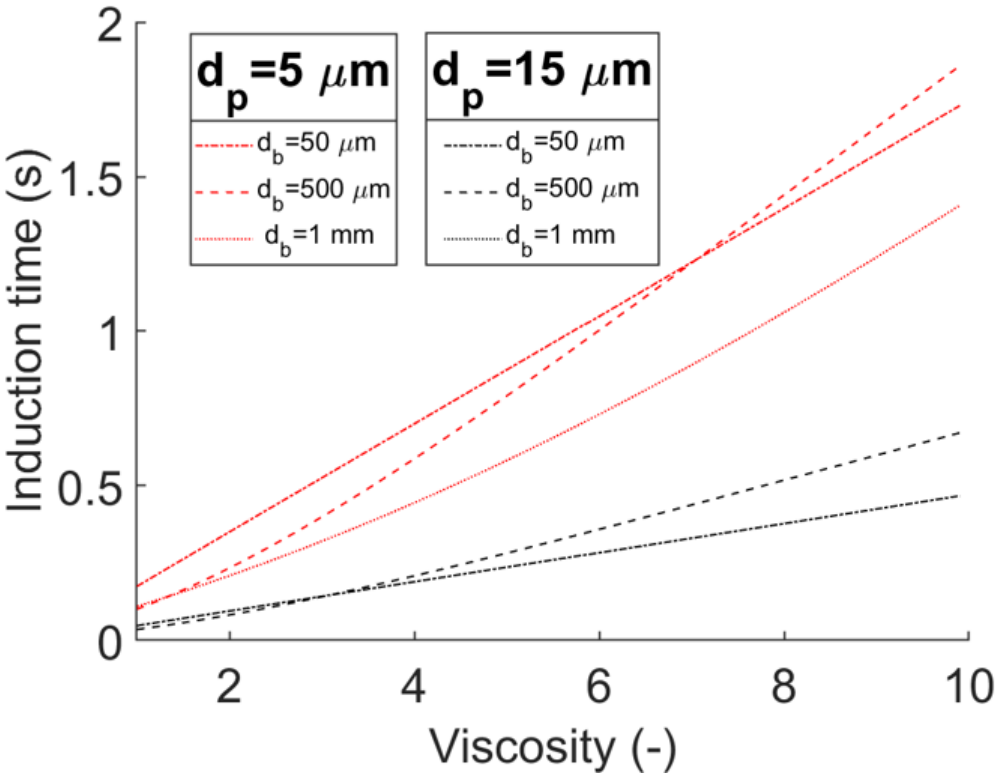

Figure 3.7: Evolution of the induction time t_i function of adimensionnal viscosity for different size of bubble and droplet

Figure 3.7 shows the evolution of the induction time function of an adimensionnal viscosity (viscosity divided by that of water) for different situations. First in red is the evolution of t_i for $5\mu m$ droplets. This induction time goes from a hundred milliseconds to around a second or two when the viscosity is multiplied by 10. It can be seen that for low viscosities, the larger the bubble, the shorter the induction time. However, for intermediate bubbles (bubbles around 500 μm) this trend tends

to reverse as the viscosity becomes higher (around 7 Cp). This means that for this particular bubble size, attachment should be less likely at this viscosity. Looking at the black curve, for $15\mu m$ droplets the same observation can be made as for $5\mu m$ droplets. However, the viscosity at which the intermediate bubble induction time becomes greater than that for smaller bubbles occurs earlier (around 3 Cp). The fact that the larger the droplet, the more likely it is to adhere. In fact, the sliding time, which is mainly due to hydrodynamics, is not really modified by a change in droplet size.

We have shown that the induction time is highly dependent on viscosity and droplet size. The higher the viscosity, the longer the induction time. Conversely, the larger the droplet or bubble, the shorter the induction time. Except for intermediate bubbles, where at a certain viscosity the induction time starts to be much higher than for smaller bubbles. However, the effect of bubble size on induction time is strongly dependent on particle size. In fact, the larger the droplet, the smaller the effect of bubble size. This reduction in induction time with increasing droplet size is also found experimentally in several studies [Nguyen et al., 1998, Ye et al., 1989, Yoon and Yordan, 1991].

Basically, we have shown that the induction time increases as the viscosity increases and as the size of particles (bubbles or droplets) acting on the film decreases. As there is a close relationship between the attachment efficiency and the induction time, let us see if the same trend can be found for the attachment efficiency.

2.2.2 Attachment efficiency

The attachment efficiency is calculated from the Nguyen attachment model and is essentially a function of the ratio of the induction time to the sliding time (equation 3.8).

$$E_A = sech^2\left(\frac{t_i}{t_s}\right)$$

This equation is based on several hypotheses:

- Droplet velocity, much lower than bubble velocity, is neglected
- Droplets behave as tracers and follow the flow line, their inertia is neglected
- Bubble surface is contaminated, behaves like a solid sphere
- Fore-and-aft symmetry situation

However, in most of the cases studied here, the latter is not verified and, as already mentioned, in order to calculate the induction time, we have suppressed the fact that the droplets behave as tracers. The results shown below are therefore not in the limit of the application of the model, but allow us to have a first idea of the evolution of the attachment efficiency.

As with collision efficiency and induction time, attachment efficiency E_A is strongly influenced by bubble diameter d_b and droplet diameter d_d. Indeed, Table 3.5 and Table 3.6 show that attachment efficiency varies with bubble and droplet size, but this evolution does not seem monotone. For very small droplets ($1\mu m$) attachment seems to increase as the bubble size increases. However, for larger droplets it seems to decrease first before increasing with bubble size. In fact, in the DAF mode (for bubbles smaller than 200 μm), the attachment efficiency tends to decrease as the bubble size increases. However, the opposite phenomenon is observed for the IAF mode. The attachment efficiency increases with the bubble size. This could be explained by the fact that the larger the bubble, the shorter the induction time. Therefore, the ratio of induction time to sliding time is lower and therefore the hyperbolic secant is smaller for larger bubbles. This means that the more likely it is for attachment to occur.
In addition, attachment efficiency tends to be lower for small droplets in DAF mode. This effect of droplet size tends to be attenuated and even reversed as the bubble size increases (and more generally in IAF mode). This phenomenon is also explained to some extent by the variation in induction and sliding time. In fact, as the droplet diameter increases, the induction time decreases, reducing the probability of droplet attachment.

d_b (μm) \ d_d (μm)	1	15	30
50	3.3×10^{-1}	7.0×10^{-1}	9.8×10^{-1}
500	6.1×10^{-1}	6.2×10^{-1}	7.1×10^{-1}
1000	7.6×10^{-1}	7.5×10^{-1}	7.9×10^{-1}

Table 3.5: Values of attachment efficiency in water at 1 Cp

d_b (μm) \ d_d (μm)	1	15	30
50	3.2×10^{-1}	6.9×10^{-2}	9.8×10^{-1}
500	4.7×10^{-1}	4.6×10^{-1}	5.7×10^{-1}
1000	6.6×10^{-1}	6.4×10^{-1}	7.1×10^{-1}

Table 3.6: Values of attachment efficiency in water at 2 Cp

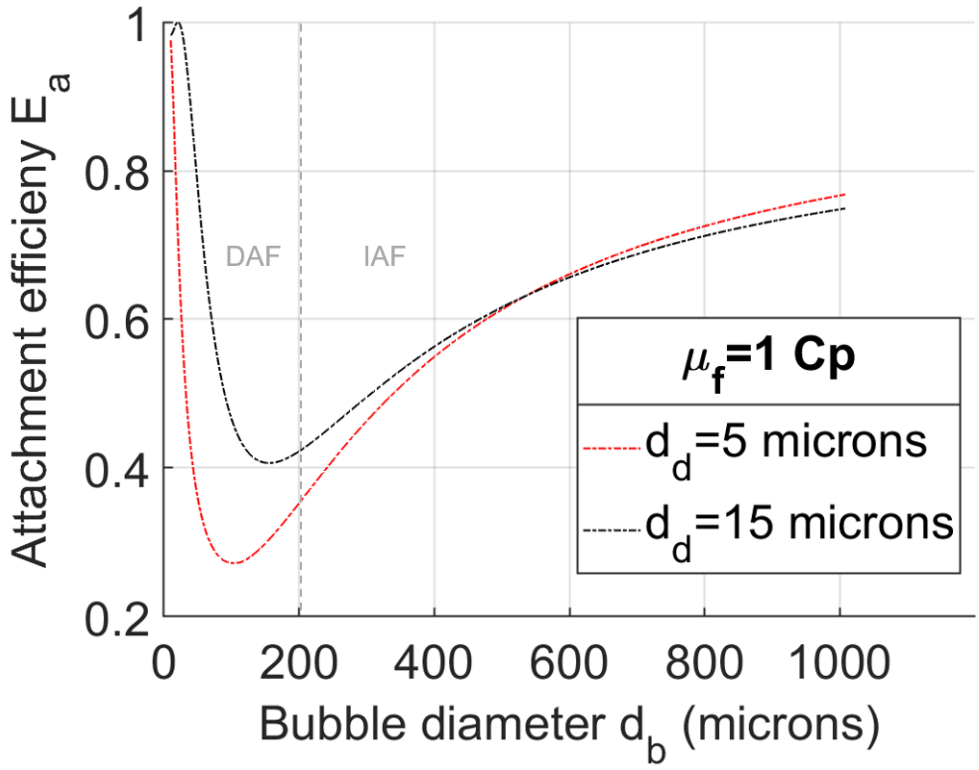

Figure 3.8: Evolution of the attachment efficiency function of bubble diameter for two droplet size (5 & 15 μm) in fresh water

It can then be said that the effect of viscosity on attachment efficiency depends on both bubble and droplet size ranges. Tables 3.5 & 3.6 shows that attachment efficiency tends to decrease with increasing viscosity.

However, this variation in attachment efficiency needs to be qualified. To do this, figure 3.9 shows the evolution of the attachment efficiency function of bubble size for a 5 μm droplet and three viscosities (one for permuted water 1 Cp, two for viscosified water 2 & 5 Cp).

This figure shows that in DAF mode (considering a mean diameter of 50μm) the viscosity has almost no effect (loss of less than 3% when the viscosity is multiplied by 5). However, for large bubbles in the IAF range, the effect of viscosity is much greater. In fact, a drop in attachment efficiency of more than 85% is observed when the viscosity is multiplied by a factor of 2. This drop in efficiency becomes more significant as viscosity increases.

Therefore, the effect of viscosity on attachment efficiency also depends mainly on bubble and droplet size. In terms of collision efficiency, the larger the bubble, the greater the effect of viscosity on attachment efficiency. This logically leads to a

decrease in entrainment efficiency with increasing viscosity.

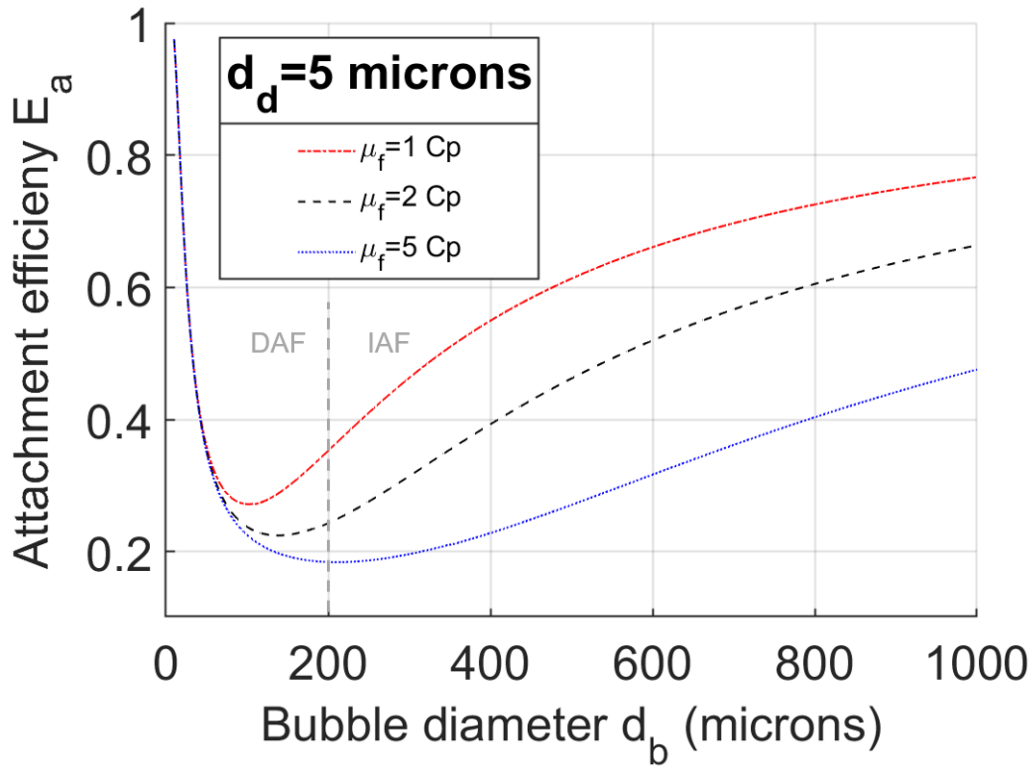

Figure 3.9: Evolution of the attachment efficiency function of bubble diameter for a $5\mu m$ droplet in various water viscosity

2.3 Impact of viscosity and particles size on capture efficiency

As capture efficiency is the product of collision and attachment efficiencies, its evolution should logically follow the same trends. Looking at the results shown in table 3.7 and 3.8, it is possible to see that the capture efficiency E_{capt} actually shows the same trends. In fact, its evolution is strongly influenced by the droplet and bubble diameters.

d_b (μm) \ d_d (μm)	1	15	30
50	4.1×10^{-3}	7.9×10^{-2}	4.2×10^{-1}
500	2.9×10^{-4}	2.6×10^{-3}	1.2×10^{-2}
1000	1.6×10^{-4}	1.4×10^{-3}	6.1×10^{-3}

Table 3.7: Values of capture efficiency in water at 1 Cp

d_b (μm) \ d_d (μm)	1	15	30
50	3.9×10^{-3}	7.7×10^{-2}	4.2×10^{-1}
500	1.5×10^{-4}	1.3×10^{-3}	6.6×10^{-3}
1000	9.5×10^{-5}	8.3×10^{-4}	3.6×10^{-3}

Table 3.8: Values of capture efficiency in water at 2 Cp

Figure 3.10 shows the variation of capture efficiency as a function of bubble diameter for two droplet sizes (5 & 15 μm). This figure shows that the effect of droplet size on capture efficiency varies in the same way as collision efficiency. As the droplet diameter increases, the capture efficiency increases.
Similarly, the effect of bubble size on the capture efficiency mainly follows the collision efficiency as the capture efficiency decreases across the bubble range. As the bubble diameter increases, the capture efficiency tends to decrease. This effect of bubble diameter on capture efficiency was demonstrated experimentally by Anfruns and Kitchener in 1977 [Dobby and Finch, 1987].
Thus, collision efficiency appears to be the critical step in capture. This may explain why collision has been studied more than adhesion. It is also interesting to note that the effect of bubble size seems to be more important for the DAF unit than for the IAF one. In fact, the capture efficiency is divided by more than 1000 when the droplet diameter goes from 10 to 200 μm, but only by 5 when the diameter goes up to 1 mm.

Tables 3.7 and 3.8 also show that the capture efficiency tends to decrease with increasing viscosity.

As with collision and adhesion, it is necessary to quantify the effect of viscosity on capture efficiency. To do this, the capture efficiency function of bubble size has been plotted (Figure 3.11) for 5 micron droplets and three viscosities (one for permuted water 1 Cp, two for viscosified water 2 & 5 Cp). This figure shows that in DAF mode for bubbles less than 200 μm, viscosity has almost no effect. In DAF mode the average bubble is often around 50 to 70 μm, the increase in viscosity is then completely negligible with a variation of less than 5% when the viscosity is multiplied by five. It is important to note that for a flotation unit operating in DAF mode, 200 μm bubbles are not very present. But for this worst case scenario, multiplying the viscosity by 5 induces a variation of around 40% of the separation efficiency. However, in the IAF range, for millimetre-sized bubbles, the effect of viscosity is much more important. In fact, multiplying the viscosity by 2 reduces the capture efficiency by 50% and this effect becomes more important as the viscosity increases.

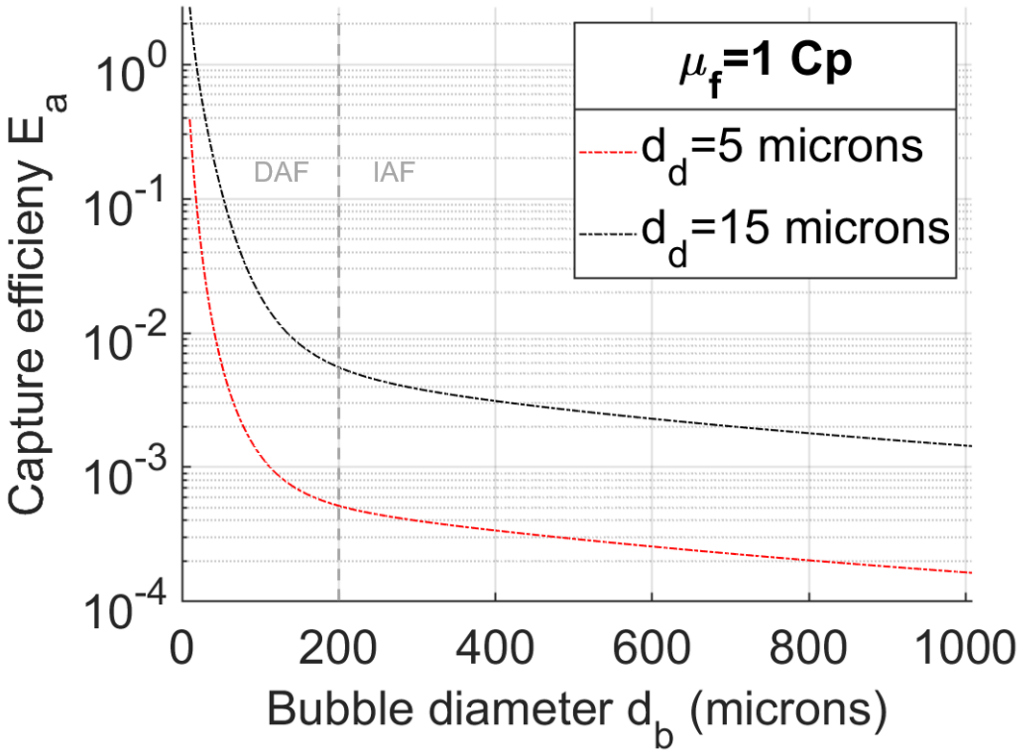

Figure 3.10: Evolution of the capture efficiency function of bubble diameter for two droplet size (5 & 15 μm) in fresh water

We have shown here that the effect of viscosity on HPAM depends mainly on bubble size. Indeed, for the small bubbles as in DAF mode, viscosity has almost no effect on the capture efficiency, whereas for the millimetre bubble as in IAF mode, its effect is huge. The overall effect of viscosity tends to reduce the capture efficiency. These trends can also be observed for collision and attachment efficiency. We have also found these trends in the literature for the effect of bubble and droplet size on capture efficiency. The larger the bubble, the lower the capture efficiency. The opposite is true for droplets; the larger the droplets, the more efficient the capture. However, the effect of HPAM is not just an increase in viscosity, it can also change physico-chemical properties.

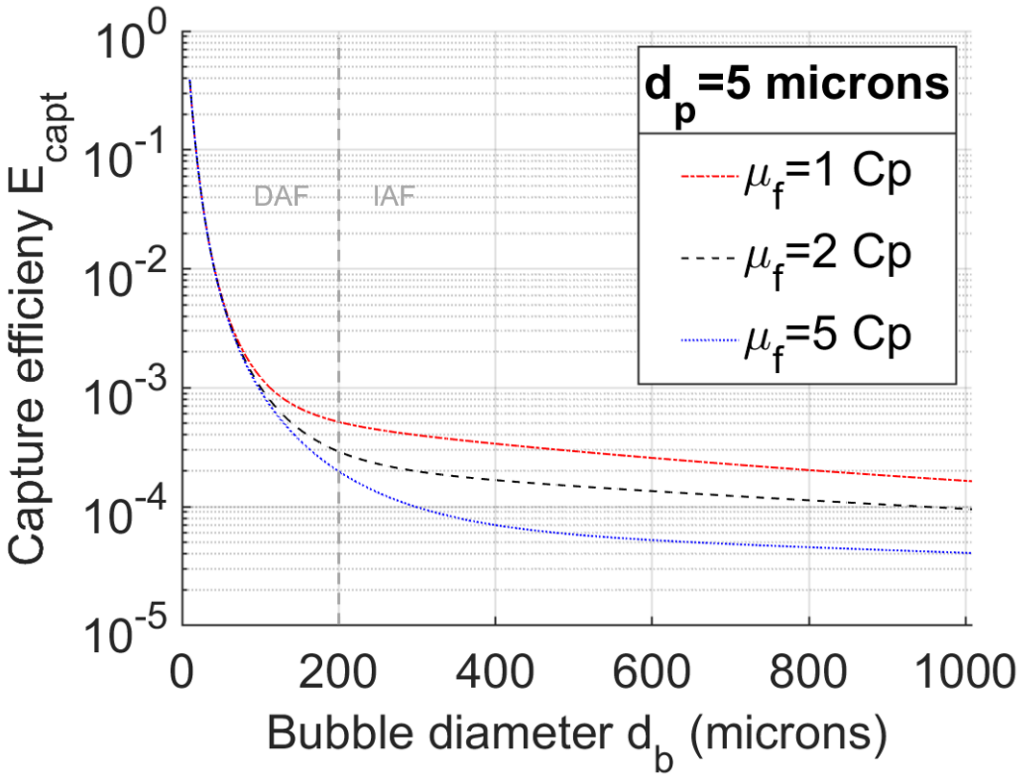

Figure 3.11: Evolution of the capture efficiency function of bubble diameter for a $5\mu m$ droplet for various water viscosity

3 Impact of HPAM on capture efficiency : other polymer effects

The presence of polymer and even salts in the brine can have an effect on the capture efficiency other than viscosity. In fact, as seen in the experimental part, the polymer also modifies the conductivity of the solution and thus the ionic strength. A modification of the ionic strength, either by the presence of polymer or salts, has an effect on the capture efficiency by modifying the electrostatic force and thus the induction time. HPAM can also modify other physico-chemical properties that affect the attachment efficiency, such as the surface tension between different phases, the zeta potential or even the Hamaker constant. Such parameters affect adhesion efficiency by modifying electrostatic or van der Waals forces or even the critical film thickness at which the film breaks.

The effect of changing the surface tension on the deposition efficiency is studied first, then the effect of changing the zeta potential, and finally the effect of changing the ionic strength. The effect of varying the Hamaker constant on the capture efficiency

is not studied as no data have been found on the effect of HPAM on it.

3.1 Surface tension variation

Surface tension is a key parameter in several physical phenomena, including flotation. Indeed, the attachment phase shows a dependence on it through the critical thickness calculation h_{cr} (equation 3.23).

However, according to [Chakibi, 2017], the presence of HPAM does not affect the surface tension between air and water. Surface tension measurements were therefore carried out with a du Noüy ring to confirm these results at our concentrations and with our polymer. Table 3.9 shows the variation of surface tension as a function of water type. These results show that the presence of the polymer does not affect the surface tension between air and water. However, it does have a small effect on the oil/water surface tension. Since only the surface tension between water and air

Kind of water / Interfaces	Deionized	Viscosified
Water/air	71 mN/m	71 mN/m
Oil/water	28 mN/m	30 mN/m

Table 3.9: Values of surface tension in deionized and viscosified water

plays an explicit role in the capture efficiency, it can be concluded that the presence of a polymer has no effect on the capture efficiency via the surface tension.

3.2 Ionic strength modification

3.2.1 Ionic strength range in presence of HPAM or salts

Firstly, according to measurements made prior to the flotation experiments (results shown in Chapter 2, Table 2.2), conductivity is multiplied by 4 when HPAM is added to deionised water. Since conductivity is closely related to ionic strength, an increase in conductivity also means an increase in ionic strength. As mentioned above, this change in ionic strength has a direct effect on the attachment efficiency by changing the electrostatic force and thus the induction time. However, the conductivity remains in the order of $\mu S/cm$.

In the case studied experimentally and numerically, the emulsion consists of brine with polymer and oil; the presence of brine containing salts has a much greater influence on ionic strength and conductivity than the polymer. Indeed, as the results presented in the experimental part table 2.2 shows, in the presence of salts, the conductivity order of magnitude changes to the mS/cm, so is more than 100 times

greater. Therefore, the study presented in this part shows the effect of an increase in ionic strength, mainly due to the presence of salts which is easy to calculate, meanwhile the one due to HPAM remains difficult to access without the exact knowledge of the charges but stays lower than the charge due to salts. The ionic strength is calculated as follows:

$$I = \frac{1}{2}\sum_i C_i z_i^2 \tag{3.27}$$

In our brine with a salt mixture equivalent to a solution of 6 g/L of NaCl, the ionic strength has a value of 0.12 mol/L.
The fact that the ionic strength increases in presence of HPAM or even more of salts imply a reduction of the electrostatic force due to a screen effect. The presence of charged component in the water screens the charges present at the bubble and droplet surface. This reduced the electrostatic force range of action allowing theoretically an easier drainage of the film and thus a smaller induction time. Basically, the presence of salts and in a lesser extent HPAM should enhanced the attachment step. If charges have the same sign.

3.2.2 Effect of ionic strength on flotation

Several studies have been carried out on the effect of salts on the recovery efficiency or on even the flotation process. These studies mainly show the effect of salts on bubble size and flotation efficiency considering the whole process. In fact, as already mentioned in the experimental part, in the presence of salts or with an increase in ionic strength, the bubble size is smaller than in fresh or permuted water. [Fanaie and Khiadani, 2020] try to explain this by the way the bubbles are generated. Bubbles are generated in DAF mode by a sudden depressurisation of the water. This is done by cavitation, which creates a bubble nucleus. If this nucleation is considered to be homogeneous, the diameter of the bubble nucleus can be given by the following formula [Edzwald, 2010]

$$d_{b,crit} = \frac{4\sigma_{water}}{P_{pressurisation} - P_{atm}} \tag{3.28}$$

This nuclei size is not dependent on salts or HPAM concentration, as the surface tension is not significantly modified (at least for our concentrations, see paragraph 3.1). The difference in bubble size distribution can then be explained by their growth, which is due to several phenomena. The main phenomenon influencing the bubble size is the coalescence of the nuclei or of the bubbles generated.
This effect of ionic strength on the bubble size has a direct effect on capture efficiency

as already explained in paragraph 2.3: the increase of ionic strength decreases the bubble size and, all other parameters being constant, increases the capture efficiency.

Furthermore, the coalescence depends on exactly the same parameters as the attachment. In fact, the coalescence of two bubbles is basically equivalent to the draining of a liquid film present between them. [Cain and Lee, 1985] shows experimentally that the rupture thickness of this film decreases with increasing salt concentration. This means that bubbles are less likely to coalesce. This result should be similar for the film between the bubble and the oil droplet. This means that the induction time should increase and the attachment efficiency should decrease as the ionic strength increases.

3.2.3 Direct influence of ionic strength on capture efficiency

Ionic strength does not play any role on collision so it has no effect on collision efficiency E_{col}. However, ionic strength changes the physico-chemical condition and plays a role on attachment.
Concretely, ionic strength have an impact on electrostatic force range and magnitude. So an increase in ionic strength (which is the case in brine or when HPAM is added), leads to a decrease of electrostatic force F_{elec}. This mean that the F_{elec} can be neglected when compared to the Van der Waals force F_{VdW}.

If the electrostatic force is neglected then the resultant of surface force. Thus the Taylor velocity V_{Taylor} (equation 3.21), being proportional to this resultant, increases. The drainage of the liquid film between the droplet and the bubble should therefore be faster and the induction time t_i shorter.

3.3 Zeta potential variation

As for the ionic strength, the zeta potential has an effect on the electrostatic force and the adhesion time. [Chakibi et al., 2018] has studied the evolution of the flotation efficiency as a function of the variation of the zeta potential (due to the presence of salts). He shows that as the absolute value of the zeta potential decreases, the flotation efficiency increases. This is explained by the fact that a reduction in this absolute value leads to a reduction in electrostatic repulsion. This reduction allows easier attachment between the bubble and the droplet. This ultimately leads to an increase in the separation efficiency and therefore the efficiency of the whole installation.

Experimental studies carried out by [Deng et al., 2002] or [Li et al., 2007] (Figure 3.12) show that the zeta potential at the surface of the droplet decreases in the presence of the polymer. In our case, measurements of zeta potential, with the material present in the laboratory, were not possible due to the high salts concentration. The decrease in zeta potential (according to figure 3.12) in the presence of polymer

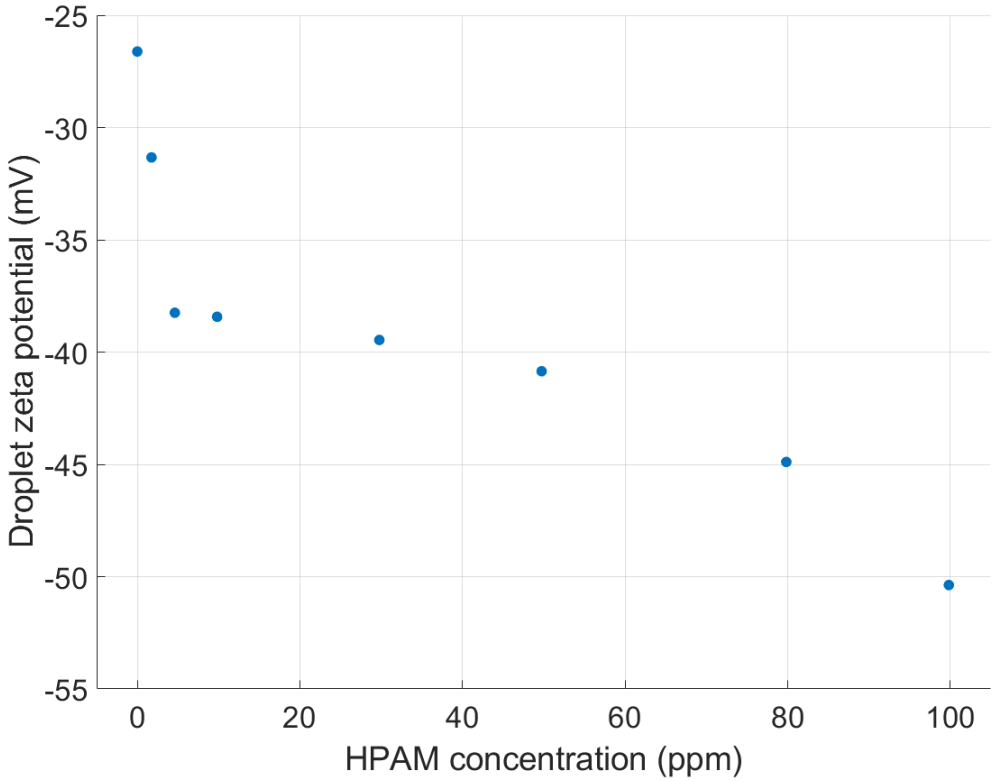

Figure 3.12: Evolution of zeta potential at the surface of the droplet function of HPAM concentration [Li et al., 2007]

combined with the observation of Chakibi allows to conclude that the presence of HPAM leads to a decrease in the capture efficiency.

4 Conclusion

Nguyen's theory of capture efficiency has allowed us to get a first impression of the effect of HPAM collision, attachment and capture efficiency. The effect of this polymer through viscosity depends mainly on the size of the bubble or droplet. For very thin bubbles, viscosity has little or no effect on any of these efficiencies. However, for larger bubbles such as millimetric ones, an increase in viscosity will generate a decrease in all of the efficiencies.

Furthermore, an increase in bubble size generally leads to a decrease in collision and capture efficiency. This is also verified for very thin bubbles such as in DAF mode for attachment, but for bubbles in IAF mode the trend is reversed and attachment efficiency tends to increase.
Overall, collision, attachment and capture efficiencies decrease as droplet size decreases.
Modification of physico-chemical parameters such as zeta potential, ionic strength or surface tension in the presence of polymer seems to have very little effect on the capture efficiency. In fact, the surface tension is not modified by the presence of HPAM. In industrial water, the presence of salt is the main component of the ionic strength, so the presence of polymer has no effect on it. If the ionic strength is drastically reduced, our method for calculating the induction time no longer works. Thus, capture seems to be impossible (but this is outside the scope of our study). The only physico-chemical parameter that could have a real impact on the attachment or capture efficiency is the zeta potential, which decreases in the presence of HPAM. This means that the electrostatic force is reduced and capture or attachment should be easier.

However, there are several problems with this way of calculating attachment and capture efficiency. Some assumptions that Nguyen made to create it are verified, but the anterior-posterior symmetry is not verified in all situations and we suppress the one that considers the particle velocity negligible to create a drag force that allows us to calculate h_0. Therefore, new modelling methods are proposed in the following chapter.

Conclusion

La théorie de Nguyen sur l'efficacité de la capture nous a permis d'avoir une première impression de l'effet de la collision HPAM, de l'attachement et de l'efficacité de la capture. L'effet de ce polymère à travers la viscosité dépend principalement de la taille de la bulle ou de la gouttelette. Pour les bulles très fines, la viscosité n'a que peu ou pas d'effet sur l'une ou l'autre de ces efficacités. Cependant, pour les bulles plus grosses, telles que les bulles millimétriques, une augmentation de la viscosité entraînera une diminution de toutes les efficacités.
En outre, une augmentation de la taille des bulles entraîne généralement une diminution de l'efficacité de collision et de capture. Ceci est également vérifié pour les bulles très fines comme en mode DAF pour l'attachement, mais pour les bulles en mode IAF la tendance est inversée et l'efficacité de l'attachement tend à augmenter.

Dans l'ensemble, les efficacités de collision, d'attachement et de capture diminuent à mesure que la taille des gouttelettes diminue.
La modification des paramètres physico-chimiques tels que le potentiel zêta, la force ionique ou la tension de surface en présence de polymère semble avoir très peu d'effet sur l'efficacité de capture. En effet, la tension de surface n'est pas modifiée par la présence de HPAM. Dans l'eau industrielle, la présence de sel est la principale composante de la force ionique, et la présence de polymère n'a donc aucun effet sur celle-ci. Si la force ionique est drastiquement réduite, notre méthode de calcul du temps d'induction ne fonctionne plus. Le capture semble donc impossible (mais cela sort du cadre de notre étude). Le seul paramètre physico-chimique qui pourrait avoir un réel impact sur l'efficacité de l'attachement ou de la capture est le potentiel zêta qui diminue en présence de HPAM. Cela signifie que la force électrostatique est réduite et que la capture ou l'attachement devrait être plus facile. L'effet des paramètres physico-chimiques qui n'ont pratiquement aucun effet ne sera pas étudié par la suite.

Cependant, cette façon de calculer l'efficacité de l'attachement et de la capture pose plusieurs problèmes. Certaines hypothèses formulées par Nguyen pour la créer ne sont pas vérifiée. La symétrie antéro-postérieure n'est pas vérifiée dans toutes les situations et nous supprimons celle qui considère que la vitesse des particules est négligeable pour créer une force de traînée qui nous permet de calculer h_0. Une nouvelle méthode de modélisation est donc proposée dans le chapitre suivant.

Chapter 4

Impact of HPAM on flotation at bubble scale: perspectives for a new model

Notre utilisation du modèle de Nguyen présente plusieurs problèmes. Certaines des hypothèses de ce modèle ne sont pas valables dans notre façon d'effectuer les calculs. Dans notre cas, la vitesse des particules n'est plus négligée par rapport à celle du fluide. Elle est utilisée pour générer une force de traînée, ce qui nous permet de modéliser notre épaisseur initiale de film h_0. Sans cela, il est impossible de calculer le temps d'induction (et donc l'efficacité de l'attachement). De plus, l'hypothèse de la symétrie avant-arrière de l'écoulement autour de la bulle n'est pas valable dans tous les cas.
L'objectif est ici de voir l'impact de la viscosité en développant un modèle plus précis, afin de vérifier les tendances obtenues dans le chapitre précédent.

Our use of Nguyen's model presents several problems. Some of the assumptions of this model are not valid in our way of performing the calculations. In our case, particle velocity is no longer neglected. It is actually used to calculate a drag force, enabling us to model our initial film thickness h_0. Without this, it is impossible to calculate the induction time (and thus the attachment efficiency). What's more, the fore-and-aft symmetry is not valid when Re_b becomes greater than 1.
The aim here is to see the impact of viscosity on a more accurate model, in order to verify the trends obtained in the previous chapter.

1 A complete deconstruction of existing model

We have seen that the capture efficiency E_{capt} is traditionally seen as the product of collision and attachment efficiency. However, this breakdown of capture efficiency raises an issue. If the collision efficiency is widely studied [Gaudin et al., 1942, Dai et al., 2000, Sarrot et al., 2005, Huang, 2009, Basaová et al., 2010, Schulze, 1989, Nguyen-Van and Kme, 1994, Nguyen et al., 1998], and easily model, the study of attachment efficiency is more complex. There is currently very few studies on attachment efficiency and all are based on the definition given by Dobby & Finch [Dobby and Finch, 1987]. This definition relies on two main parameters: (i) a maximum angle of collision θ_{col} from which collision no longer occurs and (ii) θ_{cr} angle from which attachment does not occur.
To obtain this critical angle, there is 2 possibilities: (i) performing experiments (that are almost impossible for small bubble) or (ii) calculating the induction time and use its definition. However, induction time calculation relies on the definition of a film initial thickness and no source on how to define or calculate the initial thickness of the film h_0 have been found. The numerical calculation of an induction time is then difficult as seen in the previous chapter. Indeed, formulas found in the literature does not depend on viscosity [Dai et al., 1999] or depends on unknown parameters such as h_0 usually given by experimental work [Wang et al., 2005, Li, 1994, Li et al., 1990, Albijanic et al., 2010].

To address this issue, we decided to model the capture efficiency from scratch and solve the motion equation of the droplet to calculate it directly.

1.1 Model of capture derived from movement equation

To model the capture efficiency from scratch, we have decided to solve the trajectory of each droplet. Figure 4.1 shows the three possible cases:
(i) The droplet collides and is attached to the bubble if it collides before the red trajectory, the droplet is therefore captured.

(ii) The droplet collides with the bubble after the red trajectory, the droplet is not captured. Indeed, the red trajectory is the last trajectory where the droplet is captured. It allows to define r_{att}, the radius of the circular surface where all the droplets attach. This radius is define for a given initial distance d_{ini} (because the flow at a given distance from the bubble center is not vertical).

(iii) The droplet follows a stream line after the black one, and does not collide with the bubble (so cannot attach). The black trajectory is the last trajectory where the

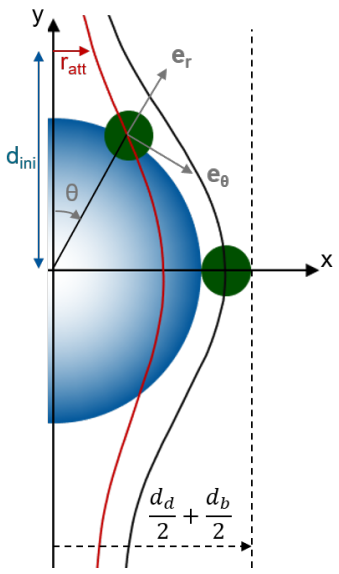

Figure 4.1: Critical droplets trajectories: trajectory of the last droplet to collide in black and the one of the last to attach or to be captured in red

droplets collide. It allows to define r_{col}, the radius of the circular surface where all the droplets collide. This radius also is defined for a given initial distance d_{ini}.

r_{col} and r_{att} allows to calculate the collision and capture efficiencies. Indeed, capture efficiency (equation 4.1) is defined as the ratio of the number of captured droplet on the number of droplets in the volume swept by the bubble. This translate into a ratio of flow rate. One going through the circular surface defined by r_{att} and the other through the one defined by the bubble and the droplet diameter.

$$E_{capt} = \frac{\int_0^{r_{att}} V_{f,y} 2\pi r dr}{\left(\frac{d_d}{2} + \frac{d_b}{2}\right) V_b} \tag{4.1}$$

To access to a droplet trajectory, we solve the droplet's equation of motion:

$$\rho_d \frac{4}{3}\pi \left(\frac{d_d}{2}\right)^3 \frac{d\mathbf{V_d}}{dt} = \sum \mathbf{F} \tag{4.2}$$

The droplet is subjected to two kinds of forces:

(i) The hydrodynamics forces representing the collisional component of capture. Those forces, independent of the film thickness, are in this work:

- The flotability (gravity effect):
  $\mathbf{F_{flotability}} = (\rho_d - \rho_f)\frac{4}{3}\pi \left(\frac{d_d}{2}\right)^3 \mathbf{g}$.

- The added mass force, inertia due to continuous phase moving with the object: $\mathbf{F_{addedmass}} = C_M \rho_f \frac{4}{3}\pi \left(\frac{d_d}{2}\right)^3 \left(\frac{D\mathbf{U_f}}{Dt}|_d - \frac{d\mathbf{V_d}}{dt}\right)$.

- The drag force: $\mathbf{F_{drag}} = \frac{C_d \rho_f \pi \left(\frac{d_b}{2}\right)^2}{2} \|\mathbf{U_f} - \mathbf{V_d}\| (\mathbf{U_f} - \mathbf{V_d})$.

In those formula, ρ_d is the density of the droplet, ρ_f is the fluid density, μ_f is the fluid viscosity, g is the earth gravity, Ω is the vorticity, U_f and V_d are respectively the fluid and droplet velocities, C_M, C_L and C_D are respectively the added mass, lift and drag coefficients.

(ii) The forces linked to the drainage of the liquid film representing the attachment component of the capture. Those forces, explicitly dependent of the liquid film thickness, are:

- The lubrication force opposed to the film draining: $\mathbf{F_{lubrication}} = -\frac{6\pi\mu_f a^2}{h} V_{p,r}$.

- The Van der Waals force, a component of the interfacial forces: $\mathbf{F_{VdW}} = -\frac{Aa}{6h^2}$

- The electrostatic force, the other component of the surface forces: $\mathbf{F_{electrostatic}} = \frac{\epsilon\epsilon_0 2\pi a\kappa \left(2\zeta_d\zeta_b exp(\kappa h) - \zeta_d^2\right)}{exp(2\kappa h) - 1}$

In those formula, h is the liquid film thickness, a is the reduced radii $\left(a = \frac{d_d d_b}{d_d + d_b}\right)$. The resultant of the Van der Waals forces depends on: (i) bubble and particle diameter, (ii) the Hamaker constant of the system (see chapter 3). The electrostatic force depends on physico-chemical properties such as ζ_b (and ζ_p) the bubble surface potential (and the particle surface potential), ϵ the solution permittivity and ϵ_0 the vacuum permittivity. The Debye constant κ reflects the presence of charges in the solution and $\frac{1}{\kappa}$ the thickness of the electrical double layer.

Other various forces can be taken into account such as steric or hydrative forces. Those forces are usually neglected [Nguyen and Evans, 2004, Hewitt et al., 1993] Hydrophobic forces should also be used but several experiments are needed to have access to integration constant and decay lengths. Therefore, it has been chosen here not to take them into account.

Once equation A.4 is written with the correct forces, the trajectory of each droplet can be found in two cases:
(i) If only the hydrodynamics forces are taken into account, the trajectory of the

droplet is then the one for collision. The droplet collides with the bubble if the distance h between the droplet and the bubble reaches zero.

(ii) If all the forces are considered, the trajectory of the droplet accounts for all mechanisms of capture. The droplet is captured by the bubble if the thickness of the liquid film h reaches its critical value h_{cr} where the film collapses.

To follow the evolution of h, equation A.4 is projected radially and becomes:

$$\rho_d \frac{4}{3}\pi\left(\frac{d_d}{2}\right)^3 \frac{dV_{d,r}}{dt} = (\rho_d - \rho_f)\frac{4}{3}\pi\left(\frac{d_d}{2}\right)^3 gcos(\theta) - C_M\rho_f\frac{4}{3}\pi\left(\frac{d_d}{2}\right)^3\frac{dV_{d,r}}{dt}$$
$$+\frac{C_D\rho_f\pi\left(\frac{d_d}{2}\right)^2}{2}\left\|U_f - V_d\right\|(U_{f,r} - V_{d,r}) - \frac{6\pi\mu_f a^2}{h}V_{p,r} - \frac{Aa}{6h^2} + \frac{\epsilon\epsilon_0 2\pi a\kappa\left(2\zeta_d\zeta_b exp(\kappa h) - \zeta_d^2\right)}{exp(2\kappa h) - 1} \tag{4.3}$$

Assuming the droplet is small enough to behave as a solid sphere, the drag coefficient follows Stokes model and can be written as:

$$C_D = \frac{24}{Re_d} \tag{4.4}$$

The drag force is then simplified as follows:

$$F_{drag} = \frac{24}{Re_d}\frac{\rho_f\pi\left(\frac{d_d}{2}\right)^2}{2}\left\|U_f - V_d\right\|(U_{f,r} - V_{d,r}) = 6\pi\mu_f\frac{d_d}{2}(U_{f,r} - V_{d,r}) \tag{4.5}$$

Then, with some reorganization, equation 4.3 becomes:

$$\frac{dV_{d,r}}{dt} + \frac{9\mu_f\left(\frac{a^2}{h} + \frac{d_d}{2}\right)}{2\left(\frac{d_d}{2}\right)^3(\rho_d + C_M\rho_f)}V_{d,r} = \frac{\rho_d - \rho_f}{\rho_d + C_M\rho_f}gcos(\theta) + \frac{9}{2}\frac{\mu_f U_{f,r}}{\left(\frac{d_d}{2}\right)^2(\rho_p + C_M\rho_f)}$$
$$-\frac{aA}{8h^2(\rho_p + C_M\rho_f)\pi\left(\frac{d_d}{2}\right)^3} + \frac{\epsilon\epsilon_0 3a\kappa(2\zeta_d\zeta_b exp(\kappa h) - \zeta_d^2 - \zeta_b^2)}{(exp(2\kappa h) - 1)(\rho_p + C_M\rho_f)2\left(\frac{d_d}{2}\right)^3} \tag{4.6}$$

Putting it in canonical form to solve the equation analytically:

$$\frac{dV_{d,r}}{dt} + \frac{1}{\tau}V_{d,r} = \gamma \tag{4.7}$$

With τ the relaxation time (equation 4.9) and γ the part non time dependent

(equation 4.9).

$$\tau = \frac{2\left(\frac{d_d}{2}\right)^3(\rho_d + C_M\rho_f)}{9\mu_f\left(\frac{a^2}{h} + \frac{d_d}{2}\right)} \tag{4.8}$$

$$\gamma = \frac{\rho_d - \rho_f}{\rho_d + C_M\rho_f} g cos(\theta) + \frac{9}{2}\frac{\mu_f U_{f,r}}{\left(\frac{d_d}{2}\right)^2(\rho_p + C_M\rho_f)} - \frac{aA}{8h^2(\rho_p + C_M\rho_f)\pi\left(\frac{d_d}{2}\right)^3} + \frac{\epsilon\epsilon_0 3a\kappa(2\zeta_d\zeta_b exp(\kappa h) - \zeta_d^2 - \zeta_b^2)}{(exp(2\kappa h) - 1)(\rho_p + C_M\rho_f)2\left(\frac{d_d}{2}\right)^3} \tag{4.9}$$

$V_{d,r}$ have then the following form (with the initial radial velocity $V_{d,r,ini}(h,\theta)$ given by the approximate flow field resolution given by Nguyen [Nguyen and Schulze, 2004] presented in the supporting material):

$$V_{p,r} = C_1 exp\left(\frac{t}{\tau}\right) + C_2 \tag{4.10}$$

With C_1 and C_2 given by equation 4.11 and 4.12.

$$C_1 = V_{d,r,ini}(h,\theta) - \gamma\tau \tag{4.11}$$

$$C_2 = \gamma\tau \tag{4.12}$$

Now that we have the radial velocity of the droplet, it is enough to integrate the latter to obtain the radial position. Combining this integration with the one of the angular velocity obtain through COMSOL simulation, the trajectory of the droplet is obtained.

The evolution of the liquid film thickness h allows to know whether the droplet is captured or not. Capture occurs if h becomes smaller than h_c. The critical thickness is obtained from Manev et al. (equation 4.13) [Manev and Nguyen, 2005] formula for foam film. This expression depends mainly on physico chemical properties such as fluid viscosity μ_f, surface tension σ or Hamaker constant $K_{VdW} = \frac{A}{6\pi}$. It also depends on the radial velocity of the particle $V_{d,r}$.

$$h_c = \frac{0.97(k_bT)^{\frac{1}{10}}K_{VdW}^{\frac{2}{5}}}{\mu_f^{\frac{1}{5}}\sigma^{\frac{3}{10}}V_{d,r}^{\frac{1}{5}}} \tag{4.13}$$

r_{att} is then the last trajectory where h becomes smaller than h_{cr}. To find it, we simply have to calculate the variation of the thickness h function of the distance to the axis of the bubble until it reaches a trajectory where h does not go under h_{cr}. r_{att} is then the initial position of the n-1 trajectory.
Now that r_{att} is defined, we have to calculate the flow rate going through the surface

it defines.

The surface defined by r_{att}, S_{att}, is perpendicular to the y axis and set at a define distance of the bubble surface d_{ini}. This distance can vary and define where the fluid velocity along the y axis, $V_{f,y}(r,\theta)$ is calculated. Thanks to the flow field resolution done with COMSOL (see next part), we obtain $V_{f,r}(r,\theta)$ and $V_{f,\theta}(r,\theta)$, the velocities of the fluid in a polar base. $V_{f,y}(r,\theta)$ results of the projection of these two velocities in a cartesian base (equation 4.14).

$$V_{f,y}(r,\theta) = V_{f,r}(r,\theta)cos(\theta) - V_{f,\theta}(r,\theta)sin(\theta) \tag{4.14}$$

With these two parameters, the flow rate crossing S_{att} is easily given by $Q_{att} = \int_0^{r_{att}} V_{f,y} 2\pi r dr$.

We now have almost all the tools to calculate the variation of capture efficiency E_{capt} function of the viscosity or bubble and droplet size. To do this study, we still need the velocity flow field around the bubble.

1.2 Simulation of the velocity flow field around the bubble

As the behavior of the liquid around the bubble plays a huge part in our model to simulate the capture efficiency, we have decided to obtain it through simulations with the COMSOL software.

Thanks to previous study made by Dani [Dani, 2007] who performed those kind of simulations, we have an idea on how to chose our simulation domain. As shown on figure 4.2a, our domain of simulation is circular with a size depending on the bubble diameter.

Indeed, according to the recommendations of [Legendre et al., 1998, Magnaudet et al., 1995] different computational domains have been chosen depending on bubble Reynolds number. The radius of the domain r_∞ is:

- $r_\infty = 120\frac{d_b}{2}$ for creeping flows ($Re < 1$)
- $r_\infty = 60\frac{d_b}{2}$ for intermediate flows ($1 < Re < 300$)

Once the computational domain set, it has been decided to use a triangular mesh refined at the bubble surface (figure 4.2b) to best resolve what's happening at this critical place for collision or attachment study.

The classical boundary conditions used in this case are as follows (figure 4.2):

- at the inlet, a uniform velocity of V_b is imposed

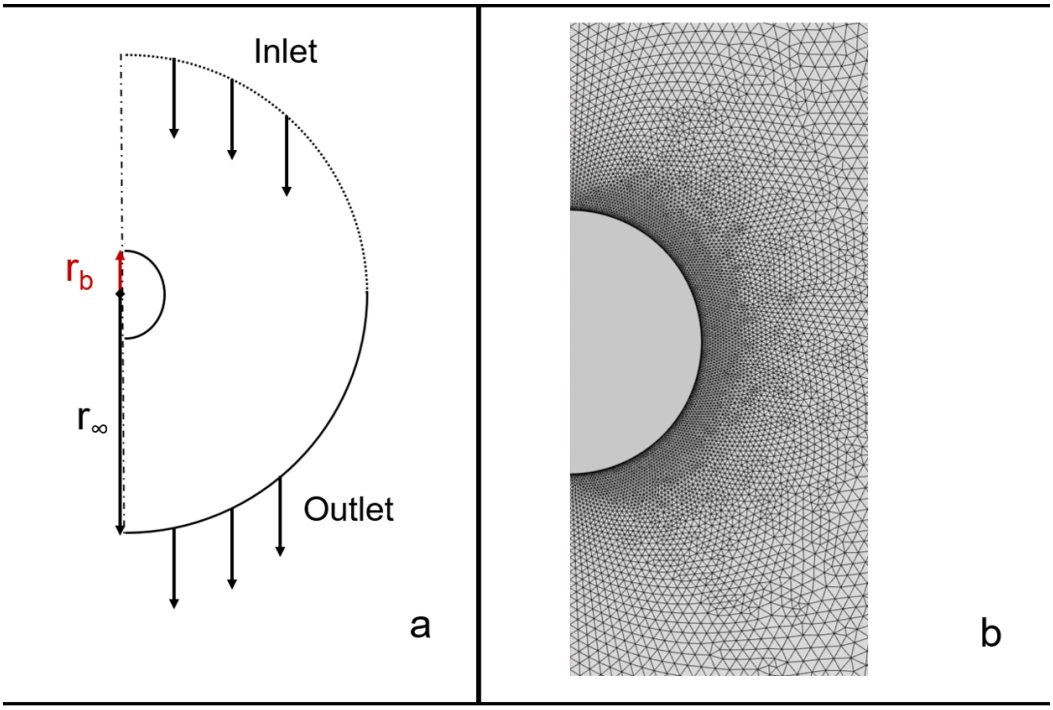

Figure 4.2: Computational domain with boundary conditions (a) and mesh (b)

- at the outlet, a pressure of zero is set
- on the bubble's horizontal axis, a symmetry condition is applied
- the surface of the bubble is considered contaminated, so $V_f = 0$

With this set up, it is possible to obtain the velocity field of the liquid around the bubble. Once obtained, this is exported to each of the mesh nodes for subsequent use in solving the droplet equation of motion.
To exploit and use it without worrying about meshing in the matlab software, it was decided to pass an interpolation function . This function (ScatterInterpolant) allows us to obtain the velocity field at any point in the simulation domain. We can thus have easily access to the velocity field and calculate droplet trajectories.

1.3 Model validation

To try and validate this new model based on the equation of motion and an initial velocity field calculated using COMSOL software, it was decided to carry out the calculations without taking into account the new forces (drainage and surface forces). In this way, we should recover the collision efficiency results from the literature as the one of Nguyen or Sarrot [Nguyen et al., 1998, Sarrot et al., 2005].

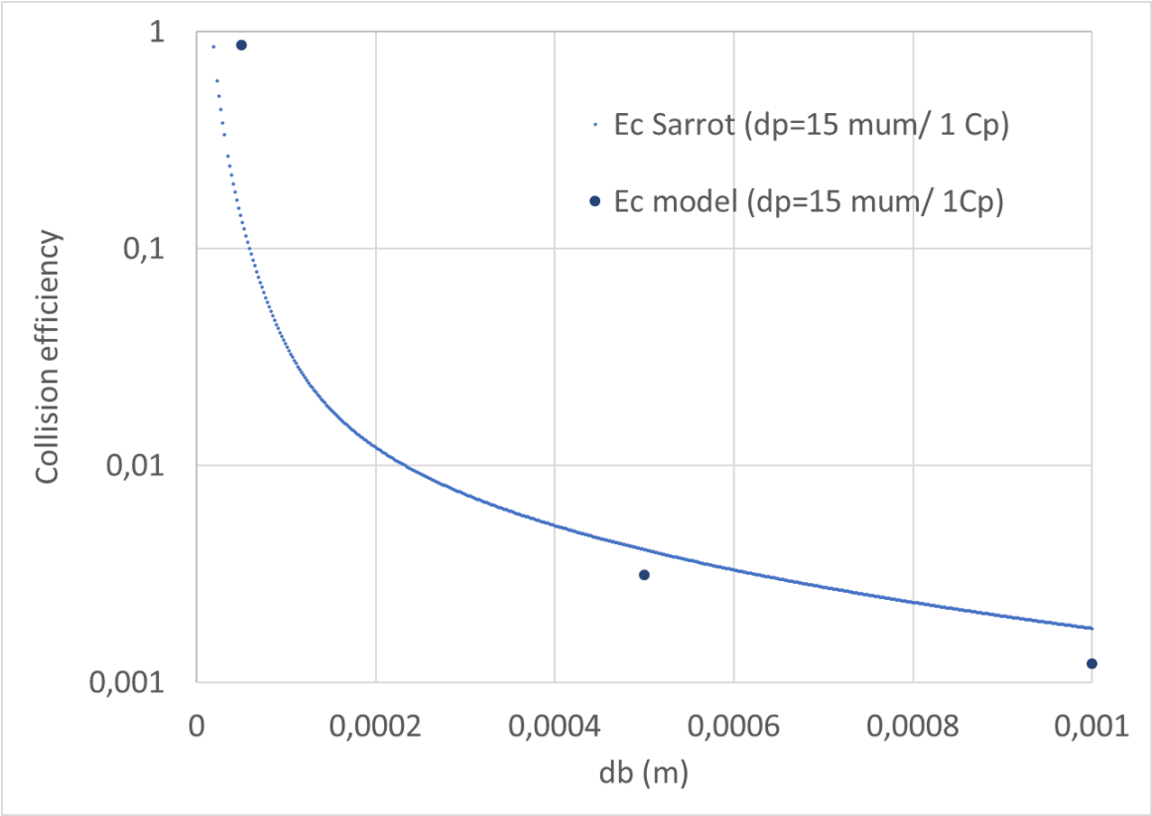

(a) E_C at 1 Cp

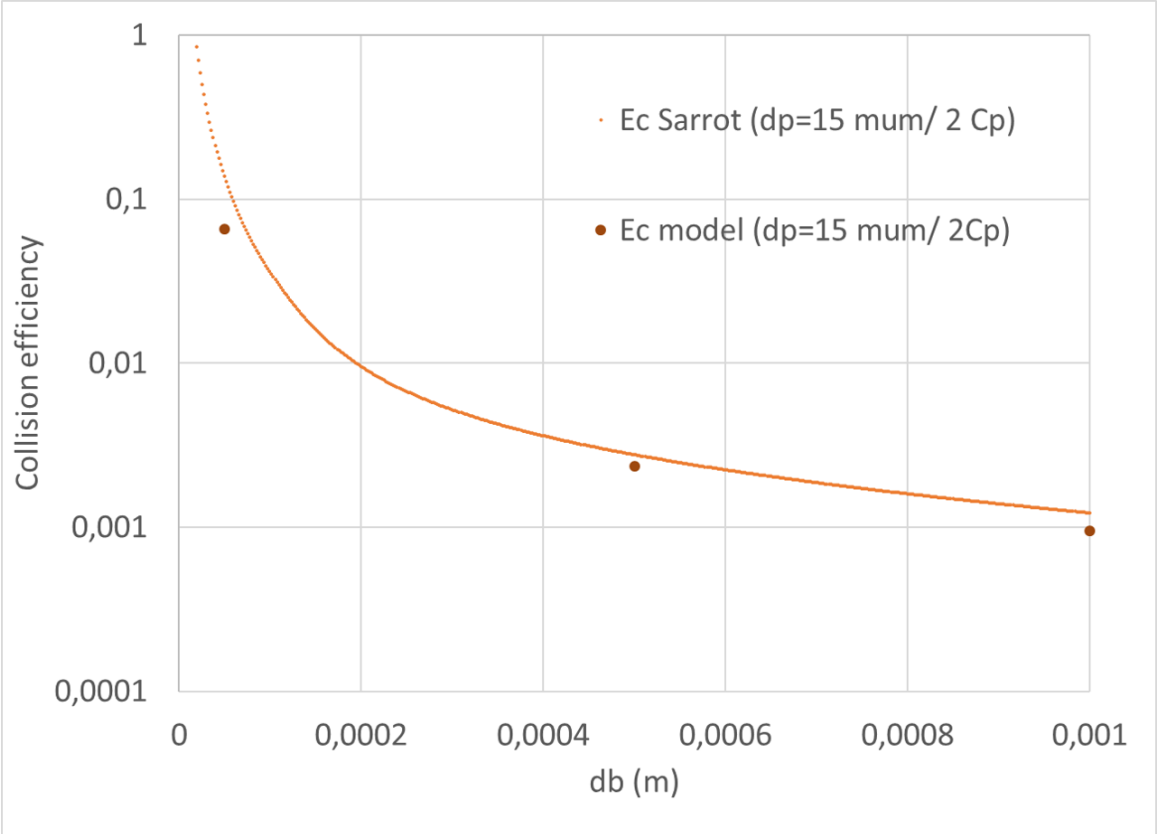

(b) E_C at 2 Cp

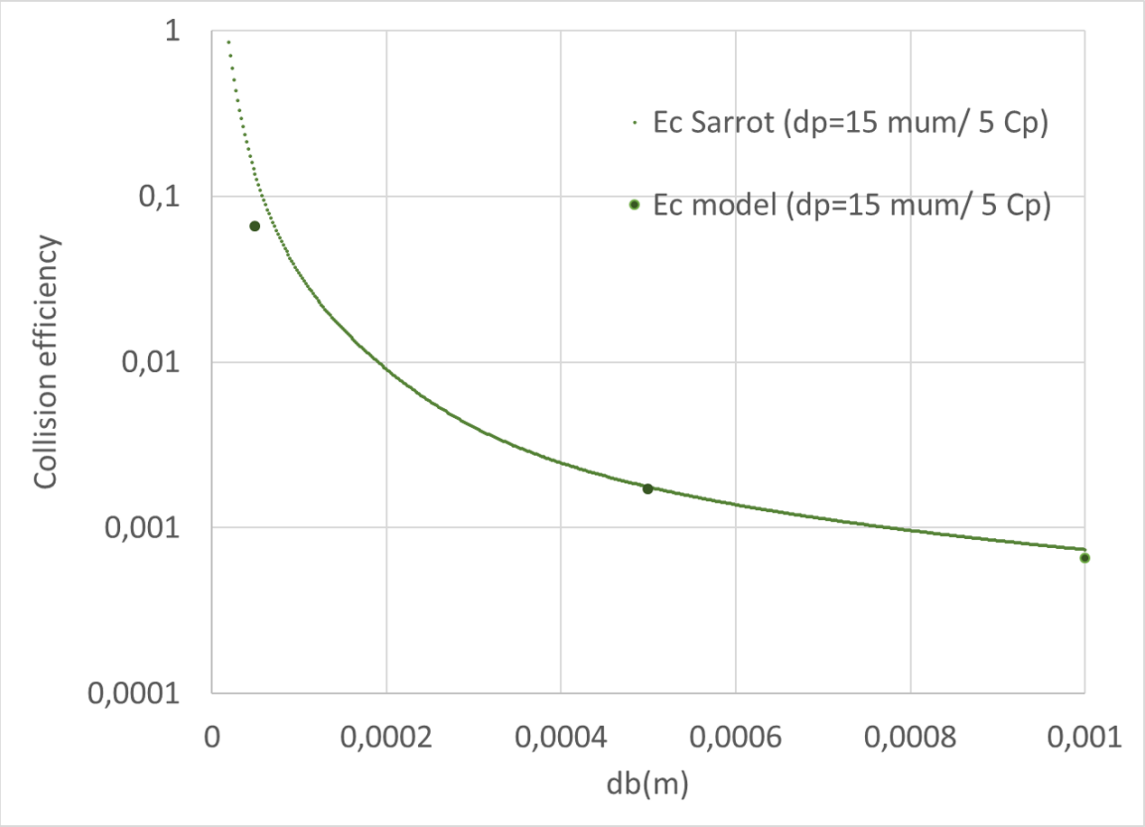

(c) E_C at 5 Cp

Figure 4.3: Comparison of our collision model with that of Sarrot for $15\mu m$ droplets and various viscosities function of bubble diameter

Figure 4.3 shows the evolution of collision efficiency for our model and Sarrot's one as a function of the bubble size for different viscosities and a $15\mu m$ droplet. This figure shows that our results are very similar to Sarrot's one for $500\mu m$ bubble with a relative difference generally around 10%. However, for this bubble size at the lowest viscosity (1 Cp) the error is a bit higher. This can be explain by the fact that at this viscosity the bubble velocity and thus the fluid velocity is the highest. The mesh might not be fine enough to solve properly the velocity variation close to the bubble surface. This issue with the mesh was not solve due to the fact that we are limited in the size file for the export. Beyond a certain number of meshes, the file cannot be exported. This can potentially cause other problems later on. One solution would be to simulate the velocity field and trajectories with the same software (in the same simulation). Unfortunately, we haven't had the time to do this.
The same problem applies to larger bubbles. The relative difference is also quite low around 10% but for the lower viscosity it goes up to 30%. Otherwise, the model seems quite reliable for large bubbles.

However, the model seems to be less reliable for smaller bubble. Once again the relative difference is bigger for lower viscosity. It goes from 500% to 50% when the viscosity goes from 1 to 2 Cp. Again the issue might be the fact that the mesh is not fine enough to capture all the phenomena near the bubble surface.

For smaller droplets, the same trend are observable. Our model is less reliable for lower viscosity and smallest bubble. The relative error is even a little bigger with $5\mu m$ droplet than for $15\mu m$ one. Nevertheless without regarding the relative error, our model results seems to be relatively close to the one in the literacy. With that in mind, we still have to see how droplets trajectories are impacted when other surfaces and drainage forces are taken into considerations.
The use of a more precise code such as the one used by Sarrot and Huang could be the best way for the future.

1.4 Impact of polymer on forces impacting droplet trajectories

Once the model is validated for collision, let see how the polymer is impacting the capture or at least the forces having an impact in the droplet trajectories. First, we will see the forces evolution in general. Then we will see the impact of HPAM on forces it impacts through droplet & bubble size, then trough the evolution of viscosity.

1.4.1 Forces evolutions & capture efficiency

As the capture efficiency depends on the critical trajectory (last trajectory where the capture is possible) of the droplet near the bubble and this trajectory depends on the forces acting on the droplet, a study of these forces can give us an idea of the evolution of the capture efficiency. As in our case such a trajectory is not found, the following results depicts the first trajectory simulated.

Figure 4.4 shows the variation of all forces acting on the droplet function of the distance between the droplet and bubble surface. The added mass force is not plotted in because it is more complex to be extracted from the simulations as the droplet acceleration involved is not stored along the the trajectory. We can see on this figure that some forces could have more impact on the droplets trajectory than others. Indeed, on this figure the flotability, electrostatic force and Van der Waals force variation are not observable. This is explain by the fact that their magnitudes are far lower than the one of lubrication and drag forces. The fact that the surface forces variation can not be on figure 4.4 is due to the large scale of distance between the bubble and droplet surface. Indeed, the range of surface forces is around 250 nm and in our case such distance is not reached. The droplet trajectory does not go close enough to the bubble for this force to be relevant.

This issue with the surface forces is explained by the variation of the lubrication and drag forces. In our case, it appears that the drag force is at the key to bring the droplet closer to the bubble. However, its magnitude stays lower than the one of the lubrication force at short distance (inferior to the millimeter). Thus at this point the lubrication force is too strong to allow the liquid film present between the droplet and the bubble to drain. This leads to the droplet to drift away the bubble when its angular position reaches 90°.

Figure 4.5 shows the evolution of the angular position of the droplet function of the distance between the droplet and bubble surface. This figure shows that the

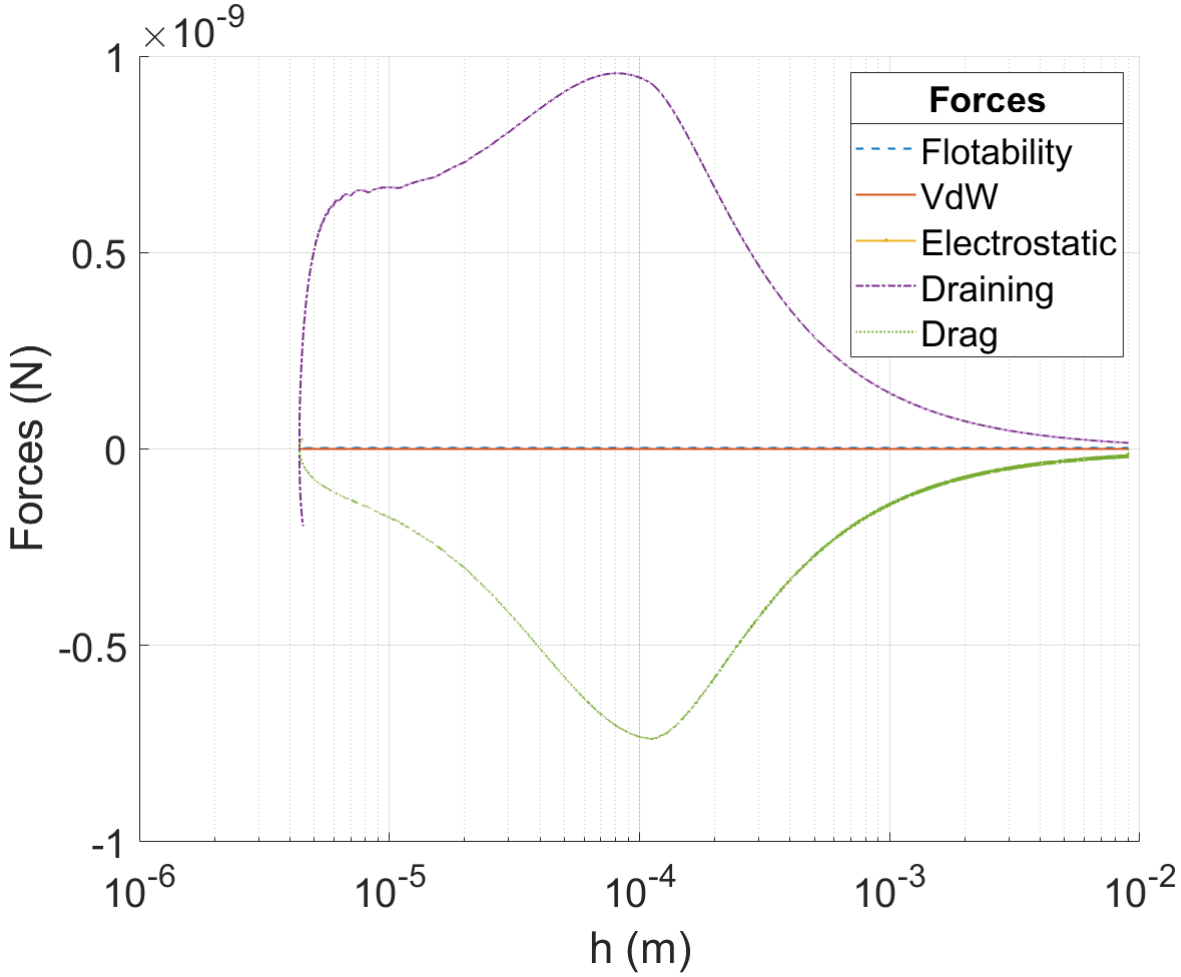

Figure 4.4: Evolution of flotability, drag, lubrication, Van der Waals and electrostatic forces for $d_b = 500\mu m$ & $d_b = 15\mu m$ in a water at 1 Cp

distance between the droplet and the bubble surface is quickly reduced until the tens of micron where it begins to stagnates. During this time the angular position of the dropet does not change much. However, when the distance between the bubble and the droplet begins to stagnate, the angular position increases suddenly.
By looking at figure 4.5, it is possible to conclude that the attracting forces are too small for the droplet to get close enough to attach to the bubble. Indeed, after the thickness corresponding to the pick value of drag and lubrication force on figure 4.4, the droplet begin to drift away the bubble surface as the liquid velocity begin to increase when becoming closer to the angular position of 90°.

All these trends leads us to conclude that the capture of a droplet by a bubble is not possible unless some attractive forces (other than the drag force) can overcome the lubrication force. Thus no capture efficiency can be define for now. A study of

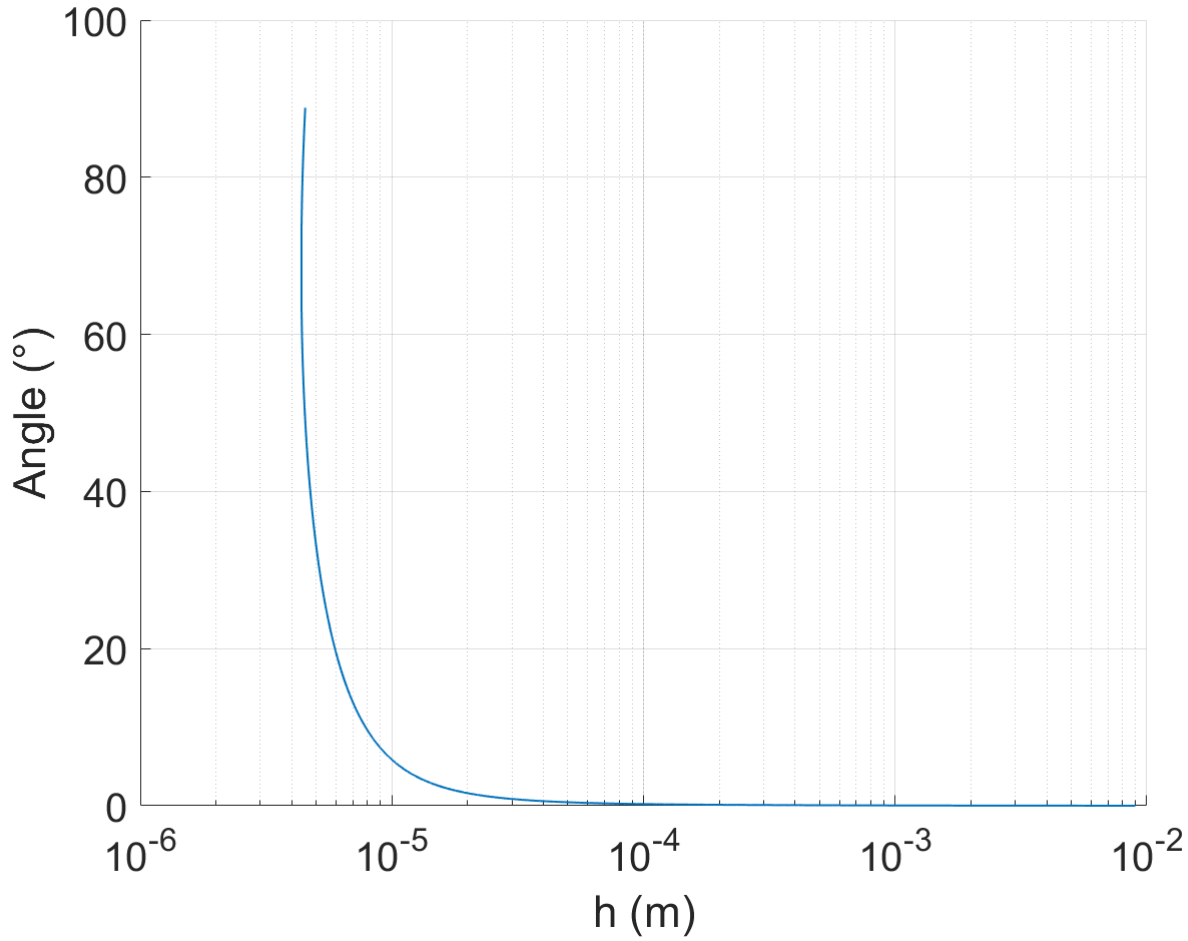

Figure 4.5: Evolution of angular position of the droplet θ function of the distance between bubble and droplet surface h for $d_b = 500\mu m$ & $d_b = 15\mu m$ in a water at 1 Cp

the sum of all forces can still be done and allows us to conclude on the impact of HPAM on flotation efficiency (though an increase of viscosity or bubble and droplet diameter).

1.4.2 Impact of droplet & bubble size

As stated before, we study here the impact of bubble and droplet size on the sum of all the forces acting on the droplet when it is near to a bubble.

First, the impact of bubble size is on the sum of the forces is studied and represented on figure 4.6. This figure represents the evolution of the sum of the forces acting on the droplet near a bubble (of $50\mu m$ with blue dashed line, $500\mu m$ with the orange dotted line, and 1 mm with the yellow solid line).

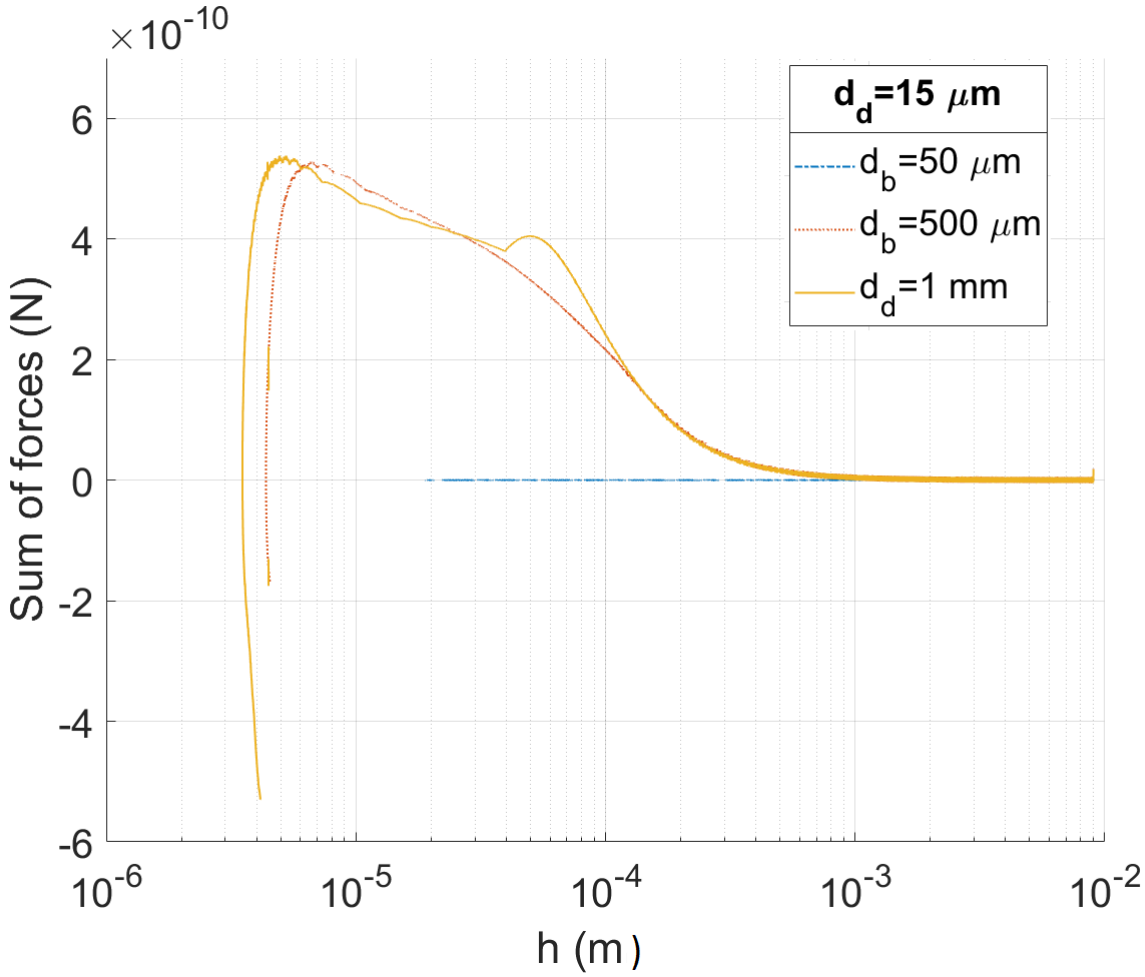

Figure 4.6: Evolution of the sum of the forces acting on a droplet of $d_d = 15\mu m$ in a water at 1 for 3 bubble diameter

It is possible to see that the resultant of the forces for a small bubble of $50\mu m$ in diameter (in DAF range) is quite low compare to the one for bigger bubbles. Its evolution, even if not visible on figure 4.6 (due to is lower magnitude) follows the same trend as for bigger bubble in IAF range. However, its lower magnitude allows us to say that the capture of the droplet is more likely for this small kind of bubble. Furthermore, it is also possible to say that for bubble in IAF range, the same conclusion is found. Indeed, the smaller the bubble is, the lower the magnitude of the sum of the forces acting on the droplet, meaning that the capture of the droplet is more likely to happen.

These variations of the resultant of the sum of all the forces are the same as the variation of the capture efficiency found in the previous chapter. This means that our model should represent correctly the capture phenomena if forces were able

to counter the lubrication force. Anyway, the smaller bubbles are, the more likely capture is at a local scale.

Our experiments on droplet distribution size and chapter 3 shows us that HPAM can have an indirect impact on capture efficiency through droplet size. This is why, figure 4.7 represent the evolution of the sum of the forces acting on the droplet near a $500\mu m$ bubble for a droplet of 5 (the blue dashed line) & 15 μm (the orange dotted line).

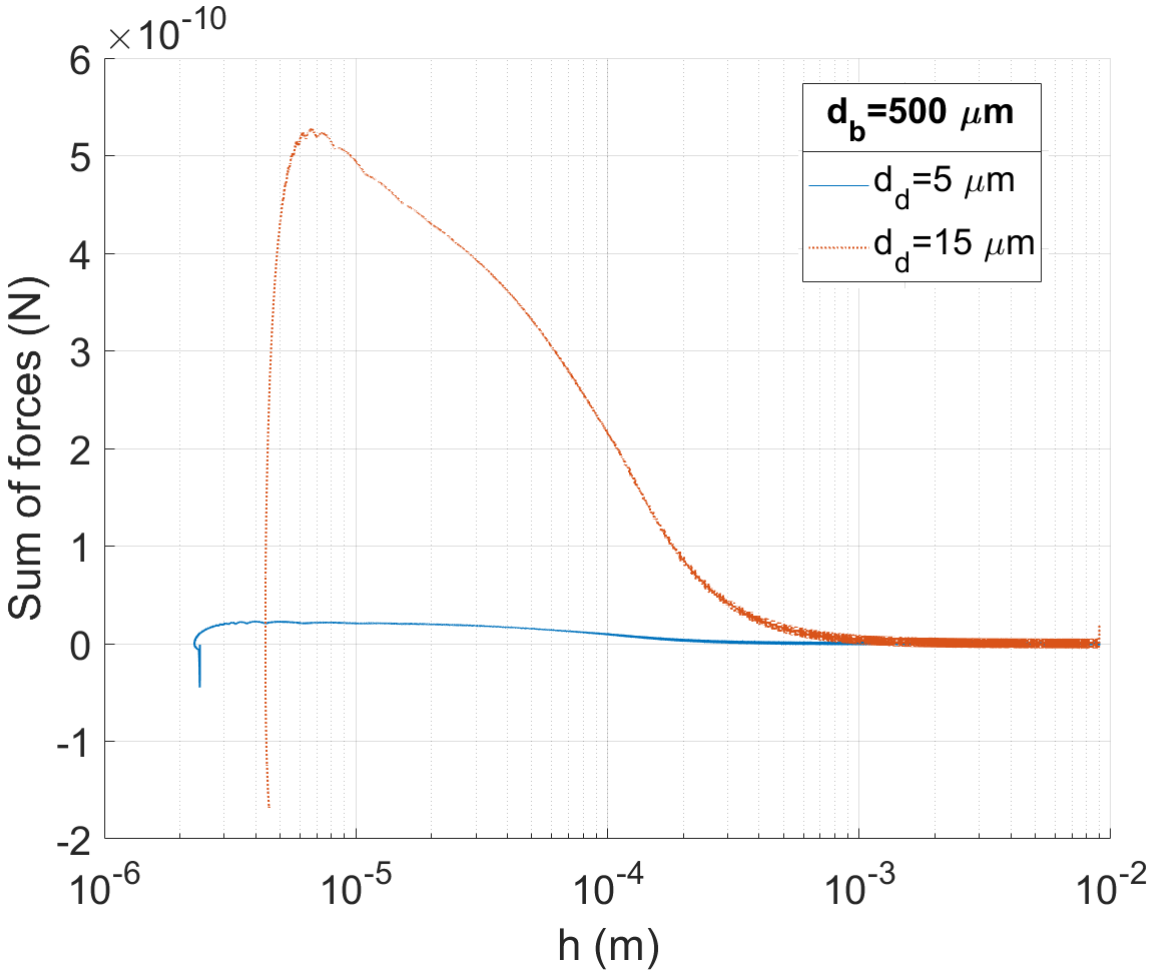

Figure 4.7: Evolution of the sum of the forces acting on a droplet for a bubble of $d_b = 500\mu m$ in a water at 1 Cp for 2 droplet diameters

As for the bubble size, figure 4.7 shows a close relation between droplet size and magnitude of the sum of the forces acting on the droplet. Indeed, this magnitude is smaller for the smaller droplet.
However, these forces applied to a droplet 27 times (3^3) smaller in volume when a 5 μm droplet is considered instead of a 15 μm one. This is also true for the added

mass which depends also on this volume. That means that the relative effect of these forces is more important in the case of a smaller droplet. This should mean that the greater the droplet, the more likely the capture is to happen. Thus, the capture efficiency should increase with an increase in droplet size. The capture efficiency should then decrease with the addition of HPAM that creates smaller droplets.
This conclusion follows the one given by Nguyen model in chapter 3.

1.4.3 Impact of viscosity

As we have done before, we study the impact of viscosity on capture efficiency with our model through the evolution of the sum of the forces acting on the droplet near a bubble.

Figure 4.8 shows the evolution of the sum of the forces acting on a droplet for given bubble (and droplet) diameter of $500\mu m$ (respectively $15\mu m$) as a function of viscosity. This figure shows that when viscosity increases this sum increases at long distance ($h > 2 \times 10^{-4}$ m) meanwhile the situation reverses for lower h. This means that the more the viscosity increases the less capture is probable.

Considering this evolution of the sum of the forces acting on a droplet translated to the capture efficiency, we can conclude that our model shows the same trend as Nguyen model concerning the impact of viscosity. Indeed, when the viscosity is increasing, the sum of the forces acting on a droplet close to the bubble surface is decreasing meaning that the capture efficiency is also decreasing.

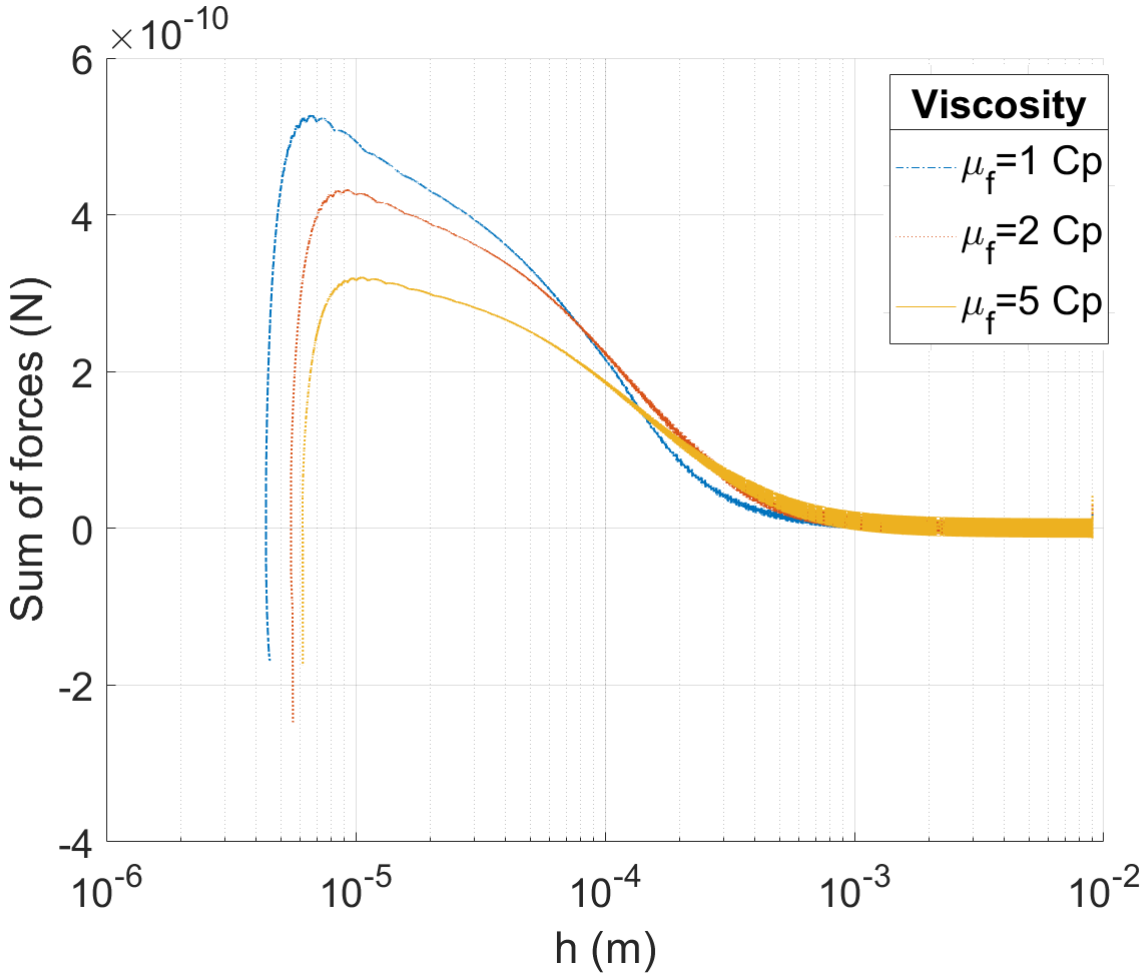

Figure 4.8: Evolution of the sum of the forces acting on a droplet for $d_b = 500\mu m$ & $d_d = 15\mu m$ in a water at 1, 2 & 5 Cp

2 Conclusion

This chapter, dedicated to overcoming the simplifying assumptions we have made in using Nguyen's model, allows us to develop a new way to model the capture efficiency based on the resolution of the droplet trajectory near a bubble. This new way of modeling the capture efficiency already gives us trends similar to Nguyen capture model.

The study of the impact of viscosity on forces acting on the droplet shows us that when the viscosity is increasing, the capture efficiency should decreases. Likewise, when the bubble diameter increases (in our case due to the presence of HPAM), the evolution of the forces shows that the capture efficiency should also decrease. When the droplet size is decreasing, the study of the forces acting gave results are in accordance with Nguyen model as it tends to shows that the capture efficiency

should decrease with this decrease of diameter.
This model set the first step to a more general way to model the capture efficiency. To have access to a capture efficiency and be truly able to compare our results to the one given by Nguyen model, other attractive forces have to be considered to overcome the strong lubrication force.

Conclusion

Ce chapitre, consacré au dépassement des hypothèses simplificatrices que nous avons faites en utilisant le modèle de Nguyen, nous permet de développer une nouvelle façon de modéliser l'efficacité de capture basée sur la résolution de la trajectoire des gouttelettes à proximité d'une goutte. Cette nouvelle façon de modéliser l'efficacité de capture, nous donne déjà des tendances similaires au modèle de capture de Nguyen. L'étude de l'impact de la viscosité sur les forces agissant sur la gouttelette nous montre que lorsque la viscosité augmente, l'efficacité de capture devrait diminuer. De même, lorsque le diamètre des bulles augmente (dans notre cas en raison de la présence de HPAM), l'évolution des forces montre que l'efficacité de capture devrait aussi diminuer. Lorsque la taille des gouttelettes diminue, l'étude des forces en présence donne des résultats en accord avec le modèle de Nguyen puisqu'elle tend à montrer que l'efficacité de capture devrait décroître avec cette diminution de diamètre.
Ce modèle constitue une première étape vers une modélisation plus générale de l'efficacité de capture. Pour avoir accès à une efficacité de capture et pouvoir réellement comparer nos résultats à ceux du modèle de Nguyen, d'autres forces d'attraction doivent être prises en compte pour surmonter la forte force de lubrification.

Chapter 5

Impact of HPAM on flotation at process scale

Ce chapitre vise à étudier l'impact du polymère à plus grande échelle. En effet, nous avons vu dans les chapitres précédents l'effet du polymère sur l'efficacité de capture à l'échelle de la bulle et ce chapitre montrera comment cela se traduit à l'échelle de l'opération unitaire. Tout d'abord, le modèle utilisé pour réaliser cette évaluation est présenté, puis l'étude est divisée en fonction du type de technologie choisie. Une étude à l'échelle du laboratoire avec une configuration en batch est d'abord étudiée avant de passer à l'échelle industrielle avec une configuration en co-courant.

This chapter aims to study the impact of polymer at a bigger scale. Indeed, we've seen in the previous chapters the effect of polymer on capture efficiency at bubble scale and this chapter will show how it translates to the process scale. First, the model used to perform this objective is presented, then the study is divided according to the used technology. A laboratory-scale study with a batch configuration is first studied before moving on to an industrial scale with a co-current configuration.

1 Overview: Flotation, two issues at two length scales

An industrial flotation device is made of several compartments that have different objectives. Figure 5.1 depicts a flotation pilot that was designed for this research purpose, and that contains the typical compartments of an industrial unit. Wastewater and air are injected at the bottom of the unit in compartment (1), which is the capture zone. In this compartment, the air bubbles and the oil droplets get into contact and form objects of different sizes. We have already focused on the capture

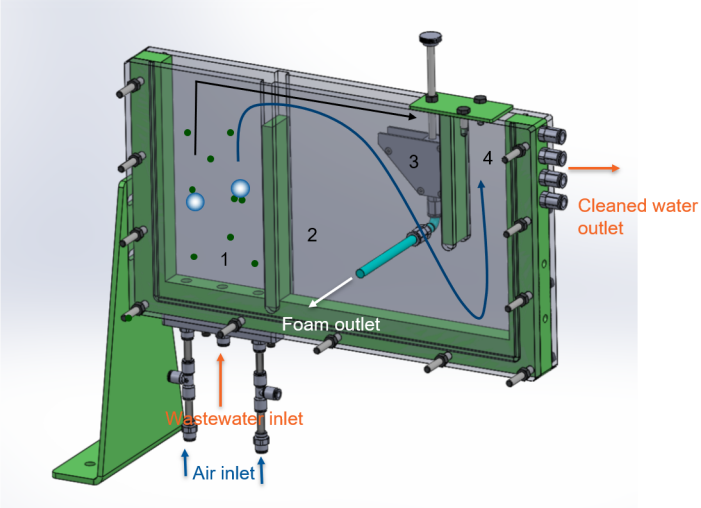

Figure 5.1: Principle of a typical flotation unit. The clusters of bubbles (open circles) and oil droplets (solid circles) are formed in compartment (1). The black path, which goes from compartment (1) to compartments (2) and (3), is when the separation is successful. The blue path, from (1) to (2) and (4), is when some objects are re-entrained by the water flux

efficiency of one bubble in the capture zone. It is then time to broaden our study in this zone. Indeed, thanks to our study of the capture efficiency of a bubble, we will be able to evaluate the efficiency of the whole capture zone. However once bubble or cluster goes out of compartment (1), two possibilities occurs. Either the cluster follows the black path and is floated (flotation is successful and oil can be gathered) or it follows the blue path and is re-entrained toward the water outlet by the water flux.

The viscosity can impact the efficiency of the installation at two different stages, during the capture (in the capture zone) or the re-carrying. The global capture inside the capture zone is first studied through the evolution of concentration in the first compartment. Then, the re-carrying phenomenon is tackled.

1.1 Evolution of concentration in the contact zone

Droplet concentration evolves in the contact zone in the same way as concentration evolves in a bubble column. It obviously depends on how the liquid to be treated and the bubbles are injected. In a typical flotation unit as the one in figure 5.1, this is close to a co-current configuration where both effluents and air are injected at the bottom of the column. This configuration will be dealt with later, as will the batch configuration, also widely used in the laboratory (flotation test).

In all these configurations, concentration varies as a function of bubble capture efficiency. This efficiency, previously calculated using one of the models presented in the previous chapters, is used to help us calculate a disappearance coefficient for the droplets (a decrease in the concentration of free droplets). It obviously depends on viscosity, bubble and droplet diameter. It remains to see at this point which of these parameters also have an impact on the efficiency of a flotation unit. This study is carried out on the assumption that there is only one bubble size present in the column, in order to facilitate the calculations. It is then be extended by weighting the capture efficiency of a bubble by its percentage presence in the initial distribution.

1.2 Recarrying

Once the clusters are formed, they are carried towards the surface of compartment (1) (Fig. 5.1); not only because the water flux goes in that direction, but also because they have a negative buoyancy. Their velocity depends both on the fluid velocity V_f and on their velocity relative to the fluid, V_c. As the oil droplets are small compared to the bubbles, we make the reasonable assumption that the size and densities of the bubble-droplets clusters are the same as for the 'naked' bubbles; meaning that V_c is equal to V_b. In most cases, V_b can be approximated using the Stoke's law, which implies that the bubble velocity depends on the square of its diameter:

$$V_b = V_{Stokes} = \frac{d_b^2 g(\rho_f - \rho_b)}{18\mu_f} \tag{5.1}$$

where d_b is the diameter of the bubble, ρ_b its density, ρ_f the density of the fluid, μ_f the dynamic viscosity of the fluid, and g is the gravitational field strength.
V_c could be evaluated more exactly with experiments of rising velocities for clusters.

In the compartment (2), where separation of cluster and 'cleaned' water is performed, V_f and V_b have opposite directions. In that case, and depending on the viscosity conditions, part of the smaller clusters may have an ascension velocity that is not sufficient to counteract V_f, so that they are re-entrained by the water (Fig. 5.1, blue path). This is what we call the recarrying phenomena, which of course negatively impacts the process. This recarrying effect is a *process-scale* indicator of the flotation efficiency, as it sets the global limit of the flotation device capacity. We discuss its importance as a function of the viscosity and the sizes of the bubbles and droplets in the last section of this chapter. This discussion is based on simple hypothesis about how to determine the involved velocities, and the calculations are performed taking into account the typical distribution of bubble sizes in

a flotation unit.

2 Process scale modeling

2.1 General equations of the 1D model

To evaluate the effect of viscosity at the process scale, the flotation device is assimilated to a bubble column. This assumption is quite logical for IAF devices as in the oil industry flotation columns are usually used. For DAF devices, the focus is on the first part of the device, in the capture zone which behaves as a co-current flotation column.

Once the location of the study is set, some hypothesis are needed. First, the bubble concentration is considered to be low enough, for the bubbles to not interact during their ascension. Bubbles are not saturated by oil droplets during their ascent, so that they rise at a constant velocity, and capture droplets at a constant rate (with the same capture efficiency). Finally, the capture efficiency is constant along the column.
With these hypothesis, it is possible to realize a mass balance of oil inside a thin slice of a flotation column. Two different configurations are considered here.
Co-current: in this device, bubbles are injected at the bottom of the unit with the emulsion. Both flow in the same ascending direction.
The second one is a semi-batch, where the column is initially filled with emulsion and the only inlet is the bubbles one. The cleaned water is sampled at the bottom of the column over time at height H_{sample}. This kind of device is mainly used at lab scale to perform flotation experiments and is the one use by [Argillier et al., 2013] or [Chakibi et al., 2018] to study the impact of HPAM and salts experimentally.

The axial variation of the emulsion concentration C follows equation 5.2.

$$\frac{dC}{dt} + U_C \frac{dC}{dz} = D \frac{d^2C}{dz^2} + r_C \tag{5.2}$$

In equation 5.4, U_C is the liquid velocity and C is the oil concentration at height z. Q_{ww} is the white water flow rate, Q_L is the flow rate of the liquid to treat and r_C is the disappearance term which translates the quantity of floated oil droplet. This rate can be calculated thanks to the following formula:

$$r_C = \frac{3}{2} \frac{E_{capt} U_b C \alpha}{d_b} \tag{5.3}$$

In this formula, E_{capt} is the capture efficiency for a bubble (see previous chapter), U_b is the bubble velocity relative to the fluid (its value comes from Schiller & Naumann correlation) and α is the gas hold up. Assuming that axial mixing is not accounted in a first approach, $D = 0$ and $\frac{d^2C}{dz^2}$ is equal to zero. This is why equation 5.4 can be simplified as follow:

$$\frac{dC}{dt} + U_C \frac{dC}{dx} = r_C \tag{5.4}$$

Once this general equation is set, it is possible to differentiate it for each column configuration.

2.2 Semi-batch configuration

In batch configuration, the concentration C is uniform inside the column, therefore, the evolution of concentration depends only on time:

$$\frac{dC}{dz} = 0 \tag{5.5}$$

This means that equation 5.4 combining with equation 5.3 becomes:

$$\frac{dC}{C} = \frac{3}{2} \frac{E_{capt} U_b \alpha}{d_b} dt \tag{5.6}$$

2.3 Co-current configuration

Co-current columns are treated on stationary regime. This means that enough time have been waited and the concentration no longer depends on time (equation 5.8) because:

$$\frac{dC}{dt} = 0 \tag{5.7}$$

The reference equations can then be sum up as:

$$\frac{dC}{C} = \frac{3}{2} \frac{U_b}{U_C d_b} \alpha dz \tag{5.8}$$

We can notice the well known equivalence, $dt = \frac{dz}{U_C}$ between the two configurations.

2.4 Gas hold-up and liquid velocity

In these equations(5.8 & 5.6), two parameters are still to be determined: the gas holdup α and the liquid velocity U_C. These parameters depend on the initial conditions of the system. Thus, their expressions differ in each case (batch & co-current).

Expressions for U_C are sum up in table 5.1, with Q_g as the gas flow rate, Q_L as the emulsion flow rate and S the cross section of the column.

Batch	Co-current
$U_C = 0$	$U_C = \frac{Q_{ww}+Q_L}{S}$

Table 5.1: Expression of liquid velocity U_C depending on configuration

The general expression of the gas holdup given in equation 5.9 depends on the gas flow rate Q_g , and the velocity of the bubble in the Cartesian system link to the column $U_{b/z}$. This last parameter is the one depending on the configuration of the flotation column. Its expression is described in table 5.2, it is basically $U_b + U_C$.

$$\alpha = \frac{Q_g}{U_{b/z}S} \tag{5.9}$$

Batch	Co-current
$U_{b/z} = U_b$	$U_{b/z} = U_b + \frac{Q_g+Q_L}{S}$

Table 5.2: Expression of bubble velocity along the z-axis in a Cartesian system $U_{b/z}$ depending on column configuration

Once every parameter is defined, equations 5.6 & 5.8 can be integrated along time (for batch configuration) or along column height (for co-current stationary cases) to obtain an expression of the variation of concentration inside the column. These expressions are sum up in table 5.3.

Batch	Stationary
$C(t) = C_0 exp\left(-\frac{3}{2}\frac{U_b}{d_b}E_{capt}\alpha t\right)$ (5.2.1)	$C(z) = C_0 exp\left(-\frac{3}{2}\frac{U_b}{U_C d_b}E_{capt}\alpha z\right)$ (5.2.2)

Table 5.3: Expression of concentration function of: time for batch and column heigth for stationary co-current

Equations 5.2.1 & 5.2.2 (table 5.3) depicts the evolution of concentration inside the column. The concentration varies as a function of three parameters besides the height or time: the capture efficiency E_{capt}, the bubble size d_b and the gas hold up inside the column α. As seen before, the polymer has an impact on capture efficiency and bubble size. Furthermore, the impact of polymer on capture efficiency

depends on bubble size.
It is then decided to study the impact of the polymer on both configurations. For each case, the impact of the viscosity is seen first, before looking at the impact of the bubble and droplet size on the flotation efficiency to finish with the impact of the gas hold up.

3 Impact of HPAM in batch configuration

In this study, the height H_{column} will be fixed at 50 cm to be able to compare our results with the experimental one of Argillier et al., 2013.

For his experiments Argillier used the following flotation device (figure 5.2). This flotation device can be assimilated to a flotation column working in batch mode. This column (50 cm tall with a circular cross section of 6.5 cm in diameter) is filled at the beginning of the experiment with an oil emulsion. Once experiments are launched a regular sampling is done at the bottom of the column (at the outlet valve numbered 6 on figure 5.2). Bubbles being generated by injecting air through a porous medium the gas hold up α is defined with the following formula (equation 5.9):

$$\alpha = \frac{Q_g}{U_{b/z} S}$$

The air flow rate used in general is 200 L/h.

Figure 5.3 [Argillier et al., 2013] shows the expected evolution of flotation efficiency function of the HPAM concentration. They used the brine presented in chapter 2 as process water. In such brine, as shown in our experiments the viscosity is twice the one of water when 500 ppm of HPAM are added. This figure shows that this multiplication by 2 of the viscosity leads to a slowdown of the separation process efficiency. At the first sampling, the flotation efficiency is 30% lower in this viscosified brine. However, the last sample has the same oil concentration, thus the flotation process is 10 time longer in presence of 500 ppm of HPAM.

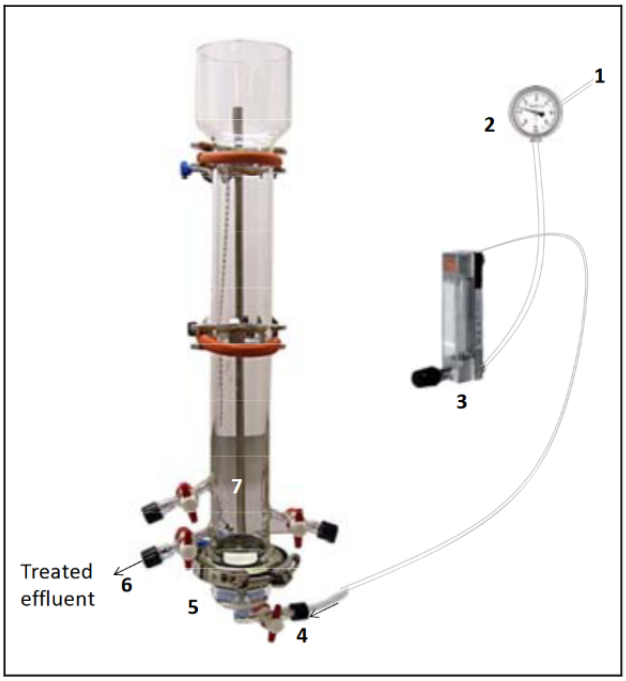

Figure 5.2: Schematic of the gas flotation system: (1) gas source, (2) manometer, (3) flowmeter, (4) inlet valve, (5) glass filter, (6) outlet valve and (7) oily wastewater introduced in the column [Argillier et al., 2013]

We first study the impact of the polymer for a similar batch configuration before looking into its impact on the other configuration. For this study, we mainly look at the evolution of flotation efficiency in batch mode function of viscosity and bubble diameter. To be able to compare our results with the study of Argillier, the droplet diameter d_d is set at 15 μm and the gas flow rate at 200 L/h. The bubble size distribution in Argillier experiments is unknown and depend of the porous media, we chose to take as bubble reference diameter 150 μm.

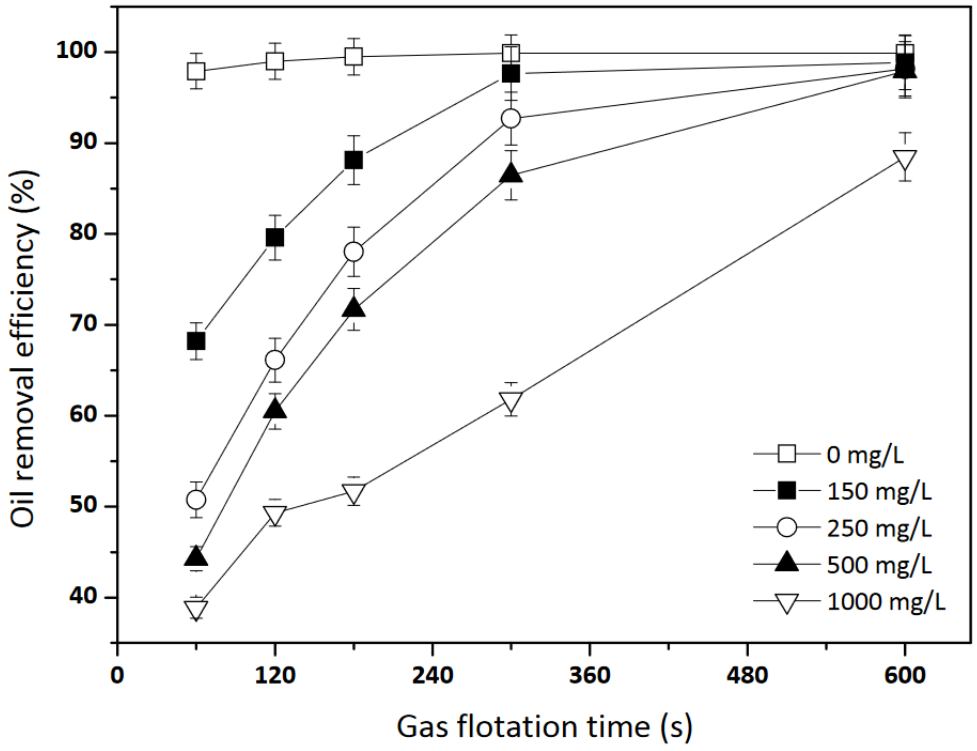

Figure 5.3: The effect of HPAM concentration (from 0 mg/L up to 1000 mg/L) on the oil removal efficiency at different flotation time. The mean diameter of oil droplets is around 15 μm whatever the polymer concentration [Argillier et al., 2013]

3.1 Impact of the viscosity on flotation efficiency in batch configuration

The first and direct impact of polymer presence is an increase in viscosity. This is why, figure 5.4 represents the evolution of flotation efficiency function of the experiment duration function of three viscosity (1,2 and 5 Cp) for a 150 μm bubble. The flotation efficiency E_f is given by the following formula, identical to the one used by Argillier:

$$E_f = \left(1 - \frac{C(t)}{C_i}\right) \times 100 \tag{5.10}$$

Figure 5.4 shows that the impact of viscosity on flotation efficiency is quite low for 150 μm bubble and batch configuration. Indeed, at the end of the flotation time no difference in flotation efficiency exists when the viscosity is multiply by 5. By comparison with the one of Argillier, our results are very similar to the one found experimentally for brine without HPAM. Note that the bubble diameter is here estimated as we do not have any information from the original paper of Argillier.

As we will see later on, the effect of bubble size is very important. We choose not to optimize the bubble size in the simulation because it has no real scientific interest.

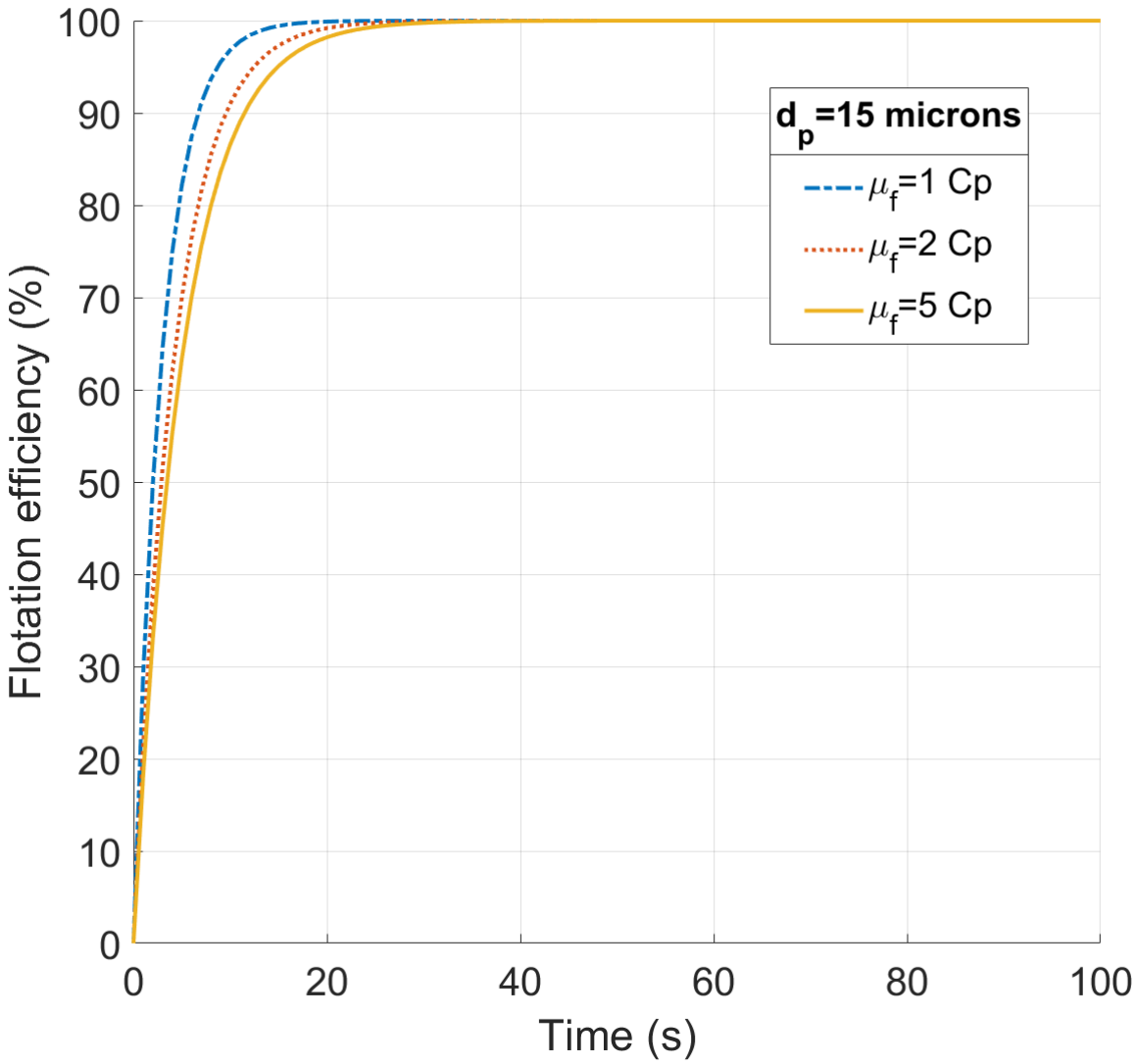

Figure 5.4: Effect of the viscosity on flotation efficiency for a $15\mu m$ droplet and $150\mu m$ bubble in batch configuration

Figure 5.3 shows that in the same configuration the presence of HPAM has a huge impact (around 55% for the first sample when the viscosity is multiply by 2 *i.e* for 500 ppm HPAM solution in brine) on flotation efficiency. In our case for the same sample no decrease in flotation efficiency is found. The only effect found in our case, when the viscosity increases, is that the time to reach the maximum flotation efficiency increases by a few seconds (around 5 when the viscosity is multiply by

2 and around 15 hen the viscosity is multiply by 2). This difference between our results and the one of Argillier shows that HPAM has a huge impact on flotation outside of the increase of viscosity.

3.2 Impact of bubble & droplet size on flotation efficiency in batch configuration

In this work we have seen in the experimental part that the presence of HPAM tends to increase the diameter of bubbles generated to perform the flotation. Furthermore, in chapter 3 & 4 we have shown that an increase in bubble diameter tends to decrease the capture efficiency of a bubble.

This same effect of bubble size is also seen at the global scale. Indeed, figure 5.5, presenting the evolution of flotation efficiency function of the experimental duration time for 3 bubbles size, shows that when the bubble size is increasing the flotation efficiency is decreasing. When the bubble diameter is multiply by 3, the flotation efficiency decreases by 5% in the worst case scenario at the end of the time of study. Furthermore, increasing the bubble size also slow down the separation as it takes almost 10times more time to reach the same flotation efficiency when the bubble size is multiply by 3.

The observed effect of HPAM presence on figure 5.3 is explained mainly by an increase of the bubble diameter in presence of the polymer. Indeed, we have shown here that in batch configuration, the flotation efficiency is reduced mainly by the increase of bubble size.

Furthermore, even if in Argillier study, the droplet size does not vary we have seen in the previous chapters that HPAM can also have an impact on flotation through droplet size. Indeed, the droplet size tends to be reduced by the presence of HPAM. This is why, figure 5.6 presents the evolution of flotation efficiency function of the experimental duration time for 2 droplets size for bubbles of $150\mu m$ diameter. This figure shows that when the droplet size is decreasing, the flotation efficiency is also decreasing. Once again, the effect of droplet size is far more important than the one of viscosity. Indeed, when the diameter is divided by 3, the flotation efficiency see a drop of at most 55%.

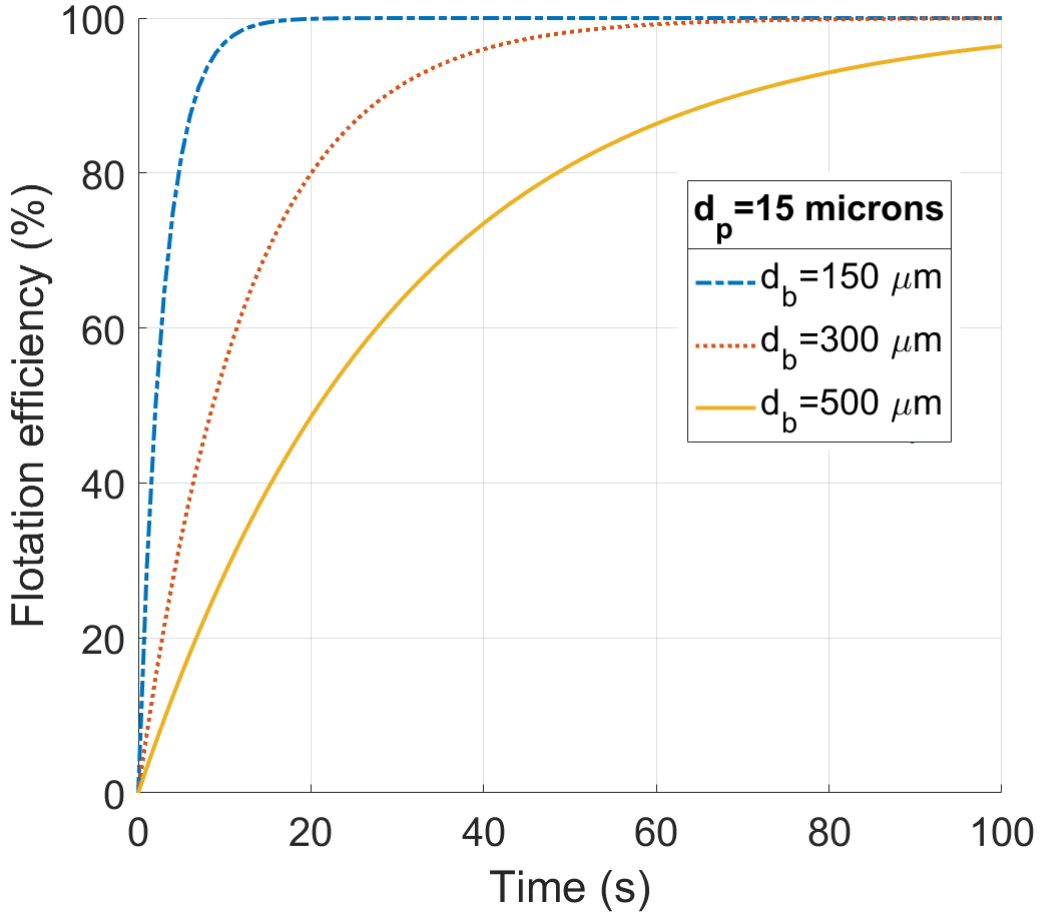

Figure 5.5: Effect of the bubble size on flotation efficiency for a $15\mu m$ droplet and water viscosity at 1 Cp in batch configuration

3.3 Impact of gas hold up on flotation efficiency in batch configuration

The last parameter worth studying is the gas hold up which varies as a function of the gas flow rate. Figure 5.7 shows the evolution of flotation efficiency function of the experimental duration time for 3 different gas hold up for $15\mu m$ droplets and $150\mu m$ bubbles. As stated before, the gas hold up varies with the gas flow rate, this is why the legend of this figure relies on the value of the gas flow rate.

This figure shows that when the gas hold up is decreasing, the flotation efficiency is also decreasing. As for other parameters, the impact of gas hold up is more important than the one of viscosity. Indeed, when the flow rate is divided by 4, the flotation efficiency see a drop of at most 45%.

We have to note that at at these so great gas volume fractions, the drag function

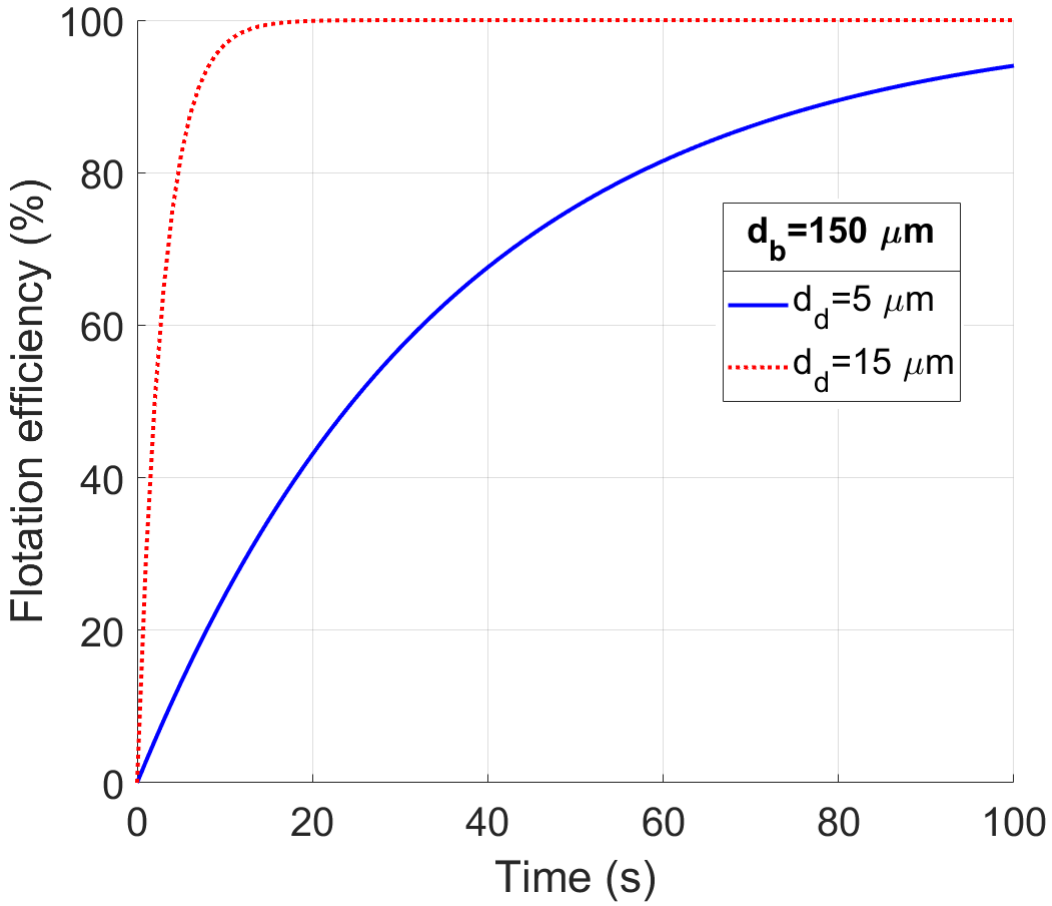

Figure 5.6: Effect of the droplet size on flotation efficiency for a 150μm bubble in batch configuration

needs to be modified to account for the decrease of the drag force with the gas hold-up increase. Furthermore, collision and attachment efficiencies models at the bubble scale also supposes that there is no effect of the gas volume fraction on their values. Both hypothesis should be revisited in the future, numerically, or experimentally.

The study of the impact of HPAM on the flotation efficiency in a batch configuration already shows interesting results. The impact of polymer through the droplet and bubble size found at local scale in chapter 3 & 4 is also found at a more global scale. When the droplet size is decreasing, the flotation efficiency is also decreasing. Inversely, when the droplet size is increasing, the flotation efficiency also tends to decrease. The effect of viscosity is also found even if its impact is relatively low compared to the one of bubble or droplet size.
Additionally, it is important to not that, even if its variation is not HPAM related, the gas hold up has also an impact on flotation efficiency. The flotation efficiency

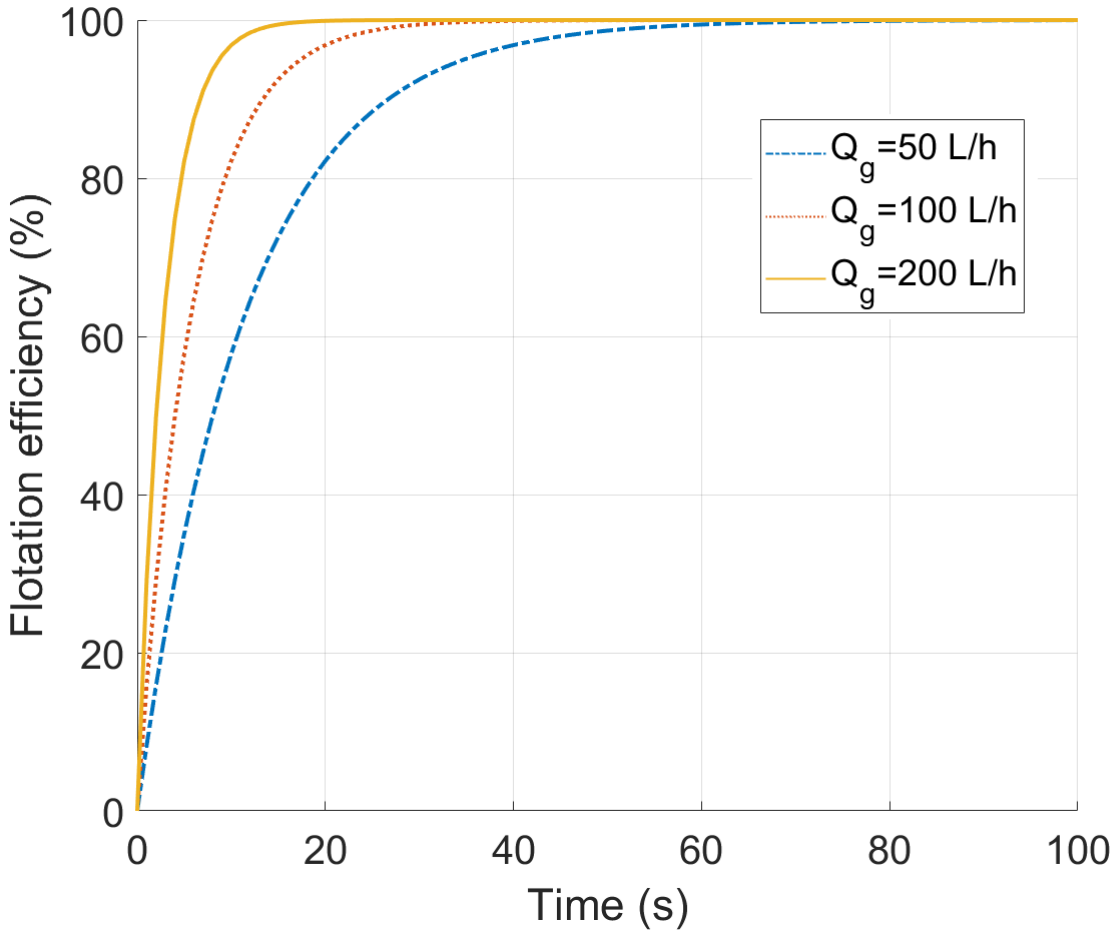

Figure 5.7: Effect of the gas flow rate on flotation efficiency for a $15\mu m$ droplet & a $150\mu m$ bubble in batch configuration ($Q_g = 50L/h \Rightarrow \alpha = 0.1027$; $Q_g = 100L/h \Rightarrow \alpha = 0.2054$; $Q_g = 200L/h \Rightarrow \alpha = 0.4109$)

increases along with the gas hold up.

4 Impact of HPAM mode for co-current

The previous part tackles the subject of flotation efficiency working in batch. Although this situation is used on a laboratory scale, it is rarely used in industry. A more realistic alternative is the co-current similar to the one used in the first part of flotation cells similar to to the one use in our experiments and in classical flotation devices.

We choose to keep a 50 cm tall column with a circular cross section of 6.5 cm in diameter and a gas flow rate of $200L/h$, as used by Argillier et al. .

The study of this mode is done as was the study of the batch configuration.

First, the effect of viscosity on flotation efficiency is looked upon before looking to the impact of bubble and droplet sizes. The impact of the gas hold up on flotation efficiency, not due to the presence of HPAM, is studied afterward.

4.1 Impact of the viscosity on flotation efficiency in co-current configuration

As stated before, a direct impact of HPAM presence is an increase in the water or brine viscosity. Figure 5.8 represents the evolution of flotation efficiency function of the column height for three viscosities (1,2 and 5 Cp) for a 50 μm bubble. This figure shows an obvious effect of viscosity on flotation efficiency. Indeed, if at the local scale (see chapter 3) or at the global scale in batch mode the viscosity as little to no effect of such small bubble, for a column of flotation its impact on flotation efficiency is far bigger. Indeed, when the viscosity is multiply by 2, the flotation efficiency drops of a few percents. However, along the height of the column a larger drop in efficiency can be observed (at most around 20%). Even worth, an increase of viscosity from 1 to 5 Cp may generate a loss in flotation efficiency of more than 50%. Even if at the top of the column a drop of only 5 % is observed.

This global impact of viscosity on the flotation efficiency in a flotation column close to the situation found in the contact zone explains why industrial reports that the increase of viscosity is the main reason for the drop in efficiency of their flotation unit. The impact of HPAM might even be worsen by the modification of droplet and bubble size distribution.

4.2 Impact of bubble & droplet size on flotation efficiency co-current configuration

We have shown that the presence of polymer tends to increase bubble size (see chapter 1 & 2), thus we are going to study its impact on flotation efficiency. Figure 5.9, presenting the evolution of flotation efficiency function of the column height duration time for 3 bubble sizes, shows that the more the bubble diameter increases the more the flotation efficiency is decreasing. The passage from DAF to IAF mode (passage from 50μm bubble to 500μm or 1 mm bubble) generate a huge decrease in flotation efficiency. This loss of efficiency can be evaluated at more than 85% in the worst case scenario. Even in IAF mode, an increase in bubble size still have a big impact. It generates a loss of more than 60% when the bubble goes from 500μm to 1 mm.

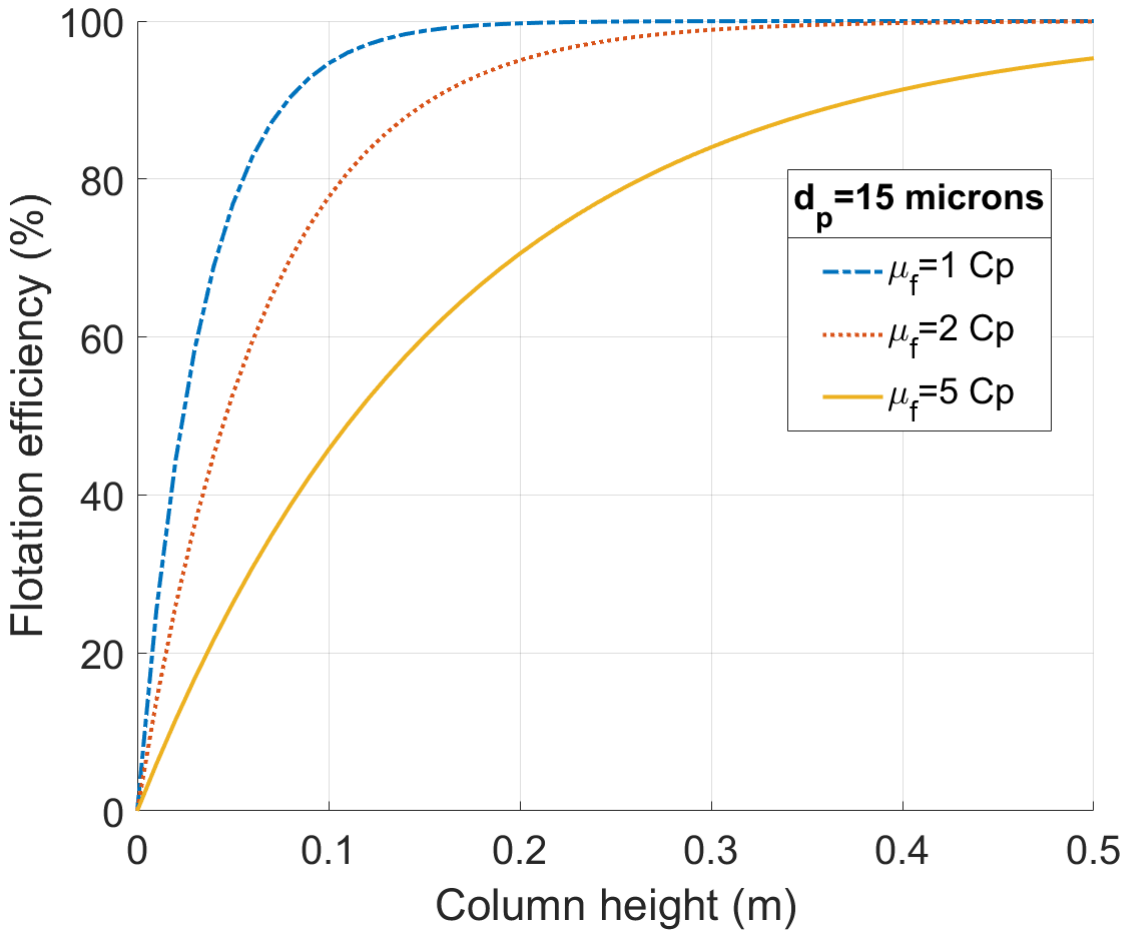

Figure 5.8: Effect of the viscosity on flotation efficiency for a $15\mu m$ droplet in co-current configuration

This impact of an increase of bubble size in presence of polymer effectively worsen the negative impact of viscosity. However, we have seen previously (see chapter 2) that the presence of polymer also impacts the droplet size distribution.

In presence of HPAM, the mean diameter of droplet size distribution tends to decrease. Figure 5.10 shows the impact of this drop in droplet size on flotation efficiency for a flotation column working in co-current configuration in DAF mode (for $50\mu m$ bubble). Again, as seen for a flotation column working in batch mode or for the local impact with the capture efficiency (see chapter 3), when the droplet diameter is reduced, the flotation efficiency drastically drop. Indeed, figure 5.10 shows a drop of more than 40% when the droplet diameter is divided by 3.

We have shown that globally in presence of HPAM, the negative effect of viscosity is increased by the increase in bubble size and decrease in droplet size experimentally

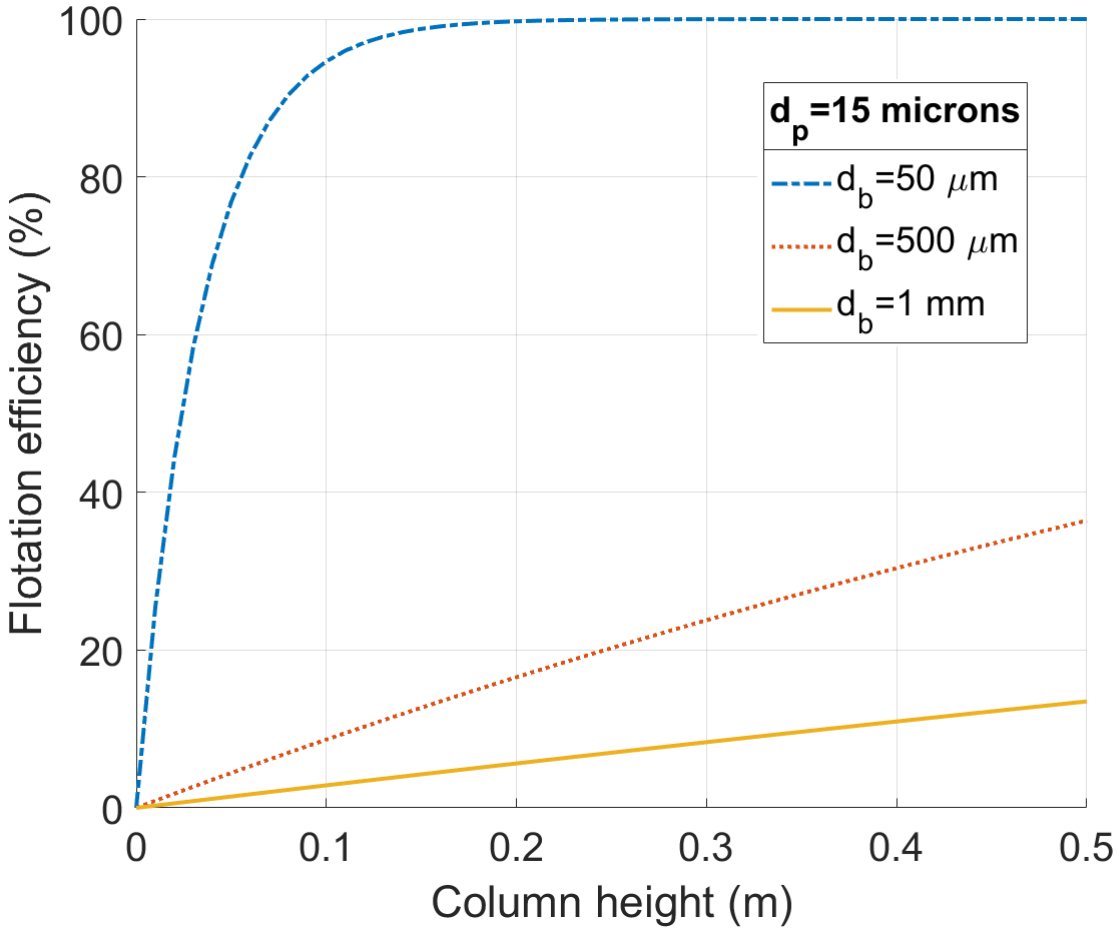

Figure 5.9: Effect of the bubble size on flotation efficiency for a $15\mu m$ droplet in a water at 1 Cp in co-current configuration

observed. However, as seen previously, the gas hold up, even if not dependent of polymer presence, has an impact at the global scale on flotation efficiency.

4.3 Impact of gas hold up on flotation efficiency in co-current configuration

As stated before, the gas hold up varies with the gas flow rate, but for a flotation unit working in continue, there is a need of a liquid or emulsion flow rate. We decided to set it at 1000 L/h. Such a value is choosen as in DAF mode, the white water flow rate is often fixed as 20% of the liquid flow rate (for example [Beneventi et al., 2008]).

Figure 5.11 shows the evolution of flotation efficiency function of the column height for 3 different gas hold up for $15\mu m$ droplets and $100\mu m$ bubbles. The legend

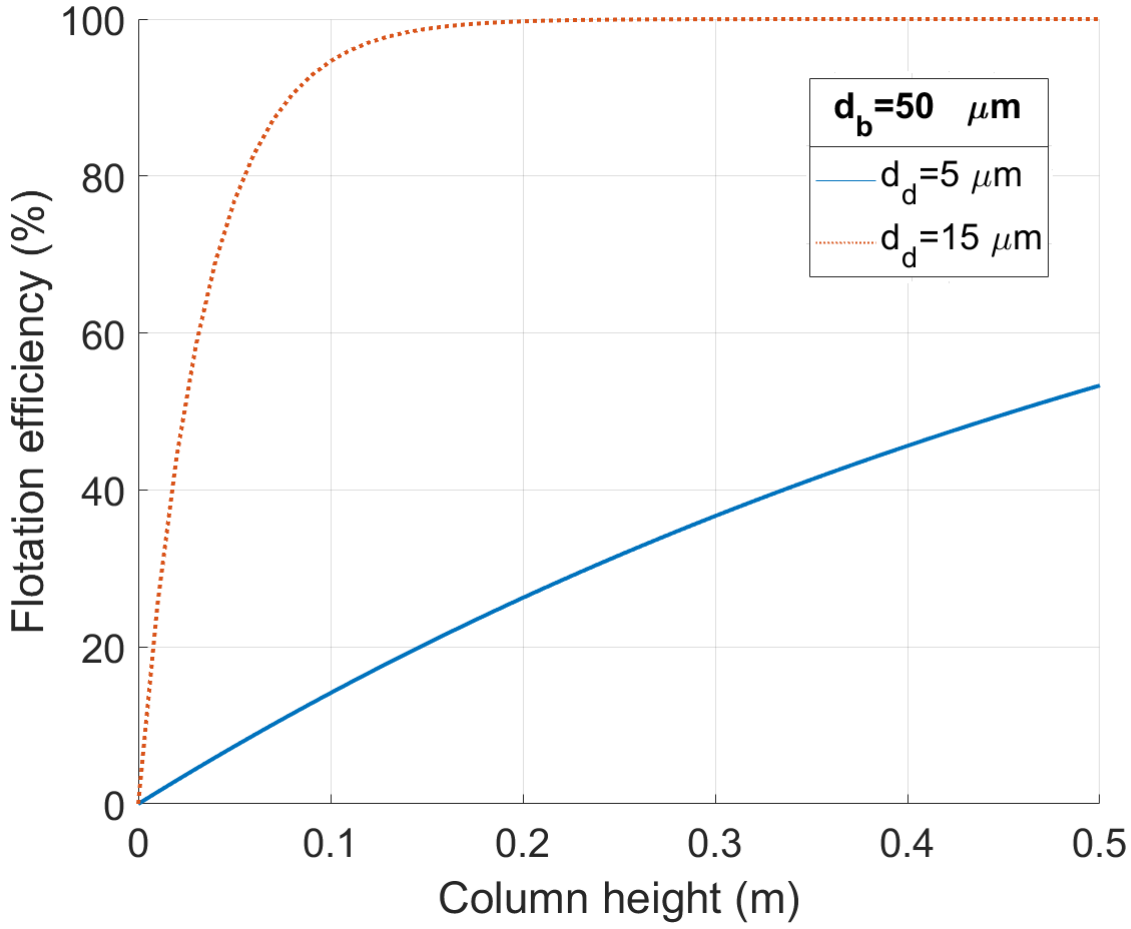

Figure 5.10: Effect of the droplet size on flotation efficiency for a $50\mu m$ bubble in a water at 1 Cp in co-current configuration

of this figure relies on the value of the gas flow rate as there is a close and simple relation between it and the gas hold up (equation 5.9) and its conversion in gas hold up.

As for the batch mode configuration, figure 5.11 shows that when the gas hold up is increasing the flotation efficiency tends to increase. This increase is not negligible, a multiplication of the gas hold up by 4 generate an increase of 35 % in flotation efficiency. This is due to the variation of gas concentration with α.

An increase of the gas hold up might be a solution to counteract the negative effect of polymer. This can be achieved either by increasing the gas flow rate as shown on figure 5.11 or reducing the liquid flow rate. Indeed, according to the equation 5.11 (resulting of equation 5.9 and the $U_{b/z}$ in table 5.2), a reduction in

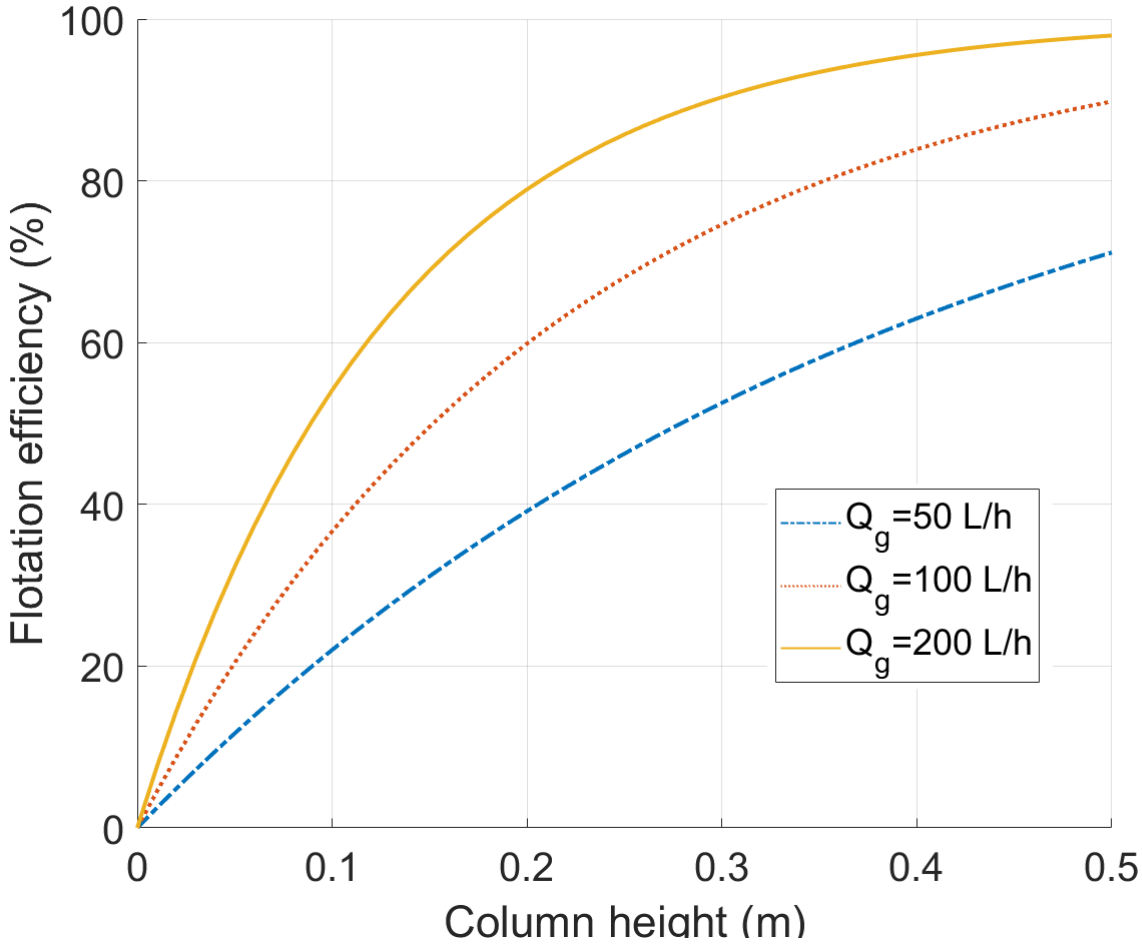

Figure 5.11: Effect of the gas hold up on flotation efficiency for a $15\mu m$ droplet & a $100\mu m$ bubble in co-current configuration ($Q_g = 50L/h \Rightarrow \alpha = 0.038$; $Q_g = 100L/h \Rightarrow \alpha = 0.0748$; $Q_g = 200L/h \Rightarrow \alpha = 0.1391$)

the liquid flow rate leads directly to an increase of the gas hold up.

$$\alpha = \frac{Q_g}{\left(U_b + \frac{Q_g + Q_L}{S}\right) S} \tag{5.11}$$

However, this diminution of liquid flow rate also generate an increase of the time needed for he water treatment. It might be interesting for industrial purpose to evaluate the loss of money generate by a slower production rate compared to the actual method to treat water properly, the use of a huge quantity of chemical products (mainly surfactants).

It is also important to note that the column used here are quite small and the flotation efficiency can be enhanced by increasing the column height or even by a

succession of flotation unit.

Finally we have found the same impact at the local and global (process scale), the polymer presence reduced the capture or flotation efficiency trough an increase in viscosity and bubble size and a decrease in droplet size. It is interesting to note that this effect are amplified at an industrial scale (when using co-current flotation column) compared to in a laboratory scale in batch configuration. At an industrial scale, increasing gas hold up or reducing the liquid flow rate might be a solution to counteract the effect of HPAM. Of course a change in the generated bubble size could be interesting, but it supposes a change in the way of producing the bubbles.

5 Cluster motion in a flotation unit : Re-carrying

As seen in the introduction clusters, assimilated here to bubbles as a first approach, rising velocity U_b calculated through the Stokes formula (when the bubble is small enough i.e inferior in diameter to 120 μm) depends on viscosity and on bubble diameter (equation 5.12).

$$V_b = V_{Stokes} = \frac{d_b^2 g(\rho_f - \rho_b)}{18\mu_f} \tag{5.12}$$

The bubble or cluster velocity U_b has to be compared to the liquid velocity V_L inside the flotation unit. The latter is usually calculated or experimentally determined in order to avoid the re-carrying of the bubbles and/or clusters. However, as shown in equation 5.12, bubble speed depends on two parameters: the viscosity and mainly the bubble size (d_b^2). Therefore, the maximum liquid velocity has to be chosen according to the average bubble size. Indeed, in order to avoid the re-carrying phenomena, it is necessary for the majority of the bubble distribution to be able to reach the surface instead of being dragged with the liquid flow.
At the end, studying the re-carrying phenomena is equivalent to study the impact of polymer on the bubble size distribution and on the viscosity.

The impact of re-carrying phenomena on flotation efficiency depends mainly on the bubble ascent velocity. Indeed as stated before, the path of the bubble inside a flotation unit depends on the bubble and the carrying liquid phase velocity. If the carrying liquid phase velocity is higher than the ascent bubble velocity, bubbles will never reach the top of the unit and are going to be carried towards the clean water outlet.
It is easy to have access to the carrying liquid phase velocity as it is simply the flow rate at the inlet of the flotation unit (either only the waste water flow rate

in IAF mode or the sum of the waste water and white water flow rate in DGF mode) divided by the separation zone section area. On the other hand, bubble velocity depends only on two parameters, the viscosity μ_f and bubble diameter d_b (according to Stokes or Schiller and Naumann correlations).

The first parameter to study is the direct impact of viscosity on the re-carrying phenomena. In order to do that, it is necessary to compare the carrying fluid velocity (in green on figure 5.12) with bubble velocities of deionized (in blue) and viscosified (in red) water function of bubbles sizes. As an example, the carrying fluid velocity is calculated when the unit is designed to carry toward the clean water outlet bubble inferior to 60 μm. Thus, this velocity is equal to a 60 μm bubble velocity in deionized water.
Figure 5.12 shows the maximum velocity of the carrying fluid inside the flotation cell in green and the one of bubble function of its size in both viscosified water (in red) and deionized water (in blue). With these velocities, it is possible to study which bubbles are going to be efficient for flotation i.e the one which are not carried away, and which velocities are above the green curve. Thus, figure 5.12 shows that in deionized water the cutoff bubble size (bubble size which velocity is represented in green on the figure) is 60μm, but in viscosified water, with the increase in viscosity, the bubble velocity is decreasing which leads to an increase in the bubble cutoff size (it goes up to 90μm). This leads to a major increase in the share of bubbles carried away towards the clean water outlet. This means that the share of efficient bubbles for flotation is decreasing.

However, viscosity can also have an indirect impact. Actually, it might impact the bubble size distribution. In order to do that, some experiments have been made in DGF mode (by pressuring water at 5 bar and then quickly depressurizing it with a needle valve. The produced bubble distribution is sized thanks to Spraytec from Malvern Instruments. Figure 5.12 shows the size distribution in viscosified water in blue bars and the distribution in viscosified water in red bars (500 ppm of HPAM in a 6 g/L NaCl brine). This figure shows that when the viscosity is increasing (in presence of HPAM), the bubble size distribution is increasing. Indeed, the mean diameter is increasing by 10 microns in comparison to the one in deionized water.
This shift might compensate the decrease of bubble velocity due to the viscosity increase. Nevertheless, in the case studied here and according to the experimental results, even with the shift of bubble size, the share of bubble carried toward the clean water outlet is still greater in viscosified water (65%) than in permuted water (40%).

This indirect impact of viscosity through the increase of bubble size (in viscosified

water), also leads to a drop in flotation efficiency. As a matter of fact, according to the model presented here, if the bubble size is increasing the impact of an increase in viscosity is much more important.

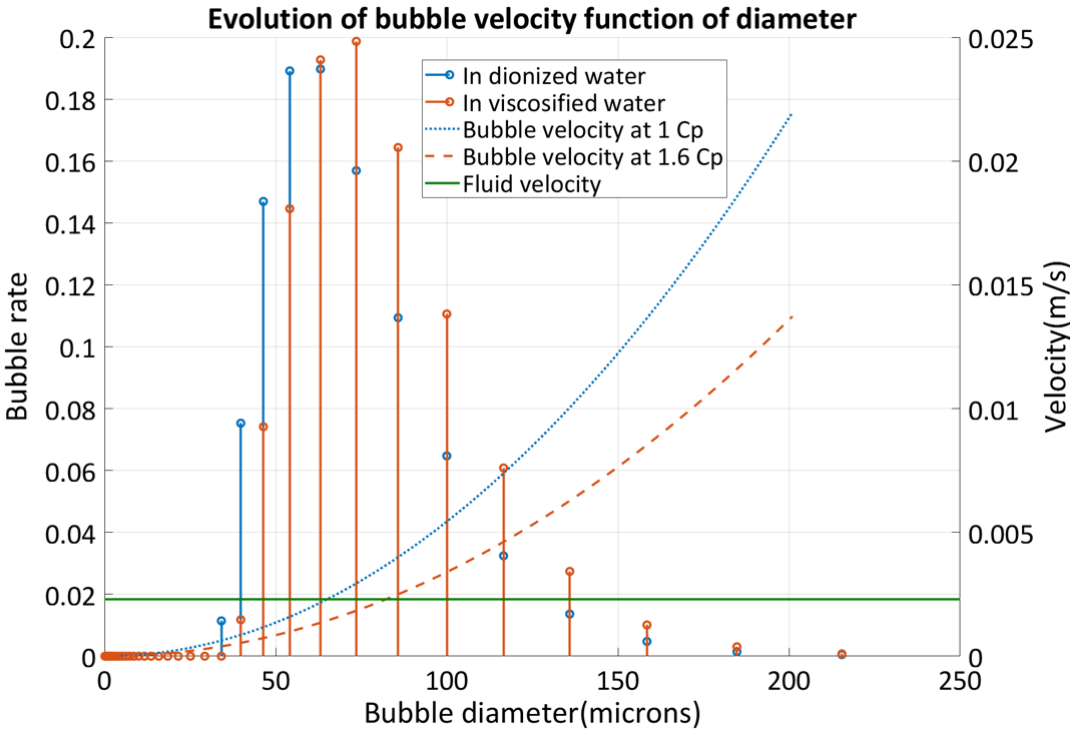

Figure 5.12: Evolution of bubble rising velocity function of their diameter in permuted and viscosified water with the bubble distribution in each kind of water

6 Conclusion

This chapter has enabled us to assess the impact of HPAM on flotation efficiency at the process scale. Firstly, we have shown that the impact of the polymer, trough the increase of viscosity and modification of bubble and droplet sizes, found at the local scale in chapter 3 translate at the global scale. Indeed, in both configurations (batch and co-current), the increase of viscosity leads to a decrease in efficiency. This decrease is not the same in both configuration. The flotation efficiency drastically decreases in co-current configuration whereas in batch mode the decrease is quite small. Likewise, when the droplet size decreases or the bubble size increases, the flotation efficiency tends to decreases.
This decrease is once again more important in co-current configuration.
However, a solution to this drop of efficiency might reside in the gas hold up in co-current configuration as the flotation efficiency is increasing with the increase in gas hold up. At the scale of the process, if the flotation cell contains a re-carrying zone, an increase of viscosity tends to decrease the share of floated bubble. This is explained by the reduction of bubble velocity with the increase of viscosity. As a matter of fact, this reduction allows bubbles normally floated to be carried by the fluid toward the clean water outlet. This leads to a diminution of flotation efficiency.

Ce chapitre nous a permis d'évaluer l'impact du HPAM sur l'efficacité de la flottation à l'échelle du procédé. Tout d'abord, nous avons montré que l'impact du polymère, à travers l'augmentation de la viscosité et la modification de la taille des bulles et des gouttelettes, constaté à l'échelle locale dans le chapitre 3 se traduit à l'échelle globale. En effet, dans les deux configurations (batch et co-courant), l'augmentation de la viscosité conduit à une diminution de l'efficacité. Cette diminution n'est pas la même dans les deux configurations. L'efficacité de la flottation diminue drastiquement dans la configuration co-courant alors qu'en mode batch la diminution est assez faible. De même, lorsque la taille des gouttelettes diminue ou que la taille des bulles augmente, l'efficacité de la flottation tend à diminuer. Cette diminution est une fois encore plus importante en configuration co-courant.
Cependant, une solution à cette baisse d'efficacité pourrait résider dans la rétention de gaz dans la configuration à co-courant, car l'efficacité de la flottation augmente avec celle de la rétention de gaz.
A l'échelle du processus, si la cellule de flottation contient une zone de ré-entraînement, une augmentation de la viscosité tend à diminuer la part de bulles flottantes. Ceci s'explique par la réduction de la vitesse des bulles avec l'augmentation de la viscosité. En effet, cette réduction permet aux bulles normalement flottantes d'être

entraînées par le fluide vers la sortie d'eau propre. Ceci conduit à une diminution de l'efficacité de la flottation.

Conclusions & perspectives

Conclusions

The objective of this work was to explain the loss in flotation efficiency in the presence of HPAM. The results can be concluded as:

- At our low concentration in HPAM, the polymer solution, because the shear stress generated in a flotation unit being small enough, can be considered as a newtonian fluid. Furthermore, the surface tension and the ionic strength (in brine) are not modified when polymer is added.
  The presence of polymer induced a decrease of the droplet size generated to created an emulsion. On the contrary, the bubble size tends to increase when HPAM is present.

- The negative impact of polymer, at the bubble scale, on the capture efficiency depends on the bubble size. For bubble between 50 μm and 100 μm (in DAF range), a variation of viscosity have little to no impact. However, for bigger bubble (in IAF range), an increase of viscosity leads to a decrease in collision, attachment and capture efficiency.
  At the local scale, the reduction of capture efficiency due to the polymer presence is increased by the reduction of droplet size and the increase in bubble size. However, the modification of physico-chemical parameters, such as ionic strength, surface tension or zeta potential, due to the presence of HPAM seems to have little to no effect on capture efficiencies.

- Nguyen and other traditional way to model the capture efficiency, as the product of collision and attachment efficiency, present some flaws when numerical study is wanted. The collision step widely studied is easy to estimate numerically but attachment model rely on many experimental parameters to work. The main issue being to find the thickness h_0 where the collision step stops and the attachment one start. A promising new model to obtain directly obtain the capture efficiency has been proposed. This model, based on the method used to calculate the collision efficiency, aim to calculate the droplet trajectory

near a bubble. Trajectories are obtained by solving the equation of movement of the droplet near the bubble considering both hydrodynamics and surface forces.

- At the process scale, when the flotation unit is assimilated to a column of flotation, the presence of HPAM has a clear negative impact on flotation efficiency due to the impact of viscosity. However, this impact is worsen by the modification of the bubble and droplet size distribution in presence of HPAM. A potential solution to this drop in efficiency is that in a co-current configuration (close to the industrial one) increasing the gas hold up allows to increase the flotation efficiency.
  Furthermore, in the type of cell study in this work, the increase of viscosity leads to a reduction of the bubble rising velocity conducting to small bubbles normally floated to be carried toward the clean water outlet and thus reducing the flotation efficiency.

At the end, our analytical methods give explanations to the observed decrease in flotation process efficiency with the presence of HPAM

Perspectives

- Further development of the new capture model are needed. Either by proving that our way of calculating the lubrication force (which opposes to film drainage) overestimates its magnitude or by finding and implementing other attractive forces to overcome it.
- Flotation experiments could be led to help the development and of the new model and see if our numerical results are translated in the reality.
- The impact of gas hold up on flotation efficiency in presence of polymer could be investigated experimentally to confirm our numerical results and see if it can be a solution applied in the industry to overcome the effect of HPAM addition without changing the technology of bubble production.

Conclusions & perspectives

Conclusions

L'objectif de ce travail était d'expliquer la perte d'efficacité de la flottation en présence de HPAM. Les résultats peuvent être conclus comme suit :

- A notre faible concentration en HPAM la solution de polymère, car la contrainte de cisaillement générée dans une unité de flottation est suffisamment faible, peut être considérée comme un fluide newtonien. De plus, la tension superficielle et la force ionique (dans la saumure) ne sont pas modifiées par l'ajout de polymère.
  La présence de polymère induit une diminution de la taille des gouttelettes générées pour créer une émulsion. Au contraire, la taille des bulles a tendance à augmenter en présence de HPAM.

- L'impact négatif du polymère, à l'échelle de la bulle, sur l'efficacité de capture dépend de la taille de la bulle. Pour des bulles entre 50 μm et 100 μm (dans la gamme DAF), une variation de la viscosité n'a que peu ou pas d'impact. Cependant, pour les bulles plus grosses (dans la gamme IAF), une augmentation de la viscosité entraîne une diminution de l'efficacité de collision, d'attachement et de capture.
  à l'échelle locale, la réduction de l'efficacité de capture due à la présence du polymère est accrue par la réduction de la taille des gouttelettes et l'augmentation de la taille des bulles. Cependant, la modification des paramètres physico-chimiques, tels que la force ionique, la tension de surface ou le potentiel zêta, due à la présence de HPAM semble avoir peu ou pas d'effet sur l'efficacité de capture.

- Le modèle proposé par Nguyen et d'autres méthodes traditionnelles de modélisation de l'efficacité de capture, en tant que produit de l'efficacité de la collision et de l'efficacité de l'attachement, présentent certaines faiblesses lorsqu'une étude numérique est souhaitée. L'étape de collision, largement étudiée, est facile à estimer numériquement, mais le modèle d'attachement repose sur

de nombreux paramètres expérimentaux. Le principal problème est de trouver l'épaisseur h_0 où l'étape de collision s'arrête et où l'étape d'attachement commence. Un nouveau modèle prometteur a été proposé pour obtenir directement l'efficacité de capture. Ce modèle, basé sur la méthode utilisée pour calculer l'efficacité de la collision, vise à calculer la trajectoire des gouttelettes près d'une bulle. Les trajectoires sont obtenues en résolvant l'équation du mouvement de la goutte près de la bulle en tenant compte à la fois de l'hydrodynamique et des forces de surface.

- A l'échelle du procédé, lorsque l'unité de flottation est assimilée à une colonne de flottation, la présence de HPAM a un impact négatif évident sur l'efficacité de la flottation en raison de l'impact de la viscosité. Cet impact est aggravé par la modification de la distribution de la taille des bulles et des gouttelettes en présence de HPAM. Une solution potentielle à cette baisse d'efficacité est que dans une configuration de co-courant (proche de la configuration industrielle), l'augmentation de la rétention de gaz permet d'augmenter l'efficacité de la flottation.
  De plus, dans le type de cellule étudié dans ce travail, l'augmentation de la viscosité conduit à une réduction de la vitesse de remontée des bulles conduisant à ce que les petites bulles normalement flottées soient emportées vers la sortie d'eau propre, réduisant ainsi l'efficacité de la flottation.

Finalement, nos méthodes analytiques expliquent la diminution observée de l'efficacité du processus de flottation en présence de HPAM.

Perspectives

- Il est nécessaire de poursuivre le développement du nouveau modèle de capture. Soit en prouvant que notre façon de calculer la force de lubrification (qui s'oppose au drainage du film) surestime son ampleur, soit en trouvant et en mettant en oeuvre d'autres forces attractives pour la surmonter.

- Des expériences de flottaison pourraient être menées pour aider au développement du nouveau modèle et voir si nos résultats numériques se traduisent dans la réalité.

- L'impact de la rétention de gaz sur l'efficacité de la flottation en présence de polymère pourrait être étudié expérimentalement pour confirmer nos résultats numériques et voir si cette solution peut être appliquée dans l'industrie.

Appendix A

Droplet and Bubble rising velocity calculation

Bubble or droplet velocity is always calculated from forces balance and motion equation. Bubbles are subjected to three forces: the flotability (the difference between the Archimede thrust and the weight), the drag and the added mass force. Once the force balance is done, the motion equation is written:

$$(m_b + C_M m_f)\frac{dV_b}{dt} = (m_b - m_f)g - C_D\frac{\pi d_b^2}{8}\rho_f V_b^2 \tag{A.1}$$

To solve this equation, there is a need to express the drag coefficient C_D. In our case, bubbles are considered small enough and contaminated to behave as solid spheres. This hypothesis can be verified by the calculation of Bond and Weber numbers (equations A.2 & A.3). These numbers are lower than 1 in the case studied in this work which validates our sphericity hypothesis.

$$Bo = \frac{\rho_f g d_b^2}{\sigma_{w/a}} \tag{A.2}$$

$$We = \frac{\rho_f V_b^2 d_b}{\sigma_{w/a}} \tag{A.3}$$

Thus, the drag coefficient depends on the bubble Reynolds number. It can be written as follow:

$$C_D = \frac{24}{Re_b}F(Re_b) \tag{A.4}$$

Equation A.4 then becomes:

$$(m_b + C_M m_f)\frac{dV_b}{dt} = (m_b - m_f)g - C_D\frac{24\pi d_b^2}{8Re_b}\rho_f V_b^2 F(Re_b) \tag{A.5}$$

$$\Leftrightarrow (\rho_b + C_M \rho_f)\frac{dV_b}{dt} = (\rho_b - \rho_f)g - C_D\frac{12\pi\mu_f}{d_b^2}V_b F(Re_b) \tag{A.6}$$

$$\Leftrightarrow \frac{dV_b}{dt} = \frac{(\rho_b - \rho_f)}{(\rho_b + C_M\rho_f)}g - C_D\frac{12\pi\mu_f}{d_b^2(\rho_b + C_M\rho_f)}V_b F(Re_b) \tag{A.7}$$

This equation is then differentiated and integrated giving the following expression for velocity:

$$V_b = \int \left[-\frac{12\mu_f}{(\rho_b + C_M\rho_f)d_p^2}(F(Re)) + \frac{\rho_b - \rho_f}{(\rho_b + C_M\rho_f)g}\right] dt \tag{A.8}$$

Once this expression is obtained two cases are studied. First, the one is very thin bubble with bubble diameter under $150\mu m$ (and $Re_b < 1$) and the other for larger bubbles. In the case of thin bubble, $F(Re)$ is equal to 1 and the Stokes formula is found. For larger bubbles the model of Schiller & Naumann is used, and $F(Re) = 1 + 0.15Re_b^{0.687}$.

In our case, Stokes formula is just use to express easily the velocity, in practice Schiller & Naumann correlation is used on all the range as bubble Reynolds number Re_b stay smaller than 800. The evolution of bubble velocity with both models is represented on figure A.1. This figure shows that when bubble Reynolds number is smaller than 1 both correlation gave identical velocities. When the Reynolds number is bigger than 1, Stokes model tends to overestimate bubble velocity.

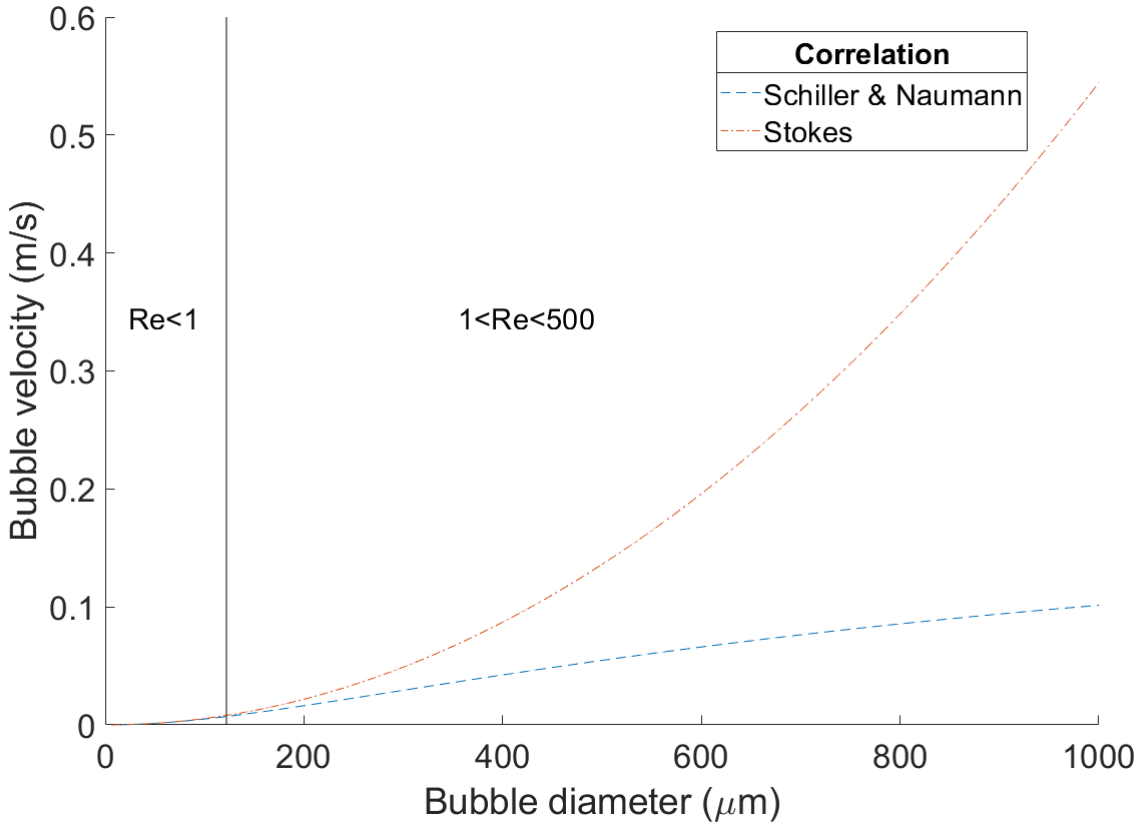

Figure A.1: Evolution of bubble velocity function of the bubble diameter and used correlation in water at 20°

Appendix B

Flotation pilot protocol

Once the preliminary studies of bubble and droplets size have been done, flotation experiments can be lead. Flotation experiments are all done with the following protocol:

- Prepare the emulsion (see the emulsion creation part)
- Make the blank on each dropsizer : record 100 frames with deionized water then average them. The computed frame is then subtracted to each frame taken during the experiment. This allow to suppress the default of the window (scratches, dust...) and the one of the light source.
- Take a sample of the initial emulsion.
- Set the flow rate of the liquid to treat at the desired value. In our general case: $150mL/min$.
- Set the flow rate of the white water at the desired value. In general 20% of the global flow rate, in our case: $40mL/min$ ($20mL/min$ in each needle valve).
- Measure the bubble size distribution.
- Level the flotation cell, and adjust the outflow in treated water (set at 90% of the global inlet flow rate).
- Launch the Dropsizers (recorded frame are used as reference later)
- Launch the experiments on the automate.
- Sample the treated water after a residency time T_r, once the steady state is reached, or around $3T_r$ (in the configuration given here $T_r = 5min$)

Bibliography

[Abidin et al., 2012] Abidin, A. Z., Puspasari, T., and Nugroho, W. A. (2012). Polymers for Enhanced Oil Recovery Technology. *Procedia Chemistry*, pages 11–16.

[Aguiar and Mansur, 2016] Aguiar, J. I. S. and Mansur, C. R. E. (2016). THE INFLUENCE OF POLYMER FLOODING ON PRODUCED OILY WATER: A REVIEW. *Brazilian Journal of Petroleum and Gas*, 10(1):49–61.

[Ait Kadi et al., 1987] Ait Kadi, A., Carreau, P. J., and Chauveteau, G. (1987). Rheological Properties of Partially Hydrolyzed Polyacrylamide Solutions. *Journal of Rheology*, 31(7):537–561.

[Al-Shamrani et al., 2002] Al-Shamrani, A. A., James, A., and Xiao, H. (2002). Separation of oilfrom water by dissolved air flotation. *Colloids and Surfaces A: Physicochemical and Engineering Aspects*, 209:15–26.

[Albijanic et al., 2010] Albijanic, B., Ozdemir, O., Nguyen, A. V., and Bradshaw, D. (2010). A review of induction and attachment times of wetting thin films between air bubbles and particles and its relevance in the separation of particles by flotation. *Advances in Colloid and Interface Science*, 159(1):1–21.

[Argillier et al., 2013] Argillier, J. F., Dalmazzone, C., Henaut, I., Mouazen, M., Noik, C., and Boufarguine, M. (2013). Methodological Approach for Analyzing the Impact of Chemical EOR on Surface Processes. In *SPE International Symposium on Oilfield Chemistry*, The Woodlands, Texas, USA. Society of Petroleum Engineers.

[Argillier et al., 2014] Argillier, J.-F., Hénaut, I., Noik, C., Viera, R., Roca Leon, F., and Aanesen, B. (2014). Influence of Chemical EOR on Topsides Produced Water Management. *Society of Petrolum Engineers*.

[Arthur et al., 2005] Arthur, J. D., Langhus, B. G., and Patel, C. (2005). Technical summary of oil & gas produced water treatment technologies. *All Consulting, LLC, Tulsa, OK*.

[Atarah, 2011] Atarah, J. J. A. (2011). The use of flotation technology in produced water treatment in the oil & gas industry.

[Barbery, 1981] Barbery, G. (1981). Flottation, Mécanismes et réactifs. *Techniques de l'ingénieur*.

[Basaová et al., 2010] Basaová, P., Macho, V., Hubika, M., and Horn, D. (2010). Collision processes involving a single rising bubble and a larger stationary spherical particle. *International Journal of Mineral Processing*, 94(1-2):58–66.

[Beneventi et al., 2008] Beneventi, D., Allix, J., Zeno, E., and Nortier, P. (2008). Influence of surfactant concentration on the ink removal selectivity in a laboratory flotation column. *International Journal of Mineral Processing*, 87(3-4):134–140.

[Bennett and Peters, 1988] Bennett, G. F. and Peters, R. W. (1988). The removal of oil from wastewater by air flotation: A review. *Critical Reviews in Environmental Control*, 18(3):189–253.

[Bensadok et al., 2007] Bensadok, K., Belkacem, M., and Nezzal, G. (2007). Treatment of cutting oil/water emulsion by coupling coagulation and dissolved air flotation. *Desalination*, 206(1-3):440–448.

[Besson, 2013] Besson, A. (2013). *Etude multi-échelle de la récolte de Dunaliella salina-Développement d'un procédé d'autofloculation-flottation de microalgues*. PhD Thesis, Toulouse, INSA.

[Burns et al., 1997] Burns, S. E., Yiacoumi, S., and Tsouris, C. (1997). Microbubble generation for environmental and industrial separations. *Separation and Purification Technology*, 11(3):221–232.

[Cain and Lee, 1985] Cain, F. W. and Lee, J. C. (1985). A technique for studying the drainage and rupture of unstable liquid films formed between two captive bubbles: Measurements on KCl solutions. *Journal of Colloid and Interface Science*, 106(1):70–85.

[Cassell et al., 1975] Cassell, E. A., Kaufman, K. M., and Matuevic, E. (1975). The effects of bubble size on microflotation. *Water Research*, 9(12):1017–1024.

[Chakibi, 2017] Chakibi, H. (2017). *Compréhension des interactions physico-chimiques complexes dans les eaux de production, en contexte EOR*. PhD thesis.

[Chakibi et al., 2018] Chakibi, H., Hénaut, I., Salonen, A., Langevin, D., and Argillier, J.-F. (2018). Role of BubbleDrop Interactions and Salt Addition in Flotation Performance. *Energy & Fuels*, 32(3):4049–4056.

[Chawaloesphonsiya et al., 2018] Chawaloesphonsiya, N., Guiraud, P., and Painmanakul, P. (2018). Analysis of cutting-oil emulsion destabilization by aluminum sulfate. *Environmental Technology*, 39(11):1450–1460.

[Choplin and Sabatié, 1986] Choplin, L. and Sabatié, J. (1986). Threshold-type shear-thickening in polymeric solutions. *Rheologica Acta*, 25(6):570–579.

[Dai et al., 1999] Dai, Z., Fornasiero, D., and Ralston, J. (1999). ParticleBubble Attachment in Mineral Flotation. *Journal of Colloid and Interface Science*, 217(1):70–76.

[Dai et al., 2000] Dai, Z., Fornasiero, D., and Ralston, J. (2000). Particlebubble collision models a review. *Advances in Colloid and Interface Science*, 85(2):231–256.

[Dalmazzone et al., 2012] Dalmazzone, C., Noïk, C., and Argillier, J.-F. (2012). Impact of Chemical Enhanced Oil Recovery on the Separation of Diluted Heavy Oil Emulsions. *Energy & Fuels*, 26(6):3462–3469.

[Dani, 2007] Dani, A. (2007). *Transfert de masse entre une bulle et un liquide : simulations numériques directes et fluorescence indute par nappe laser*. PhD thesis, Institut National des Sciences Appliquées de Toulouse.

[Deng et al., 2002] Deng, S., Bai, R., Chen, J. P., Yu, G., Jiang, Z., and Zhou, F. (2002). Effects of alkaline/surfactant/polymer on stability of oil droplets in produced water from ASP flooding. *Colloids and Surfaces A: Physicochemical and Engineering Aspects*, 211(2-3):275–284.

[Deng et al., 2005] Deng, S., Yu, G., Jiang, Z., Zhang, R., and Ting, Y. P. (2005). Destabilization of oil droplets in produced water from ASP flooding. *Colloids and Surfaces A: Physicochemical and Engineering Aspects*, 252(2):113–119.

[Derjaguin, 1993] Derjaguin, B. (1993). On the repulsive forces between charged colloid particles and on the theory of slow coagulation and stability of lyophobe sols. *Progress in Surface Science*, 43(1-4):15–27.

[Derjaguin and Dukhin, 1993] Derjaguin, B. V. and Dukhin, S. S. (1993). Theory of flotation of small and medium-size particles. *Progress in Surface Science*, 43(1-4):241–266.

[Derjaguin et al., 1984] Derjaguin, B. V., Dukhin, S. S., and Rulyov, N. N. (1984). Kinetic Theory of Flotation of Small Particles. In Matijevi, E. and Good, R. J., editors, *Surface and Colloid Science*, pages 71–113. Springer US, Boston, MA.

[Dobby and Finch, 1986] Dobby, G. S. and Finch, J. A. (1986). A model of particle sliding time for flotation size bubbles. *Journal of Colloid and Interface Science*, 109(2):493–498.

[Dobby and Finch, 1987] Dobby, G. S. and Finch, J. A. (1987). Particle size dependence in flotation derived from a fundamental model of the capture process. *International Journal of Mineral Processing*, 21(3):241–260.

[Dudek and Øye, 2018] Dudek, M. and Øye, G. (2018). Microfluidic Study on the Attachment of Crude Oil Droplets to Gas Bubbles. *Energy & Fuels*, 32(10):10513–10521.

[Edzwald, 2007] Edzwald, J. K. (2007). Developments of high rate dissolved air flotation for drinking water treatment. *Journal of Water Supply: Research and Technology-Aqua*, 56(6-7):399–409.

[Edzwald, 2010] Edzwald, J. K. (2010). Dissolved air flotation and me. *Water Research*, 44(7):2077–2106.

[Eftekhardadkhah et al., 2015] Eftekhardadkhah, M., Aanesen, S. V., Rabe, K., and Øye, G. (2015). Oil Removal from Produced Water during Laboratory- and Pilot-Scale Gas Flotation: The Influence of Interfacial Adsorption and Induction Times. *Energy & Fuels*, 29(11):7734–7740.

[Fanaie and Khiadani, 2020] Fanaie, V. R. and Khiadani, M. (2020). Effect of salinity on air dissolution, size distribution of microbubbles, and hydrodynamics of a dissolved air flotation (DAF) system. *Colloids and Surfaces A: Physicochemical and Engineering Aspects*, 591:124547.

[Frank et al., 2012] Frank, X., Charpentier, J.-C., Ma, Y., Midoux, N., and Li, H. Z. (2012). A Multiscale Approach for Modeling Bubbles Rising in Non-Newtonian Fluids. *Industrial & Engineering Chemistry Research*, 51(4):2084–2093.

[Gaudin et al., 1942] Gaudin, A. M., Schuhmann, R., and Schlechten, A. W. (1942). Flotation Kinetics. II. The Effect of Size on the Behavior of Galena Particles. *The Journal of Physical Chemistry*, 46(8):902–910.

[Ham et al., 1983] Ham, N. J. M. V., Behie, L. A., and Svrcek, W. Y. (1983). The effect of air distribution on the induced air flotation of fine oil in water emulsions. *The Canadian Journal of Chemical Engineering*, 61(4):541–547.

[Hewitt et al., 1993] Hewitt, D., Fornasiero, D., Ralston, J., and Fisher, L. R. (1993). Aqueous film drainage at the quartz/water/air interface. *Journal of the Chemical Society, Faraday Transactions*, 89(5):817.

[Huang, 2009] Huang, Z. (2009). *Efficacité de Capture dans les Procédés de Flottation*. PhD Thesis, Institut National des Sciences Appliquées de Toulouse.

[Ichikawa, 2007] Ichikawa, T. (2007). Electrical demulsification of oil-in-water emulsion. *Colloids and Surfaces A: Physicochemical and Engineering Aspects*, 302(1-3):581–586.

[Israelachvili, 1992] Israelachvili, J. (1992). Intermolecular and surface forces. Academic Press, London. *Intermolecular and surface forces. 2nd ed. Academic Press, London.*

[Ityokumbul, 1993] Ityokumbul, M. T. (1993). Selection of recovery zone height in flotation column design. *Chemical Engineering and Processing: Process Intensification*, 32(2):77–82.

[Ives, 1983] Ives, K. J., editor (1983). *The Scientific Basis of Flotation*. Springer Netherlands, Dordrecht.

[Julien Saint Amand, 1999] Julien Saint Amand, F. (1999). Hydrodynamics of deinking flotation. *International Journal of Mineral Processing*, 56(1):277–316.

[Kang et al., 2011] Kang, W., Xu, B., Wang, Y., Li, Y., Shan, X., An, F., and Liu, J. (2011). Stability mechanism of W/O crude oil emulsion stabilized by polymer and surfactant. *Colloids and Surfaces A: Physicochemical and Engineering Aspects*, 384(1):555–560.

[Koh and Schwarz, 2006] Koh, P. T. L. and Schwarz, M. P. (2006). CFD modelling of bubbleparticle attachments in flotation cells. *Minerals Engineering*, 19(6):619–626.

[Legendre et al., 1998] Legendre, D., Borée, J., and Magnaudet, J. (1998). Thermal and dynamic evolution of a spherical bubble moving steadily in a superheated or subcooled liquid. *Physics of Fluids*, 10(6):1256–1272.

[Leppinen and Dalziel, 2004] Leppinen, D. M. and Dalziel, S. B. (2004). Bubble size distribution in dissolved air flotation tanks. *Journal of Water Supply: Research and Technology-AQUA*, 53(8):531–543.

[Lewandowska, 2007] Lewandowska, K. (2007). Comparative studies of rheological properties of polyacrylamide and partially hydrolyzed polyacrylamide solutions. *Journal of Applied Polymer Science*, 103(4):2235–2241.

[Li, 1994] Li, D. (1994). Coalescence between Two Small Bubbles or Drops. *Journal of Colloid and Interface Science*, 163(1):108–119.

[Li et al., 1990] Li, D., Fitzpatrick, J. A., and Slattery, J. C. (1990). Rate of collection of particles by flotation. page 13.

[Li et al., 2007] Li, M., Xu, M., Lin, M., and Wu, Z. (2007). The Effect of HPAM on Crude Oil/Water Interfacial Properties and the Stability of Crude Oil Emulsions. *Journal of Dispersion Science and Technology*, 28(1):189–192. Publisher: Taylor & Francis _eprint: https://doi.org/10.1080/01932690600992829.

[Liu et al., 2013] Liu, Y., Tourbin, M., Lachaize, S., and Guiraud, P. (2013). Silica nanoparticles separation from water: Aggregation by cetyltrimethylammonium bromide (CTAB). *Chemosphere*, 92(6):681–687.

[Lopes and Silveira, 2014] Lopes, L. F. and Silveira, B. M. O. (2014). Rheological Evaluation of HPAM fluids for EOR Applications. *International Journal of Engineering*, 14(03):7.

[Magnaudet et al., 1995] Magnaudet, J., Rivero, M., and Fabre, J. (1995). Accelerated flows past a rigid sphere or a spherical bubble. Part 1. Steady straining flow. *Journal of Fluid Mechanics*, 284:97–135.

[Manev and Nguyen, 2005] Manev, E. D. and Nguyen, A. V. (2005). Critical thickness of microscopic thin liquid films. *Advances in Colloid and Interface Science*, 114-115:133–146.

[Meyssami, 2005] Meyssami, B. (2005). Use of coagulants in treatment of olive oil wastewater model solutions by induced air flotation. *Bioresource Technology*, 96(3):303–307.

[Mickova, 2015] Mickova, I. L. (2015). Advanced Electrochemical Technologies in Wastewater Treatment. Part II: Electro-Flocculation and Electro-Flotation. *American Academic Scientific Research Journal for Engineering, Technology, and Sciences*, 14(2):273–294.

[Mondal et al., 2021] Mondal, S., Acharjee, A., Mandal, U., and Saha, B. (2021). Froth flotation process and its application. *Vietnam Journal of Chemistry*, 59:417–425.

[Moosai and Dawe, 2002] Moosai, R. and Dawe, R. A. (2002). Oily wastewater cleanup by gas flotation. *West Indian Journal of Engineering*, 25(1):25–41.

[Nguyen, 2000] Nguyen, A. V. (2000). Improved Approximation of Water Dielectric Permittivity for Calculation of Hamaker Constants. *Journal of Colloid and Interface Science*, 229(2):648–651.

[Nguyen and Evans, 2004] Nguyen, A. V. and Evans, G. M. (2004). Attachment interaction between air bubbles and particles in froth flotation. *Experimental Thermal and Fluid Science*, 28(5):381–385.

[Nguyen et al., 1998] Nguyen, A. V., Ralston, J., and Schulze, H. J. (1998). On modelling of bubble-particle attachement probability in flotation. *International Journal of Mineral Processing*, 53:225–249.

[Nguyen and Schulze, 2004] Nguyen, A. V. and Schulze, H. J. (2004). *Colloidal science of flotation*. Number 118 in Surfactant science series. Dekker, New York. OCLC: 249254620.

[Nguyen Van, 1993] Nguyen Van, A. (1993). On the sliding time in flotation. *International Journal of Mineral Processing*, 37(1):1–25.

[Nguyen-Van and Kme, 1994] Nguyen-Van, A. and Kme, S. (1994). Probability of collision between particles and bubbles in flotation: the theoretical inertialess model involving a swarm of bubbles in pulp phase. *International Journal of Mineral Processing*, 40(3):155–169.

[Nilan et al., 2014] Nilan, M., Stang, P., Dadkhah, M. E., and Sahu, A. K. (2014). Understanding the Impact of Chemicals in Produced Water in Enhanced Oil Recovery (EOR) Projects.

[Oikonomidou et al., 2018] Oikonomidou, O., Evgenidis, S. P., Kostoglou, M., and Karapantsios, T. D. (2018). Degassing of a pressurized liquid saturated with dissolved gas when injected to a low pressure liquid pool. *Experimental Thermal and Fluid Science*, 96:347–357.

[Patel, 2005] Patel, C. (2005). TECHNICAL SUMMARY OF OIL & GAS PRODUCED WATER TREATMENT TECHNOLOGIES. page 53.

[Qi et al., 2013] Qi, W.-K., Yu, Z.-C., Liu, Y.-Y., and Li, Y.-Y. (2013). Removal of emulsion oil from oilfield ASP wastewater by internal circulation flotation and kinetic models. *Chemical Engineering Science*, 91:122–129.

[Ralston and Dukhin, 1999] Ralston, J. and Dukhin, S. S. (1999). The interaction between particles and bubbles. *Colloids and Surfaces A: Physicochemical and Engineering Aspects*, 151:3–14.

[Ralston et al., 1999] Ralston, J., Dukhin, S. S., and Mishchuk, N. A. (1999). Inertial hydrodynamic particle-bubble interaction in flotation. *International Journal of Mineral Processing*, 56:207–256.

[Ralston et al., 2007] Ralston, J., Fornasiero, D., Grano, S., Duan, J., and Akroyd, T. (2007). Reducing uncertainty in mineral flotationflotation rate constant prediction for particles in an operating plant ore. *International Journal of Mineral Processing*, 84(1):89–98.

[Ramirez et al., 1999] Ramirez, J. A., Zinchenko, A., Loewenberg, M., and Davis, R. H. (1999). The flotation rates of fine spherical particles under Brownian and convective motion. *Chemical Engineering Science*, 54(2):149–157.

[Ramírez-Muñoz et al., 2012] Ramírez-Muñoz, J., Galicia-Nequiz, O., Baz-Rodríguez, S., Colín-Luna, J., Martínez-Delgadillo, S., and Puebla, H. (2012). The Effects of Surfactants on the Drag of a Bubble. *Procedia Engineering*, 42:1840–1848.

[Reed and Woodard, 1976] Reed, S. W. and Woodard, F. E. (1976). Dissolved air flotation of poultry processing waste. *Journal (Water Pollution Control Federation)*, pages 107–119.

[Richerand and Peymani, 2015] Richerand, F. and Peymani, Y. (2015). Improving Flotation Methods to treat EOR polymer Rich Produced Water. *Society of Petrolum Engineers*.

[Ross, 1950] Ross, S. (1950). The Inhibition of Foaming. II. A Mechanism for the Rupture of Liquid Films by Anti-foaming Agents. *The Journal of Physical Chemistry*, 54(3):429–436.

[Rubinstein and Colby, 2003] Rubinstein, M. and Colby, R. H. (2003). *Polymer physics*. Oxford University Press, Oxford ; New York.

[Rubio et al., 2002] Rubio, J., Souza, M. L., and Smith, R. W. (2002). Overview of flotation as wastewater treatement technique. *Minerals Engineering*, 15:139–155.

[Rykaart and Haarhoff, 1995] Rykaart, E. M. and Haarhoff, J. (1995). Behaviour of air injection nozzles in dissolved air flotation. *Water Science and Technology*, 31(3-4):25–35.

[Sarrot, 2006] Sarrot, V. (2006). *Capture de fines particules par des inclusions fluides*. thesis, Toulouse, INSA.

[Sarrot et al., 2005] Sarrot, V., Guiraud, P., and Legendre, D. (2005). Determination of the collision frequency between bubbles and particles in flotation. *Chemical Engineering Science*, 60(22):6107–6117.

[Schers and Van Dijk, 1992] Schers, G. J. and Van Dijk, J. C. (1992). Dissolved-air flotation: Theory and practice. In *Chemical Water and Wastewater Treatment II*, pages 223–246. Springer.

[Schulze, 1989] Schulze, H. J. (1989). Hydrodynamics of Bubble-Mineral Particle Collisions. *Mineral Processing and Extractive Metallurgy Review*, 5(1-4):43–76.

[Shepitka et al., 1983] Shepitka, J. S., Case, C. E., Donaruma, L. G., Hatch, M. J., Kilmer, N. H., Khune, G. D., Martin, F. D., Ward, J. S., and Wilson, K. V. (1983). Partially imidized, water-soluble polymeric amides. I. Partially imidized polyacrylamide and polymethacrylamide. *Journal of Applied Polymer Science*, 28(12):3611–3617.

[Silset, 2008] Silset, A. (2008). Emulsions (w/o and o/w) of HeavyCrude Oils. Characterization, Stabilization, Destabilization and ProducedWater Quality.

[Spildo and Sæ, 2015] Spildo, K. and Sæ, E. I. . (2015). Effect of Charge Distribution on the Viscosity and Viscoelastic Properties of Partially Hydrolyzed Polyacrylamide. *Energy & Fuels*, 29(9):5609–5617.

[Sutherland, 1948] Sutherland, K. L. (1948). Physical Chemistry of Flotation. XI. Kinetics of the Flotation Process. *The Journal of Physical and Colloid Chemistry*, 52(2):394–425.

[Takahashi et al., 1979] Takahashi, T., Miyahara, T., and Mochizuki, H. (1979). Fundamental study of bubble formation in dissolved air pressure flotation. *Journal of Chemical Engineering of Japan*, 12(4):275–280.

[Telis et al., 2007] Telis, V., Telis-Romero, J., Mazzotti, H., and Gabas, A. (2007). Viscosity of Aqueous Carbohydrate Solutions at Different Temperatures and Concentrations. *International Journal of Food Properties*, 10(1):185–195.

[Wang et al., 2005] Wang, W., Zhou, Z., Nandakumar, K., Masliyah, J. H., and Xu, Z. (2005). An induction time model for the attachment of an air bubble to a hydrophobic sphere in aqueous solutions. *International Journal of Mineral Processing*, 75(1):69–82.

[Ward et al., 1970] Ward, C. A., Balakrishnan, A., and Hooper, F. C. (1970). On the Thermodynamics of Nucleation in Weak Gas-Liquid Solutions. *Journal of Basic Engineering*, pages 695–704.

[Ward and Martin, 1981] Ward, J. S. and Martin, F. D. (1981). Prediction of Viscosity for Partially Hydrolyzed Polyacrylamide Solutions in the Presence of Calcium and Magnesium Ions. *Society of Petroleum Engineers Journal*, 21(05):623–631.

[Wever et al., 2011] Wever, D., Picchioni, F., and Broekhuis, A. A. (2011). Polymers for enhanced oil recovery: A paradigm for structureproperty relationship in aqueous solution. *Progress in Polymer Science*, 36(11):1558–1628.

[Yan et al., 2021] Yan, Y., Yang, W., Fang, X., Yan, P., and Tu, J. (2021). Experimental investigation of multi-phase hydrodynamics and bubble-particle interactions in a Wemco 56 flotation cell. *Minerals Engineering*, 172:107115.

[Ye et al., 1989] Ye, Y., Khandrika, S. M., and Miller, J. D. (1989). Induction-time measurements at a particle bed. *International Journal of Mineral Processing*, 25(3):221–240.

[Yoon, 2000] Yoon, R.-H. (2000). The role of hydrodynamic and surface forces in bubbleparticle interaction. *International Journal of Mineral Processing*, 58(1-4):129–143.

[Yoon and Luttrell, 1989] Yoon, R. H. and Luttrell, G. H. (1989). The Effect of Bubble Size on Fine Particle Flotation. *Mineral Processing and Extractive Metallurgy Review*, 5(1-4):101–122.

[Yoon and Yordan, 1991] Yoon, R.-H. and Yordan, J. L. (1991). Induction time measurements for the quartzamine flotation system. *Journal of Colloid and Interface Science*, 141(2):374–383.

[Zaitoun and Potie, 1983] Zaitoun, A. and Potie, B. (1983). Limiting Conditions for the Use of Hydrolyzed Polyacrylamides in Brines Containing Divalent Ions. Society of Petroleum Engineers.

[Zhang and Guiraud, 2013] Zhang, M. and Guiraud, P. (2013). Elimination of TiO2 nanoparticles with the assist of humic acid: Influence of agglomeration in the dissolved air flotation process. *Journal of Hazardous Materials*, 260:122–130.

[Zouboulis and Avranas, 2000] Zouboulis, A. I. and Avranas, A. (2000). Treatment of oil-in-water emulsions by coagulation and dissolved-air flotation. *Colloids and Surfaces A: Physicochemical and Engineering Aspects*, 172(1):153–161.